A Simple Site-specific Method for Estimating Nonlinear Site Effects

2018

Haizhong Zhang

A Simple Site-specific Method for Estimating Nonlinear Site Effects

Dissertation
Presented to Faculty of Engineering, Kanagawa University in Partial Fulfillment of the Requirements for the Degree of Doctor of Engineering

Submitted by

Haizhong Zhang

Supervised by

Professor **Yan-gang Zhao**

January 2018

CONTENTS

Acknowledgments

I would like to first express my sincere gratitude to my advisor Professor Yan-gang Zhao. His support, encouragement and guidance from the initial to final level enabled me to complete this thesis. The valuable things I have learned are not only the professional knowledge, but also the way to do a research through creative thinking, hardworking and rigorous attitude. It is great honor to work with him and I would keep those things I have learned in mind and take them as my guideline for my future.

Secondly, I would like to express my deep gratitude to Associate Professor Takasuke Saito. He gave me a lot of useful help in solving the met difficulties, both in my research and life in Japan.

Special thanks to Professor Takahisa Enomoto for his useful help and professional comments from the early stage of this study.

Great thanks to the review committee members: Professor Mamoru Iwata, Professor Kazushi Shimazaki, Professor Takeshi Ohkuma for their valuable comments and suggestions on this work.

Sincere thanks are given to the member of Zhao laboratory for their help in solving the met difficulties in many aspects and understanding Japanese culture, etc: Dr. Jiao Wang, Dr. Siqi Lin, Dr. Xuanyi Zhang, Dr. Xifeng Yan, Miss Yexuan Yao, Miss Fangwen Ge, Mr. Yuma Ozawa, Mr. Yuki Kawaguchi, Mr. Haoshen Xu, Mr. Yuqi Xie, Mr. Yusuke Sukiyama, Mr. Takashi Tsumura, Mr. Ryota Fukada, Miss Wakako Mitsuhashi, Mr. Yokenn Takeuchi, Mr. Hajime Waseda, and many friends outside Zhao laboratory.

Grateful acknowledgement is given to the Ministry of Education, Science, and Culture, Government of Japan for granting me the scholarship which made this study possible.

Finally, I specially thank my wife—Miss Hua Chen and my parents for their cares, patience and devotion.

Haizhong Zhang

January, 2018

Abstract

It has long been recognized that site effects should be considered in the seismic design of structures. Generally, there are two categories of methods for estimating site effects for design purpose, namely: empirical and theoretical. The empirical methods are developed based on site classification and statistical analysis of seismic records. In most seismic codes throughout the world, such as the Eurocode 8 and the International Building Code, the empirical methods are adopted for estimating site effects. But, for some regions such as Japan, site conditions are known to vary significantly, site effects can hardly be represented using several site classes. For such regions, it has been suggested that site effects be evaluated using theoretical methods according to specific sites instead of rough site classifications, by some codes including the Japanese Seismic Code.

A number of simple theoretical methods have been developed to estimate site effects of specific sites. Almost all of these methods are developed theoretically based on a simple soil model, a single-layer soil profile on bedrock. And, for multi-layer soil profiles, the multiple soil layers are approximated as an equivalent single layer by roughly weighted averaging the soil shear wave velocity and density. However, the weighted averaging ignores the layer sequence and can't properly consider properties of every soil layers. It can be easily inferred that, the error of estimated site effects will increase as variation degree of the soil properties along the depth increases. What's worse, the method using the weighted averaging is found to significantly underestimate site effects, when the impedance contrast of the soil layers is large, which is dangerous for the seismic design of structures.

The main objective of the present research is to develop a new simple site-specific method for estimating site effects of multi-layer soil profiles. This dissertation consists of six chapters. The contents of each chapter are briefly described as follows.

In Chapter 1, the background, objective and organization of this study are described.

In Chapter 2, a function for estimating site effects characterized as response spectral ratio (RSR) is developed. To develop this function, the RSR and Fourier spectral ratio (FSR) are compared, based on ground-motion records in Section 2.2 and random vibration theory in Section 2.3.

The developed function for RSR in Chapter 2 consists of two basic parameters, namely the fundamental period and first resonance peak. In Chapter 3, three simple methods for estimation of the first resonance peak of layered soil profiles are developed.

In Chapter 4, a simple procedure to consider the soil nonlinear behavior in estimation of the site effects is developed. During the application of this method, the first mode shape is necessary; a simple method for estimating the first mode shape of layered soil profiles is proposed, in Section 4.3.

In Chapter 5, the consideration of estimating site effects in Chapter 3 is extended to calculate the fundamental period of a multiple-degree-of-freedom system.

In Chapter 6, conclusions obtained by this study are summarized.

Chapter 1

Introduction

1.1 Background

Recent earthquakes (Mexico City (1985), Armenia (1988), Loma Prieta, California (1989), Northridge, California (1994), Kobe (1995), Taiwan (1999), Central-Western India (2001), Wenchuan, China (2008), Tokoku, Japan (2011), Kumamoto, Japan (2016) etc.) [1-10] have repeatedly shown the pronounced effect of local site conditions on the level of ground shaking and damage at a site. The earthquake ground motions can be significantly modified whilst travelling from the bedrock to the soil surface. In certain soil conditions, the ground motion at bedrock level is amplified by several times though the overlying soil, thereby inducing greater damage in buildings and other structures. It is clearly that, site effects should be incorporated into the seismic design of structures.

Generally, there are two categories of methods of estimating site effects for design purpose, namely: empirical and theoretical. The empirical methods are developed based on site classification and statistical analysis of seismic records. In most seismic codes throughout the world, the empirical methods are adopted for estimating site effects. For example, in UBC 1997 [11], IBC 2003 [12], IBC 2012 [13], IBC 2015 [14], ASCE/SEI 7-05 [15] and ASCE/SEI 7-10 [16], site effects are reflected by site coefficients of five site classes; and the site coefficients are developed based on regression of seismic records of the Loma Prieta earthquake in 1989 [2,17,18]. The empirical methods are appropriate for regions that, (1) site conditions don't vary significantly, and thus can be represented by several representative classes, (2) adequate recorded ground-motion data are available for conduction of the statistical analysis.

But, for regions like Japan, geological feature is known to vary significantly through the country, site effects can hardly be reflected accurately by several classes of sites. In reality, many important site-specific characteristics can be masked by the site classifications. For example, for a site consisting of soft soil on stiffer rock, soil resonance caused by multiple reflections within the soil medium can cause significant amplification of seismic motion with a frequency near the site's fundamental frequency; however, the resonance effect of a specific site is 'averaged' by the site classification and typically cannot be accurately accounted for by a specific site class. Moreover, for regions such as Hongkong, there are few recorded strong-motion data, reliable site coefficients can

hardly be obtained based on the statistical analysis. For such regions, the theoretical methods based on wave propagation theory are more appropriate be used to estimate site effects. It has been suggested that site effects be evaluated theoretically according to specific sites, by some codes including the 2000 Japanese Seismic Code [19, 20] and Mexico's seismic code [21].

A number of simple methods have been developed theoretically to estimate site effects of specific sites. In Japanese seismic code, a site-specific method developed based on a single-layer soil profile on bedrock is adopted [19, 20 and 22]. The method uses two response spectral ratios corresponding to the site's first and second natural periods to represent site effects. In Mexico seismic code, a different site-specific method is adopted, which is also developed based on a single-layer soil profile on bedrock [21]. This method uses amplification ratio of peak acceleration to approximate site effects. In addition, many simple methods for site effects of specific sites have been developed by several studies including those by Lam [23] and Hing-hong [24-26]. Similarly, all of these methods are developed based on a single-layer soil profile on bedrock. And, these methods use a single response spectral ratio corresponding to the site's first natural period to reflect site effects.

It is noted that, all of these methods are developed based on a simplest soil model, i.e. a single-layer soil profile on bedrock. And, for multi-layer soil profiles, the multiple soil layers are approximated as an equivalent single layer by roughly weighted averaging the soil shear wave velocity and density. However, as the weighted averaging ignores the layer sequence and can't properly consider properties of every soil layers. It can be easily inferred that, the error in estimation of the site effects will increase as the variation degree of soil properties along the depth increases. What's worse, the method using the weighted averaging is found to significantly underestimate site effects, when the impedance contrast of the soil layers is large [27-29], which is dangerous for seismic design of structures.

1.2 Objective

In this study, a new simple site-specific method for estimating site effects of layered soil profiles is developed. Instead of by roughly weighted averaging the soil properties of each layer, the proposed method properly takes into account layer sequence and properties of every soil layers. In addition, the proposed method also takes account of, (1) frequency dependent properties of the site effects, (2) effect of the soil nonlinear behavior on site effects.

1.3 Organization

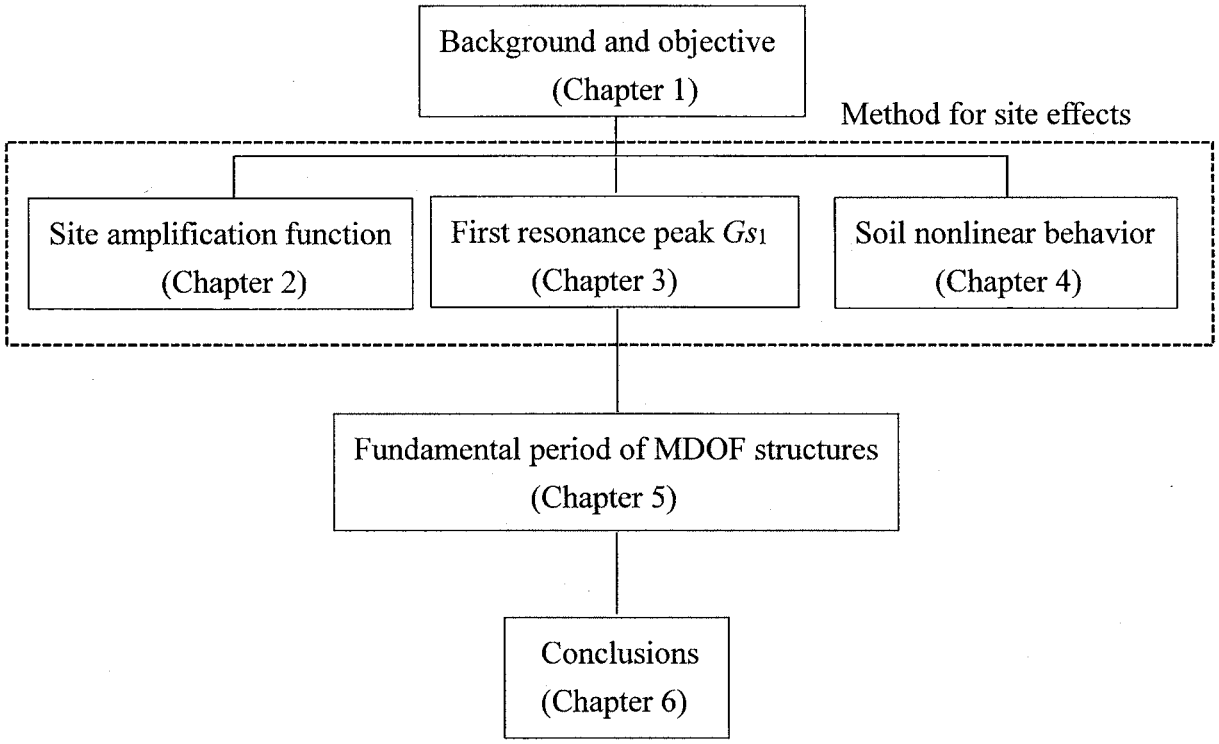

Fig.1-3-1 Relationship between chapters

This dissertation consists of six chapters and Fig.1-3-1 shows the organization. Chapter 1 is the background of this study, and Chapter 6 is the summary and conclusions. Chapters 2 to 4, show the new proposed method for estimating site effects of layered soil profiles. In Chapter 5, the consideration of estimating site effects in Chapter 3 is extended to calculate the fundamental period of a multiple-degree-of-freedom (MDOF) system. Chapters 2 to 5 constitute the main part of the dissertation. The contents of the four chapters are summarized as follows.

As the seismic motion for structural design is usually given in the form of response spectrum, the site effects are typically characterized as ratio of response spectrum at ground surface against the one specified at outcrop bedrock in seismic codes. In Chapter 2, a function for estimating the response spectral ratio (RSR) is developed. To develop this function, the response spectral ratio (RSR) and Fourier spectral ratio (FSR) are compared based on ground-motion records in Section 2.2, and random vibration theory (RVT) in Section 2.3.

The developed function for RSR in Chapter 2 consists of two basic parameters, namely the fundamental period and first resonance peak. In Chapter 3, three simple methods for estimation of the first resonance peak of layered soil profiles are developed. And, the validity of the proposed methods are investigated using a lot of actual soil profiles.

As the soil nonlinear behavior significantly influences the site response, a simple procedure to consider the soil nonlinear behavior in estimation of the site effects is developed in Chapter 4. During the application of this method, as the first mode shape is necessary, and a simple method for estimating the first mode shape of layered soil profiles is proposed, in Section 4.3. The validity of both the proposed method for soil nonlinear behavior and the method for the first mode shape are investigated using many actual soil profiles. In addition, the validity of the total proposed method for site effects are also demonstrated by estimating response spectra of several actual reprehensive soil profiles.

In Chapter 5, the consideration of estimating site effects in Chapter 3 is extended to calculate the fundamental period of a multiple-degree-of-freedom (MDOF) system. The accuracy of the proposed method is investigated by estimating the fundamental periods of many designed MDOF models and actual MDOF structures.

Chapter 2

Site amplification function for site effects

2.1 Introduction

As the seismic motion for structural design is usually given in the form of response spectrum, the site effects are typically characterized as ratio of response spectrum at ground surface against the one specified at outcrop bedrock in seismic codes. In this chapter, an equation for estimation of the response spectral ratio (RSR) is developed, and the developed equation is called site amplification function.

This chapter is organized as follows. Firstly, to develop the site amplification function, response spectral ratio (RSR) and Fourier spectral ratio (FSR) are compared, based on ground-motion records and random vibration theory, in Sections 2.2 and 2.3, respectively. Then, based on the conclusions derived from sections 2.2 and 2.3, a site amplification function is constructed in Section 2.4.

2.2 Comparison of Fourier and response spectral ratio based on ground-motion records

2.2.1 Introduction

Most analytical methods for estimating the RSR are developed based on a very simple soil model, a single-layer soil profile on bedrock, with seismic waves propagating vertically [20-26]. But even for such a simple soil model, there is not a closed form equation for the RSR in theory. To obtain the RSR, site response analysis has to be conducted in frequency or time-history domain. Moreover, values of the RSR depend on not only material properties of analyzed soil profiles but also properties of input rock motions even for linear analysis; the dependence of the RSR on rock motions are found may be significant [30, 31]. This means that, for a certain linear soil model, a unique RSR can't been determined even by means of site response analysis. Properties of input rock motions also have to be properly taken into account in determination of the RSR. Therefore, directly developing a reasonable analytical method for RSR is very difficult.

Fourier spectral ratio (FSR), known as transfer function, is also often used to characterize site effects. For the simple soil model introduced above, a closed form equation for FSR can be easily obtained without any site response analysis. In addition, if soil responds elastically, values of FSR totally depend on properties of estimated soil profiles; thus for a certain soil profile the FSR is unique. It is clear that, determination of the FSR is much easy than that of the RSR. If some systemic relationships between RSR and FSR are known, the RSR can be simply estimated based on the FRS.

Many studies have compared the FSR with the RSR statistically using actual ground-motion records [32-34]. Maximum value of FSRs and RSRs are found occur at about the same frequency, by analyses of soft clay sites on much stiffer rock or soil [32]. Moreover, FSRs are found to systematically exceed RSRs in the neighborhood of the main spectral peaks, through analyses of several sites on the valley of Mexico [33]. In addition, average spectral ratios at several period bands are compared for alluvial and bay mud sites, and found that, estimates based on RSR were consistent with similar estimates based on FSR for similar period bands computed, with some discrepancies observed at longer-period bands [34].

This section statistically investigates the relationship between RSRs and FSRs not only about the main peaks discussed previously but also the values for a wide range of periods. Moreover, this section examines, the dependence of the relationship on magnitude and epicentral distance. For the purpose above, horizontal accelerations recorded on nearby soil-rock pairs in Japan are used, and detail information about these sites and ground-motion records are introduced in section 2.2.2 and 2.2.3, respectively. Then, in section 2.2.4, relationship between RSR and FSR along with its dependence on magnitude and epicentral distance are investigated, using these selected ground motion records. Finally, the conclusions are presented in section 2.2.5.

2.2.2 Soil-rock pairs

To investigate the relationship between RSRs and FSRs, 10 actual nearby soil-rock pairs are selected from Strong-motion Seismograph Networks (K-NET, KIK-net) of Japan [13]. The rock sites are selected to have shear wave velocity of surface layer larger than 400 m/s to meet the definition of engineering bedrock in the Japanese Seismic Code. And, to reduce the path effect on spectral ratios, soil sites are selected as close as possible to the rock sites, and the maximum distance of the selected soil-rock pairs is 4.16 km. These selected soil-rock pairs are numbered from 1 to 10, and information of each pair, including station code, coordinates, distance between rock and soil site, shear wave velocity of surface layer, and average shear wave velocity in the upper 30 m (V_{S30}) are listed in Table 2-2-1. In the table, for each soil-rock pairs, the upper one is rock site and the lower one is soil site.

Table 2-2-1 Information of used soil-rock pairs

Station ID		Coordinates		--	Site Conditions	
Name	Code	Long.	Lat.	Distance (km)	*S* velocity (m/s)	V30 (m/s)
1	AOMH03	140.9896	41.234	4.10	530	653.7
	AOM006	140.9972	41.1976		100	264.8
2	CHBH20	140.0997	35.0882	3.04	1800	1909.1
	CHB020	140.1022	35.1155		150	134.4
3	ISKH04	136.7176	37.1902	4.16	440	443.5
	ISK006	136.6897	37.1602		260	344.0
4	YMGH01	131.5618	34.0494	3.22	1000	1387.7
	YMG013	131.5348	34.031		70	185.4
5	NGSH06	129.8625	32.6999	4.15	900	1421.1
	NGS010	129.8763	32.7353		150	371.6
6	GIFH20	137.2531	35.7991	0.84	460	809.9
	GIF010	137.245	35.8029		150	440.9
7	GIFH14	137.5174	36.2493	0.01	440	627.4
	GIF004	137.5174	36.2492		230	452.7
8	ISKH07	136.6357	36.515	3.07	440	440.0
	ISK010	136.6431	36.5419		110	388.2
9	SRCH10	142.0085	42.993	0.03	480	1026.8
	HKD123	142.0085	42.9933		110	627.1
10	MIE014	136.1687	34.0638	0.02	880	1009.4
	MIEH05	136.1689	34.0637		170	590.1

2.2.3 Ground-motion database

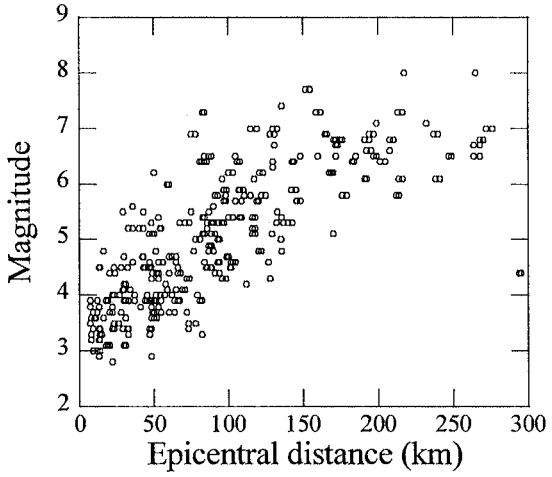

Fig.2-2-1 Magnitude versus epicentral distance

In order to obtain more general conclusions, all ground motions until May 2016, recorded on the 10 soil-rock pairs and also meeting the following characteristics, are selected from the K-NET, KiK-net. (1) Ground motions from same earthquake are recorded at both rock and nearby soil sites. (2) Ground motions with peak acceleration greater than 5gal. (3) Ground motions with Epicentral distance larger than 10 times of the distance between rock and nearby soil site (to reduce the path effect), and less than 300 km. Finally, a total of 1,020 earthquake time histories are selected. Fig.2-2-1 shows the distribution of magnitude and epicentral distance of the earthquake used in this study. It can be observed that, ground motion records with a wide range of magnitude and epicentral distance are selected. As earthquake with small magnitude can hardly be recorded at large epicentral distance, few such records are selected. Generally speaking, selected ground motion records are with reasonably balanced distribution with respect to magnitude and epicentral distance.

In addition, to remove long-period noise, baseline adjustment is applied to all records, and to eliminate effect of low-period noise, only the spectral ratios lager than 0.1s are used.

Moreover, as introduced above, for a linear soil profile subjected to vertically propagating shear waves, the FSR is constant, but RSRs are variable depending on the frequency content of rock site excitation [30,31]. Therefore, the relationship between RSR and FSR is also dependent on frequency content of rock site excitation, which is originally affected by magnitude and epicentral distance. To investigate the dependence on magnitude and epicentral distance, selected ground motions are

Table 2-2-2 Classification of accelerograms

Group	Magnitude	Epicentral distance
1	2.8～5.0	7～150
2	5.1～8.0	7～150
3	5.1～8.0	151～300

classified into three groups as shown Table 2-2-2. In the table, Group 1, 2 and 3, respectively, represent small earthquake with short distance, large earthquake with short distance, and large earthquake with long distance.

2.2.4 Results of statistical study

To compute spectral ratios, Fourier spectra and 5% damped response spectra for each earthquake at each site are computed. Fourier amplitudes are smoothed using the Parzen window function with band width equal to 0.3. And, the geometric mean of the two components, in EW and NS direction, of each earthquake are computed. Then, spectral ratios are computed for each earthquake at each nearby soil-rock pairs. To investigate the general relationship between RSRs and FSRs, the ratios for all earthquakes are averaged for each period at each soil-rock pairs, and mean value of RSRs and FSRs are compared. In addition, to explore the influence of magnitude and epricentral distance, the ratios for earthquakes in each group are averaged for each period at each soil-rock pairs.

Mean values of RSRs and FSRs, for period band from 0.1s to 10s, at the 10 soil-rock pairs are computed. For 6 of these soil-rock pairs, fundamental period can be observed obviously from spectral ratios, results for these soil-rock pairs are shown in Fig.2-2-2, and results for other 4 soil-rock pairs are shown in Fig.2-2-3. In these figures, horizontal coordinate is period, longitudinal coordinates is spectral ratio; and the thick line represents value of RSR, thin line represents value of FSR. From Fig. 2-2-2, the shape of RSR is found nearly consistent with the one of FSR. And, maximum value of FSRs and RSRs occur at about the same period, and the one of FSRs systematically exceed that of RSRs. These conclusions are consistent with those of previous studies [32, 33]. Moreover, values of RSR and FSR at periods larger and smaller than fundamental period are compared. Figs. 2-2-2 (a)-(e) shows that, at fundamental period, value of FSR systematically exceed that of RSR, but, as the period increase or decrease, value of RSR will exceed that of FSR at some period, and the shape of RSR is relatively gentler than that of FSR. In Fig. 2-2-2 (f), values of FSRs at any period are nearly equal with those of RSRs.

In addition, fundamental period obtained from RSR, T_R, and FSR, T_F, along with representative values of RSRs and FRSs at 0.1s, 2s and fundamental period are listed in Table 2-2-3. Fundamental periods obtained from RSRs can be seen nearly equal with those from FSRs. And the values of FSR at fundamental period exceed those of RSR for all sites. For most of the sites, values RSRs at 0.1s and 2s exceed those of FSR. All of these results support above conclusions.

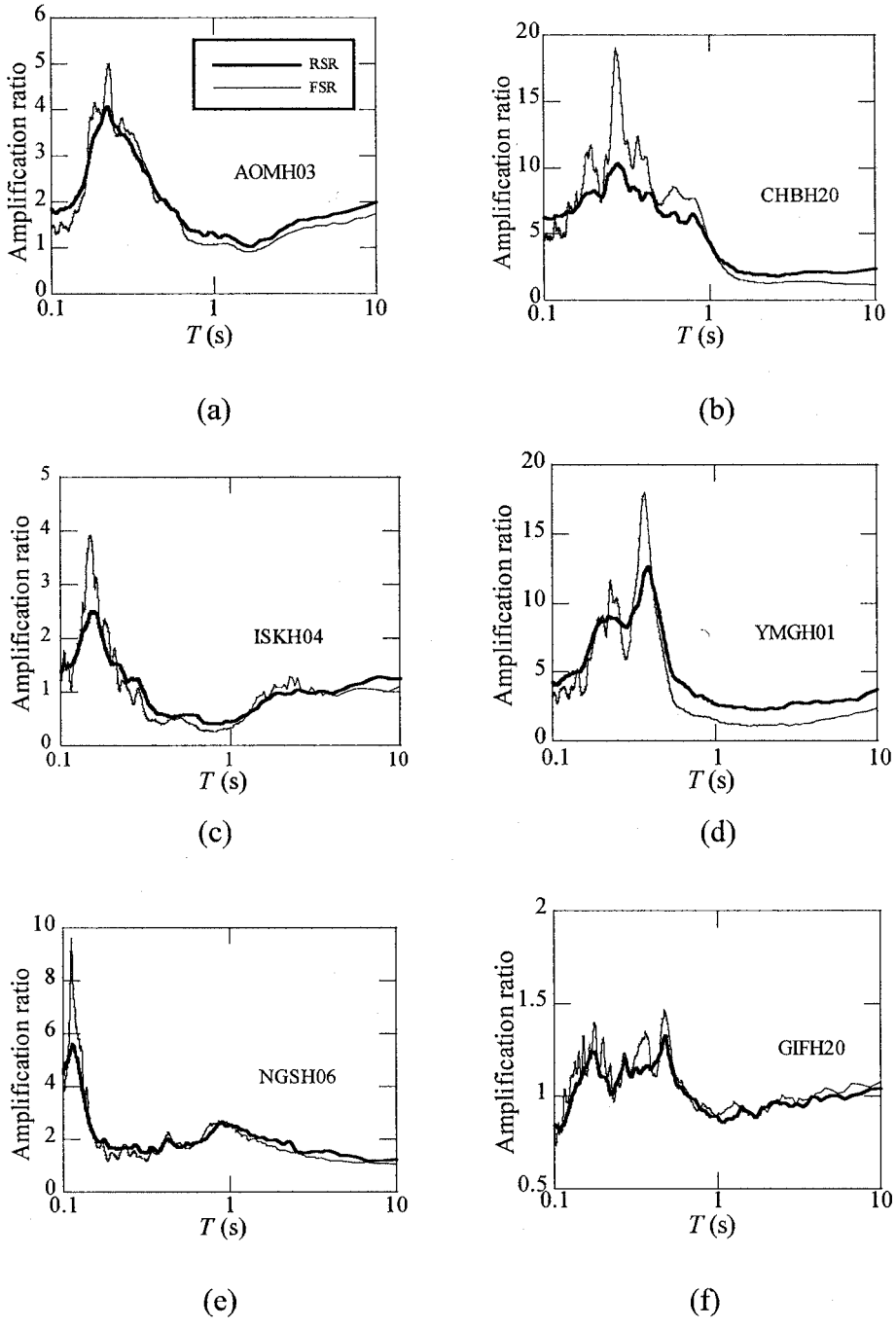

Fig.2-2-2 Comparison of mean values of RSRs and FSRs at the 6 soil-rock paris

Table 2-2-3 Results of the 6 soil-rock pairs shown in Fig.2-2-2

Name	Group	T_R (s)	T_F (s)	RSR (peak)	FSR (peak)	Ratio	RSR (0.1s)	FSR (0.1s)	Ratio	RSR (2 s)	FSR (2s)	Ratio
1	1	0.22	0.22	5.28	6.18	0.85	1.82	1.52	1.20	1.36	0.95	1.43
	2	0.20	0.23	3.69	4.45	0.83	1.77	1.45	1.22	1.05	0.99	1.06
	3	0.23	0.23	3.42	4.61	0.74	1.93	1.53	1.26	1.11	1.01	1.10
	Average	0.22	0.22	4.08	4.93	0.83	1.84	1.50	1.23	1.17	0.99	1.18
2	2	0.27	0.27	11.00	21.81	0.50	7.32	5.37	1.36	2.34	1.29	1.81
	3	0.26	0.28	9.82	17.7	0.55	5.13	3.36	1.53	1.59	1.39	1.14
	Average	0.28	0.27	10.33	18.98	0.54	6.22	4.36	1.43	1.96	1.34	1.46
3	1	0.16	0.16	3.25	4.66	0.70	1.78	1.30	1.37	0.83	1.02	0.81
	3	0.15	0.14	1.97	3.75	0.53	0.99	1.11	0.89	1.10	1.14	0.96
	Average	0.16	0.15	2.50	3.93	0.64	1.39	1.20	1.16	0.96	1.09	0.88
4	1	0.38	0.36	12.24	19.02	0.64	3.66	3.20	1.14	3.38	1.18	2.86
	2	0.38	0.37	12.46	18.47	0.67	4.78	3.24	1.48	1.86	1.25	1.49
	3	0.39	0.38	13.58	18.50	0.73	4.44	3.34	1.33	1.67	1.07	1.56
	Average	0.39	0.37	12.68	17.96	0.71	4.29	3.26	1.32	2.31	1.17	1.97
5	1	0.11	0.11	6.16	9.04	0.68	4.34	4.17	1.04	1.92	1.46	1.32
	2	0.10	0.11	5.11	10.25	0.50	4.83	4.15	1.16	1.84	1.66	1.11
	Average	0.11	0.11	5.61	9.59	0.58	4.59	4.16	1.10	1.88	1.56	1.21
6	1	0.46	0.46	1.20	1.40	0.86	0.75	0.73	1.03	0.96	0.99	0.97
	2	0.40	0.50	1.33	1.45	0.92	0.80	0.94	0.85	1.04	0.92	1.13
	3	0.48	0.47	1.47	1.66	0.89	0.97	0.90	1.08	0.83	0.84	0.99
	Average	0.47	0.47	1.33	1.47	0.90	0.84	0.86	0.98	0.94	0.91	1.03

Fig. 2-2-3 shows the spectral ratios without obvious fundamental peak. To investigate the reason why fundamental peak is not observed, shear wave velocity of surface layer and V_{30} of the 4 soil sites listed in Table 2-2-1 are analyzed. It is found that, although shear wave velocity of surface layer is small, V_{30} is large. This indicates, depth of soft surface layer is small and share wave velocity of lower soil layers are large, which lead the fundamental period of soil site smaller than 0.1s and can't be observed in the period band 0.1-10s.

Values of RSRs and FSRs at these 4 sites are also compared. Figs. 2-2-3 (a)-(c) shows that, values of RSRs and FSRs are nearly the same at any period and about equal to 1. The small value of spectral ratios is considered to be related with small contrast of V_{30} between soil and rock site. And, In Fig. 2-2-3 (d), as period increases, values of RSRs exceed those of FSRs, which is consistent with results shown in Figs.2-2-2 (a)-(e).

As introduced above, the relationship between RSR and FSR is dependent on frequency content of

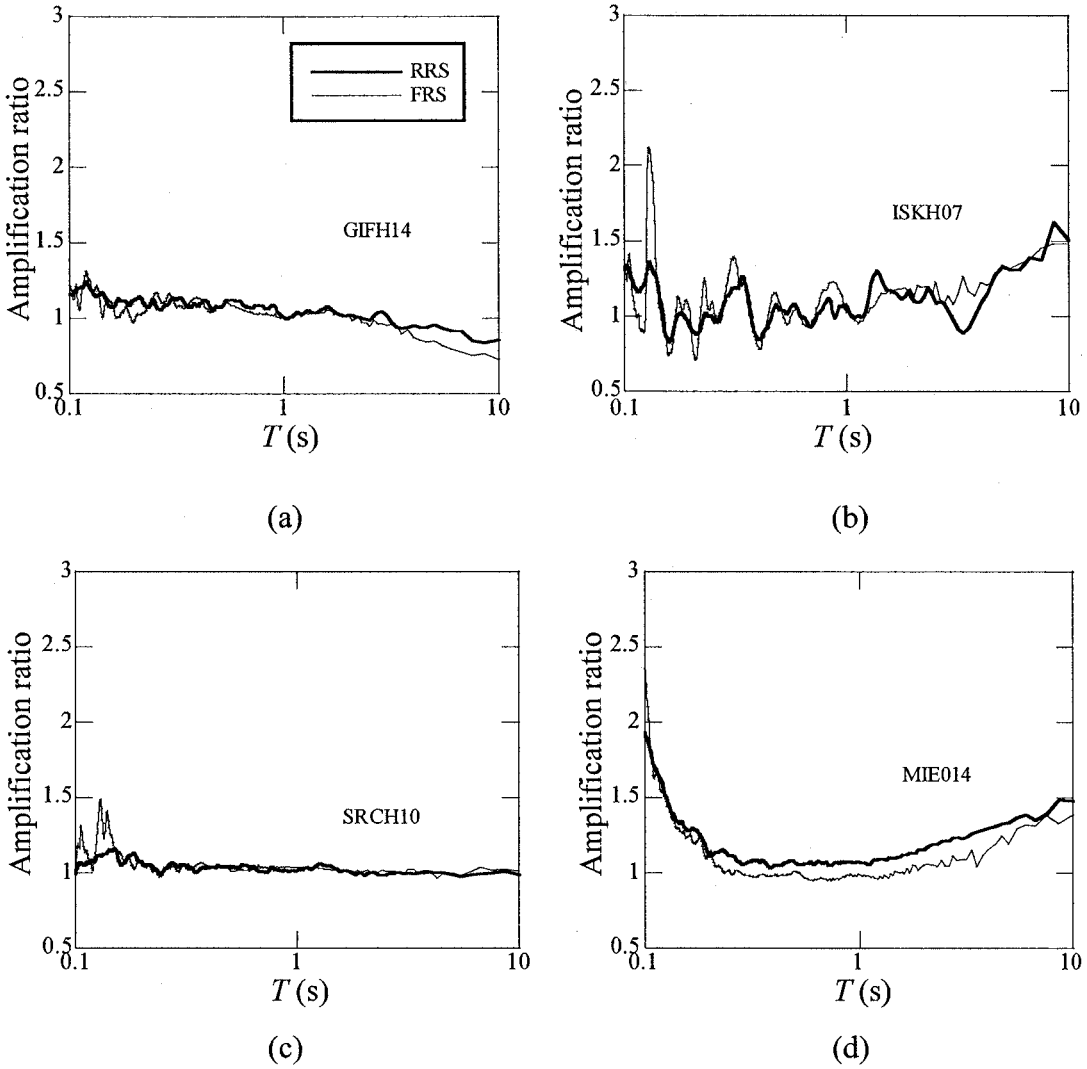

Fig.2-2-3 Comparison of mean value of RSRs and FSRs at the 4 soil-rock paris

rock site excitation. Frequency content of ground motion is affected by magnitude and distance. Thus, the relationship between RSR and FSR is dependent on magnitude and epicentral distance. To explore the dependence of the relationship on magnitude and epicentral distance, the ratios for earthquakes in each group shown in Table 2-2-2 are averaged for each period at each soil-rock pairs. Spectral ratios at number 1 rock-soil pair as representative results are shown in Fig. 2-2-4. Figs. 2-2-4 (a), (b) and (c) show, respectively, results for group 1, 2 and 3. It can be found that, at period much longer than fundamental period of soil site, difference between RSRs and FSRs decreases with increasing magnitude and epicentral distance. Besides, same with the observations above, the shape of RSR is nearly consistent with the one of FSR for each group.

In addition, values of RSRs and FRSs at 0.1s, 2s and fundamental period for each group, at the 6 soil-rock pairs in Fig.2-2-5, are computed and listed in Table 2-2-3; then, ratios between values of RSR against those of FSR are computed and shown in Fig. 2-2-5. Fig. 2-2-5 (a) indicates that, the

ratios at period equal to 2s approach 1 with increasing magnitude and epicentral distance, and the dependence on magnitude is more prominent. Dependence of ratios at period equal to fundamental period or 0.1s on magnitude and epicentral distance is not observed obviously, from Figs. 2-2-5 (b) and (c).

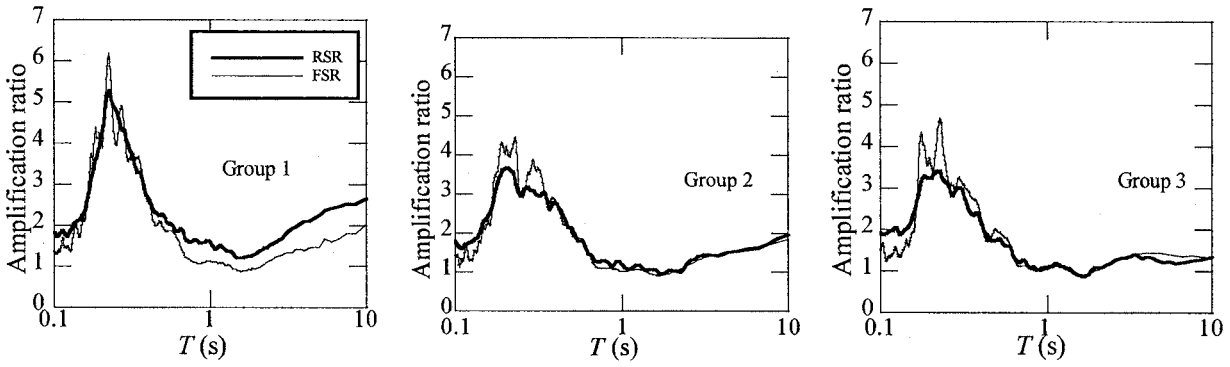

(a) (b) (c)

Fig.2-2-4 Comparison of spectral ratios at number 1 rock-soil pair for earthquake ground motions, (a) in group 1, (b) in group 2, (c) in group 3

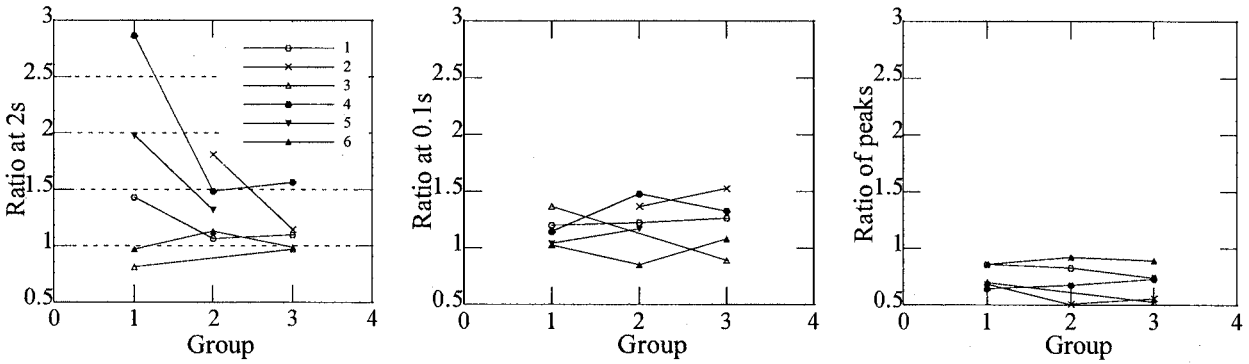

(a) (b) (c)

Fig.2-2-5 Ratios between values of RSR against those of FSR at, (a) period equaling to 2s, (b) period equaling to 0.1s, (c) the fundamental period

2.2.5 Conclusion

The Section 2.2 statistically investigates the relationship between RSR and FSR, using 1020 actual ground motions recorded on 10 nearby soil-rock pairs. The content of this section and the main conclusions are summarized as follows:

(1) Mean values of FSR and RSR for each soil-rock pairs are compared. It is found that, (1) the shape of RSR is nearly consistent with the one of FSR, the shape of RSR is relatively gentler; (2)

maximum value of FSRs and RSRs occur at about the same period, and the one of FSRs systematically exceed that of RSRs.

(2) The dependence of the relationship on magnitude and epicentral distance is examined. It is found that, at period band longer than the site fundamental period, difference between RSRs and FSRs decreases as magnitude and epicentral distance increase; and at period band equaling or shorter than the site fundamental period, dependence of the relationship on magnitude and epicentral distance is not obvious.

2.3 Comparison of Fourier and response spectral ratio based on RVT

2.3.1 Introduction

For the statistical analysis in Section 2.2, Fourier amplitude is smoothed using window functions for clear observation of frequency characteristic, as the Fourier amplitude varies according to used window function and it's band width, amplitude relationship between RSR and FSR also varies according to used window function and it's band width. Therefore, it is difficult to compare amplitudes of RSR and FSR by the statistical analysis of recorded ground motions.

In this section, theoretical analysis based on random vibration theory (RVT) is applied to investigate the physical relationships existing between RSR and FSR. This section is organized as follows. Firstly, the RVT is introduced briefly in section 2.3.2. In section 2.3.3, an equation expressing relationship between the RSR and FSR is derived based on the RVT. Subsequently, according to the derived equation, some systemic relationship between RSR and FSR are clarified. In addition, as the RSR vary depending on bedrock motion and FSR do not, the relationship between the RSR and FSR is inferred also dependent on rock motion. The dependence of the relationship on bedrock motion is investigated, in section 2.3.4.

2.3.2 Random vibration theory

The basis of the RVT is that the peak of a signal is the product of its root mean square (rms) value and an estimated peak factor (*pf*). Applying the RVT to an acceleration-time history results in:

$$a_{\max} = pfa_{rms} \tag{2-3-1}$$

in which $a_{\max}$ is peak acceleration. a_{rms} is rms acceleration computed using Parseval's theorem which states that the integral of the square of a motion in the time domain is equal to the integral of its square in the frequency domain [36].

$$a_{rms} = \sqrt{\frac{1}{D}\int_0^D |a(t)|^2 dt} = \sqrt{\frac{1}{D\pi}\int_0^\infty |A(\omega)|^2 d\omega} = \sqrt{\frac{m_0'}{D}} \tag{2-3-2}$$

in which $A(\omega)$ is Fourier amplitude spectrum (FAS) at frequency ω and m_0' is the zeroth-order spectral moment of the FAS. The nth order spectral moment of the FAS is defined by

$$m_n' = \frac{1}{\pi}\int_0^\infty (\omega)^n |A(\omega)|^2 d\omega \tag{2-3-3}$$

D represents duration of the signal. For an RVT analysis where the goal is to predict peak ground acceleration, D is taken as the duration of the ground motion, D_{gm}; when the goal is to predict response spectrum acceleration, D is taken as the duration of the oscillator response, D_{rs}. As the duration is increased due to the response of the oscillator, D_{rs} is larger than D_{gm}. And, many equations have been developed to predict D_{rs} according to D_{gm} [37-40].

The expected value of the peak factor ($\overline{pf}$) is commonly used in RVT analysis. Many equations for $\overline{pf}$ have been proposed [41-43]. Among these equations, the one by Cartwright and Longuet-Higgins (1956) has been used commonly in engineering seismology and site-response applications. Following the assumption that the peaks of a signal are independent and follow a Poisson process, Cartwright and Longuet-Higgins (1956) [41] proposed that the expected value of the peak factor can be estimated using

$$\overline{pf} = \frac{a_{\max}}{a_{rms}} = \sqrt{2}\int_0^\infty \left\{1 - [1 - \xi e^{-\eta^2}]^{N_e}\right\} d\eta \tag{2-3-4}$$

where ξ is a parameter to measure the bandwidth of the Fourier spectrum, expressed as:

$$\xi = \frac{m_2'}{\sqrt{m_0' m_4'}} \tag{2-3-5}$$

N_e represents the number of extrema, estimated by:

$$N_e = 2 f_e D = \frac{1}{\pi}\sqrt{\frac{m_4'}{m_2'}} D \tag{2-3-6}$$

and f_e represents rates of extrema.

Eq. (3-3-4) has been incorporated into most RVT procedure in engineering seismology [44] and site response [45]. For large values of N_e, Eq. (3-3-4) can be simplified as [41]:

$$\overline{pf} = [2\ln(\xi \bullet N_e)]^{1/2} + \frac{0.5772}{[2\ln(\xi \bullet N_e)]^{1/2}} \tag{2-3-7}$$

Eq. (3-3-4) can also be rewritten as:

$$\overline{pf} = [2\ln(N_z)]^{1/2} + \frac{0.5772}{[2\ln(N_z)]^{1/2}} \tag{2-3-8}$$

where N_z represents number of zero crossings, estimated by:

$$N_z = 2 f_z D = \frac{1}{\pi}\sqrt{\frac{m_2'}{m_0'}} D \tag{2-3-9}$$

and f_z represents rates of zero crossings.

Davenport [42] also derived an equation for $\overline{pf}$, which is same with the Eq. (2-3-8). Actually, this equation is a good approximation to Eq. (2-3-4) even for small values of N_z [36], thus it is widely used in engineering seismology [47-49]. For simplify, the Eq. (2-3-8) is also used for estimation of peak factor in this section. In addition, many other studies [50, 51] also proposed other peak factor models, and every peak factor models have its strong point and available range. This study doesn't intent to argue which one is better, and just applies a generally used one to investigate the

relationship between RSR and FSR.

2.3.3 Relationship between RSR and FSR

Equation for relationship between RSR and FSR

To investigate the relationship between RSR and FSR, equation for RSR expressed in term of FSR is derived based on the RVT in this section. For this purpose, a soil site subjecting to a seismic motion at outcrop bedrock is considered, and FAS of the bedrock motion equals to $A_B(\omega)$. Then, the FAS of seismic motion at ground surface, $A_S(\omega)$, can be obtained as:

$$A_S(\omega) = A_B(\omega)T(\omega) \tag{2-3-10}$$

where $T(\omega)$ is the site transfer function representing Fourier spectral ratios of ground motions at ground surface and outcrop bedrock.

Then, to calculate the ratio of response spectrum at ground surface against the one on bedrock, the response spectra should be calculated firstly. Based on the RVT, response spectrum (peak value of the oscillator response) at bedrock, $R_B(\overline{\omega}, h_0)$, can be calculated by:

$$R_B(\overline{\omega}, h_0) = \overline{pf}_B \sqrt{\frac{1}{D_B \pi} \int_0^\infty \left| AR_B(\omega, \overline{\omega}, h_0) \right|^2 d\omega} \tag{2-3-11}$$

where $\overline{pf}_B$ and D_B, respectively, are peak factor and duration of the oscillator response corresponding to the bedrock motion. And, $AR_B(\omega, \overline{\omega}, h_0)$ is FAS of the oscillator response of the bedrock motion given by:

$$AR_B(\omega, \overline{\omega}, h_0) = A_B(\omega) \bullet H_0(\omega, \overline{\omega}, h_0) \tag{2-3-12}$$

where $H_0(\omega, \overline{\omega}, h_0)$ is the transfer function of the oscillator that has fundamental frequency and damping ratio equaling to $\overline{\omega}$ and h_0, respectively. The transfer function of acceleration can be expressed as:

$$H_0(\omega, \overline{\omega}, h_0) = \frac{\sqrt{(2h_o\omega\overline{\omega})^2 + \omega^4}}{\sqrt{(2h_o\omega\overline{\omega})^2 + (\omega^2 - \overline{\omega}^2)^2}} \tag{2-3-13}$$

Similarly, response spectrum at ground surface can be calculated by:

$$R_S(\overline{\omega}, h_0) = \overline{pf}_S \sqrt{\frac{1}{D_S \pi} \int_0^\infty \left| AR_S(\omega, \overline{\omega}, h_0) \right|^2 d\omega} \tag{2-3-14}$$

where $\overline{pf}_S$ and D_S, respectively, are peak factor and duration of the oscillator response corresponding to the surface ground motion. And, $AR_S(\omega, \overline{\omega}, h_0)$ is FAS of the oscillator response of the ground

surface motion given by:

$$AR_S(\omega,\overline{\omega},h_0)=A_S(\omega)H_0(\omega,\overline{\omega},h_0) \tag{2-3-15}$$

Then, using Eqs. (2-3-11) and (2-3-14), the RSR can be calculated as:

$$RSR(\overline{\omega},h_0)=\frac{R_S(\overline{\omega},h_0)}{R_B(\overline{\omega},h_0)}=\frac{\overline{pf}_S/\sqrt{D_S}\sqrt{\int_0^\infty A_B{}^2(\omega)H_0{}^2(\omega,\overline{\omega},h_0)T^2(\omega)d\omega}}{\overline{pf}_B/\sqrt{D_B}\sqrt{\int_0^\infty A_B{}^2(\omega)H_0{}^2(\omega,\overline{\omega},h_0)d\omega}} \tag{2-3-16}$$

By defining

$$W(\omega,\overline{\omega})=A_B{}^2(\omega)H_0{}^2(\omega,\overline{\omega},h_0) \tag{2-3-17}$$

Eq. (2-3-16) can be rewritten as:

$$RSR^2(\overline{\omega},h_0)=\frac{\overline{pf}_S^2/D_S}{\overline{pf}_B^2/D_B}\times\frac{\int_0^\infty W(\omega,\overline{\omega})T^2(\omega)d\omega}{\int_0^\infty W(\omega,\overline{\omega})d\omega} \tag{2-3-18}$$

Eq. (2-3-18) expresses the relationship between RSR and FSR. In essence, Eq. (2-3-18) also represents RVT site-response analysis, which has been introduced in many studies [45]. The accuracy of the RVT site-response analysis has been discussed in many studies [52, 53], and is found affected by neglecting duration change of the oscillator response generated by the site response as well as choice of peak factor models. In Eq. (2-3-18), the duration change is taken into account. And, if ideal peak factor model is used, Eq. (2-3-18) is theoretically exact.

***Systemic relationships based on Eq.* (2-3-18)**

According to Eq. (2-3-18), the relationship between RSR and FSR is discussed in this section. Eq. (2-3-18) consists of two terms, which will be discussed in the following two subsections respectively.

The first term

The first term in Eq. (2-3-18) represents change rate about peak factor and duration of oscillator response generated by site response. The duration of oscillator response has been found is extended by site response [52, 53], i.e. D_S is longer than D_B. To further investigate change regulation of the whole $\overline{pf}^2/D$ by the site response; according to Eq. (2-3-8), the first term is obtained as:

$$\frac{\overline{pf}_S^2/D_S}{\overline{pf}_B^2/D_B}=\frac{(2\ln(N_{Sz})+1.1544+\frac{1}{2\ln(N_{Sz})})D_B}{(2\ln(N_{Bz})+1.1544+\frac{1}{2\ln(N_{Bz})})D_S} \tag{2-3-19}$$

where N_{Sz} and N_{Bz} represent the number of zero crossings of the oscillator response corresponding to the surface ground motion and bedrock motion, respectively. Then, submitting Eq. (2-3-9) into Eq. (2-3-19) result in:

$$\frac{\overline{pf}_S^2/D_S}{\overline{pf}_B^2/D_B} = \frac{(2\ln(2f_{Sz}D_S)+1.1544+\frac{1}{2\ln(2f_{Sz}D_S)})D_B}{(2\ln(2f_{Bz}D_B)+1.1544+\frac{1}{2\ln(2f_{Bz}D_B)})D_S} \tag{2-3-20}$$

where f_{Sz} and f_{Bz} represent rates of zero crossings of the oscillator response corresponding to the surface ground motion and bedrock motion, respectively. Here, change of the rates of zero crossings by the site response is considered has little effect on values of the first term in Eq.(2-3-18) , thus $f_{Sz} = f_{Bz}$ is assumed,

$$\frac{\overline{pf}_S^2/D_S}{\overline{pf}_B^2/D_B} = \frac{2\ln(rN_{Bz})+1.1544+\frac{1}{2\ln(rN_{Bz})}}{r(2\ln(N_{Bz})+1.1544+\frac{1}{2\ln(N_{Bz})})} \tag{2-3-21}$$

where $r = D_S/D_B$.

If only the first item of Eq. (2-3-8) is considered, Eq. (2-3-21) can be further simplified as:

$$\frac{\overline{pf}_S^2/D_S}{\overline{pf}_B^2/D_B} = \frac{1}{r}\log_{N_{Bz}}^{N_{Bz}r} \tag{2-3-22}$$

Fig. 2-3-1 plots values calculated by Eqs. (2-3-21) and (2-3-22) versus N_{Bz} for five values of r. An r value of 1.1 represents that the duration of the oscillator response is extended by 110% generated by the site response. It can be seen that for each considered value of r, results by Eq. (2-3-21) agree very well with those by Eq.(2-3-22) for N_{Bz} value larger than 40. In addition, the Fig. 2-3-1 also indicates that, whichever equation is used, values of the first term in Eq. (2-3-18) are always less than 1. Therefore, it can be known that, as duration of the oscillator response is extended by the site response, the whole $\overline{pf}^2/D$ is decreased, which leads the values of first term in Eq. (2-3-18) be always smaller than 1. It can also be found values of the first term decrease along with increasing of r and are not affected obviously by N_{Bz}.

Recent studies [53] find that the use of the Vanmarcke (1975) peak factor model [50] rather than the Cartwright and Longuet-Higgins (1956) peak factor model predicts RSR in better agreement with those predicted by time-history analysis. Eq. (2-3-18) indicates that the peak factor only affect the first term. Thus, it may be doubted that if the Vanmarcke peak factor model is used the conclusions about values of the first term in Eq. (2-3-18) derived above will not be true. Actually, values of RSR using either Cartwright and Longuet-Higgins (1956) peak factor model or Vanmarcke peak factor model agree very well with those by time-history analysis at most period band except near site fundamental period [52,53]. Even, near the site fundamental period, the use of the Vanmarcke (1975)

peak factor mode predicts smaller values of RSR and thus smaller values of the first term than by using the Cartwright and Longuet-Higgins (1956) peak factor model [53]. Therefore, whichever peak factor model is used, the conclusion that values of first term are always less than 1 will not change.

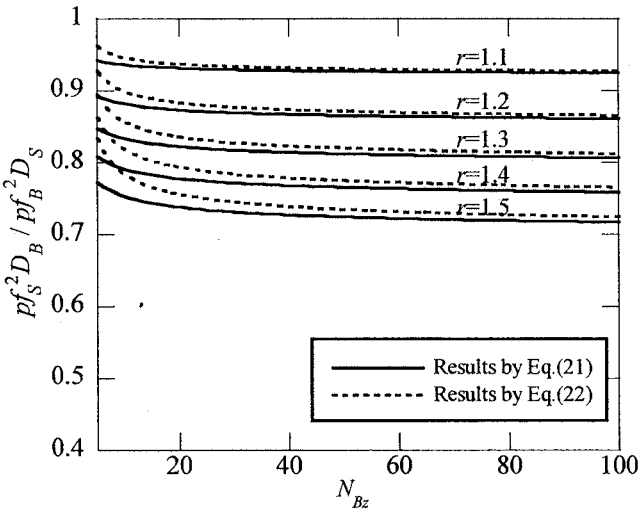

Fig.2-3-1 Values of the first term in Eq. (2-3-18)

The second term

The second term in Eq. (2-3-18) represents a weighted average of the square of FSR, $T^2(\omega)$, and the square of FAS of the oscillator response corresponding to bedrock motion, $W(\omega,\overline{\omega})$, acts as a weight function. This means that value of the second term at any frequency $\overline{\omega}$ equals to the weighted average of all values of $T^2(\omega)$ at frequencies from 0 to ∞ (Hz). As weighted average of some values can never larger than their maximum value, and smaller than their minimum value. Thus, every values of the second term are smaller than the maximum value of $T^2(\omega)$, and larger than the minimum value of $T^2(\omega)$.

For value of the second term at frequency $\overline{\omega}$, the weight function is product of the square of an oscillator transfer function, $H_0{}^2(\omega,\overline{\omega},h_0)$ with the square of FAS of the bedrock motion, $A_B{}^2(\omega)$. It should be noted that the fundamental frequency of the oscillator also equals to $\overline{\omega}$. As the oscillator transfer function acting as a narrow-band filter has a peak at fundamental frequency. Thus, generally the weighted function $W(\omega,\overline{\omega})$ is also narrow-band and has a peak at fundamental frequency $\overline{\omega}$. Fig.2-3-2 shows three examples of the weighted function. Here, FAS of the bedrock motion is generated based on the theoretical seismological model by Boore [36]. The key model parameters are presented in Table 2-3-1. The magnitude, M, and closest distance, R, are hypothesized equal 5 and 10 (km), respectively. Two oscillator frequencies, 10 Hz and 20 Hz, and two oscillator damping, 0.05 and 0.01, are considered in these examples. It is found, in every cases, weighted function is narrow-band and has a peak at the oscillator frequency. This means that, for estimation of value of the second

term at frequency $\overline{\omega}$, the value equals to the weighted average of all values of $T^2(\omega)$ at frequencies from 0 to ∞ (Hz); and the weight for value of $T^2(\omega)$ at frequency $\overline{\omega}$ is generally much bigger than that of other values. Thus, value of the second term at frequency $\overline{\omega}$ is mostly dominated by values of $T^2(\omega)$ at frequency $\overline{\omega}$, and is always near the value of $T^2(\omega)$ at frequency $\overline{\omega}$. Therefore, shape of second term is typically also similar with that of $T^2(\omega)$. In addition, as shown in Fig.2-3-2, the smaller the oscillator damping is, the weight for value of $T^2(\omega)$ at frequency $\overline{\omega}$ is bigger, thus the value of the second term at frequency $\overline{\omega}$ will agree better with value of $T^2(\omega)$ at frequency $\overline{\omega}$. Theoretically, when the oscillator damping approaches 0, values of the second term and $T^2(\omega)$ will be exactly the same.

Fig.2-3-3 shows two examples about comparison of FSR with root of the second term in Eq. (2-3-18). Here, a simple soil model, a single-layer soil profile on bedrock, is considered. The fundamental period of the soil profile equals to 0.2s. The soil damping ratio equals to 0.1. And, the impedance ratio of the soil against the bedrock equals 0.2. The oscillator damping in Figs.2-3-3 (a) and (b) equal to 0.05 and 0.01, respectively. It is found, for both the two cases, the shape of FSR is similar with that of root of the second term, and their maximum value occur at same period, site fundamental period. In addition, as shown in Fig.2-3-3 (b), for the case that oscillator damping is smaller, values of root of the second term agree better with value of FSR. It also can be noted that, for the both two cases, value of FSR at fundamental period are bigger than that of root of the second term, which support the conclusion in the first paragraph of this section.

For a single-layer soil profile on bedrock, maximum value of FSR occurs at site fundamental period. Generally, even for multi-layer soil profiles on bedrock, maximum value of FSR also occurs at site fundamental period. Therefore, for multi-layer soil profiles on bedrock, maximum values of the second term in Eq. (2-3-18) and the $T^2(\omega)$ also generally occur at site fundamental period. As introduced above, every values of the second term are smaller than the maximum value of $T^2(\omega)$, thus, value of second term at fundamental period is smaller than that of $T^2(\omega)$.

Table 2-3-1 Parameters used in development of FAS of rock motion

Parameter	Value
Source spectrum	Brune ω-squared point source
Stress drop $\Delta\sigma$ (bar)	100
Site diminution k (s)	0.04
Density of crust ρ (g/ cm^3)	2.8
Shear wave velocity of crust β (km/s)	3.7
Crust amplification	Boor and Joyner 1997

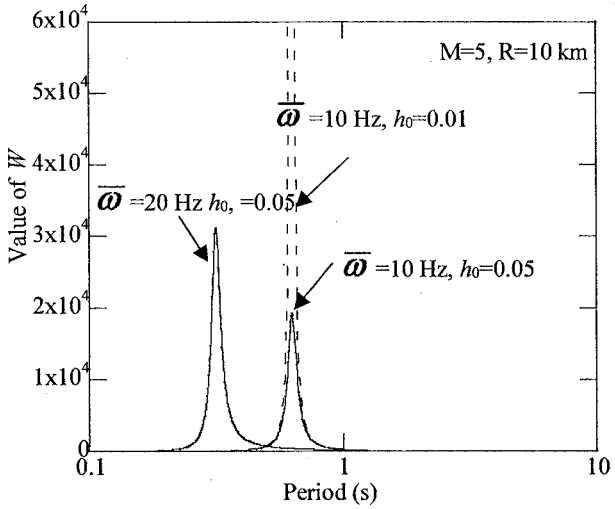

Fig.2-3-2 Three examples of the weight function $W(\omega,\overline{\omega})$

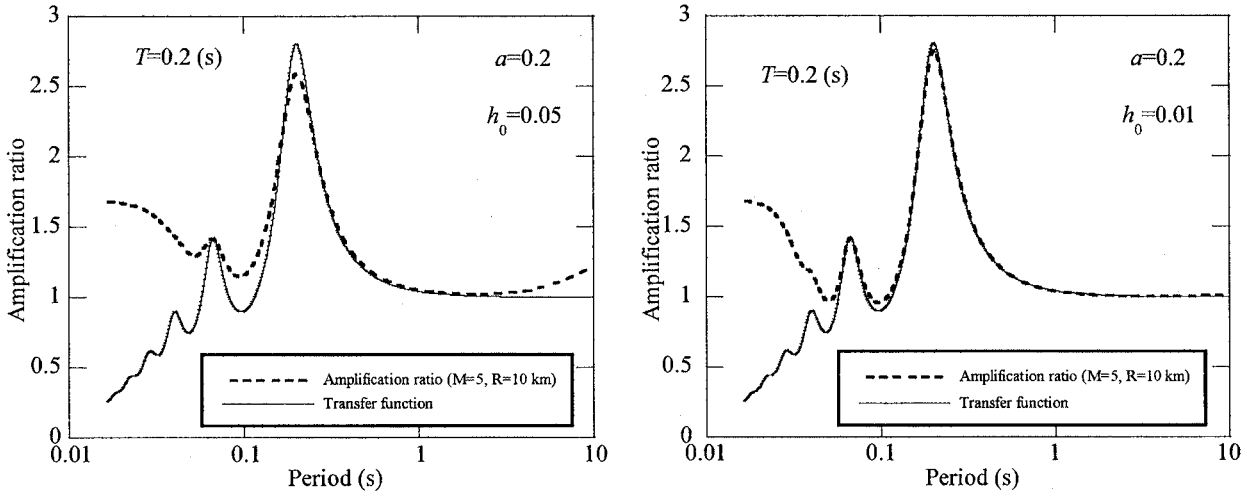

(a) (b)

Fig. 2-3-3 Comparison of site transfer function with root of the second term in Eq. (2-3-18)

Systemic relationships between RSR and FSR

According to conclusions summarized in the above two sections, systemic relationships between RSR and FSR are discussed in this section.

Firstly, relationship about global shape between RSR and FSR is discussed. The shape of the second term in Eq. (2-3-18) is kwon similar with that of square of FSR. In addition, values of the first term in Eq. (2-3-18) are not affected obviously by N_{Bz}. According to Eq. (2-3-9), the N_{Bz} is determined by spectral moments and duration of oscillator response corresponding to bedrock motion. Although for values of RSR at different frequencies, the oscillator transfer function, $H_0^2(\omega,\overline{\omega},h_0)$, in turn,

N_{Bz} are different; values of the first term don't vary appreciably with frequency. Therefore, global shape of RSR also should be similar with that of FSR. And, maximum values of FSR and RSR typically happened at same frequency.

In addition, it is indicated previously that maximum values of the second term in Eq. (2-3-18) and the $T^2(\omega)$ generally occur at site fundamental period, and value of second term at fundamental period is smaller than that of $T^2(\omega)$. And, values of the first term in Eq. (2-3-18) are always less than 1. Therefore, maximum values of RSR and FSR always occur at same period, i.e. site fundamental period, and the one of RSR is smaller.

Fig.2-3-4 shows an example of comparison between RSR and FSR. The input bedrock motion used previously is used here. And the ground motion duration, D_{gm}, is calculated by $D_{gm}=1/f_C+0.05R$ [45], where fc is the corner frequency for the source spectrum [44]. The simple soil model, a single-layer soil profile on bedrock, is used. It can be noted that, results in Fig. 2-3-4 support all conclusions summarized above.

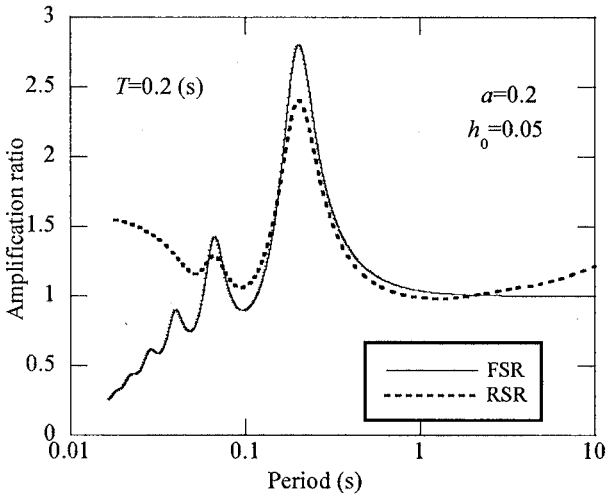

Fig. 2-3-4 Comparison between RSR with FSR

2.3.4 The dependence of the relationship on bedrock motion

For a linear certain site, FSR known as site transfer function is totally dependent on the material properties. But, as shown in Eq.(2-3-18), RSR depends on not only the material properties represented by the site transfer function, $T(\omega)$, but also input motion at bedrock reflected in the weight function, $W(\omega,\overline{\omega})$, the peak factor, $\overline{pf}$, and the duration, D. Thus, for a certain site, relationship between RSR and FSR also must be dependent on the bedrock motion. In this section, the dependence of the relationship on bedrock motion is discussed.

Although the bedrock motion can affect the first term in Eq. (2-3-18) by affecting N_{Bz} according to Eqs. (2-3-21), (2-3-12) and (2-3-9), values of the first term do not vary obviously along with N_{Bz} as introduced above. Thus, bedrock motion has little influence on the first term. As to the second term in Eq. (2-3-18), bedrock motion affect it by changing the weight function, $W(\omega, \overline{\omega})$ according to Eq. (2-3-17). As results of weighted average are strongly dependent on the weight function, thus value of the second term can be significantly affected by bedrock motion. Based on the two reasons, the dependence of RSR on bedrock motion can be known is mainly dominated by the second term.

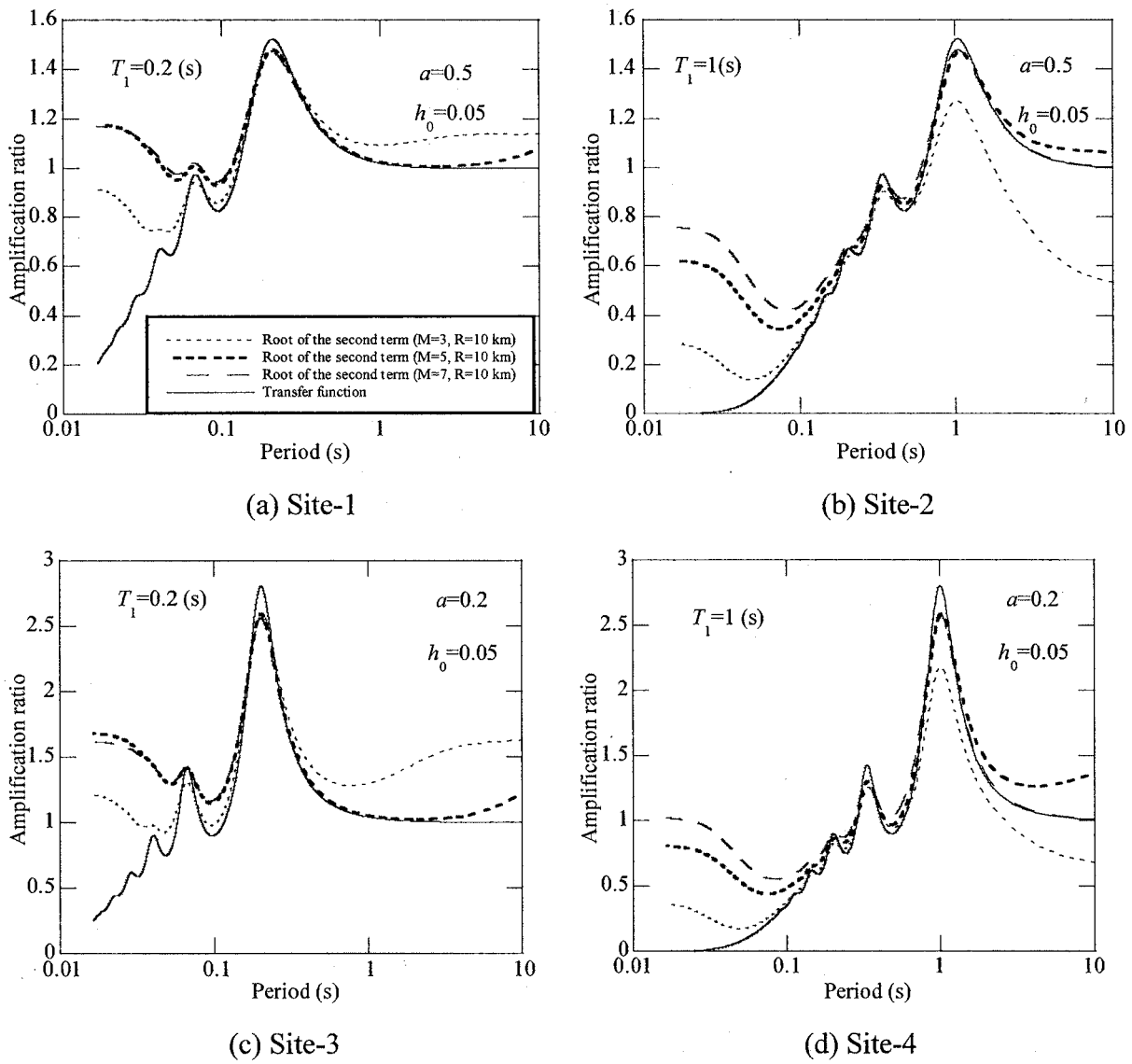

Fig. 2-3-5 Variation of the second term in Eq. (2-3-18) depending on the magnitude

In order to investigate change rule of relationship between RSR and FSR according to bedrock motion, some example calculation are conducted. Here, the simple soil model, single-layer soil profile on bedrock, is used. And, four sites with different fundamental periods, T_1, and impedance ratio

between soil and bedrock, a, are considered. Six bedrock motions with different magnitude and distance are generated based on the theoretical seismological model introduced above. In order to investigate the effects of magnitude, three levels of bedrock motion with magnitude equaling to 3, 5 and 7, and the closest distance, R, equaling 10 km are generated. And to investigate the effects of closest distance, R, three levels of bedrock motion with the distance equaling to 10km, 40km and 160km, and the magnitude equaling 10 km are generated. As the dependence of RSR on rock motion is mainly dominated by the second term, thus only the second term is considered here. For every considered sites under the three levels of bedrock motions, values of root of the second term are calculated using Eq. (2-3-18), and results are presented in Figs. 2-3-5 and 2-3-6. For the purpose of comparison with the FSR, FSRs of every considered sites are also presented in Figs. 2-3-5 and 2-3-6.

It can be noted that, for all the four sites, values of root of the second term vary depending on bedrock motion, the variation law is dependent on periods and estimated sites. Around the period band smaller than site fundamental period, the values of root of the second term for every levels of input bedrock motions are all lager than those of FSR, and tend to increase along with increasing of magnitude. Around the period band lager than site fundamental period, the values of root of the second term may be larger or smaller than that of FRS depending on input bedrock motion, but the values approach to those of FSR along with increasing of magnitude. Near the site fundamental period, values of root of the second term are smaller than those of FSR for all sites and every levels of input motions, which agree with the conclusion in section 2.3.3. And the variation degree depending on input motion is smaller for sites with small fundamental period, like Site-1 and Site-3, than those of sites with long fundamental period, like Site-2 and Site-4. The variation degree of root of the second term depending on closet distance (Fig.2-3-6) is obviously smaller than that depending on the magnitude (Fig.2-3-5).

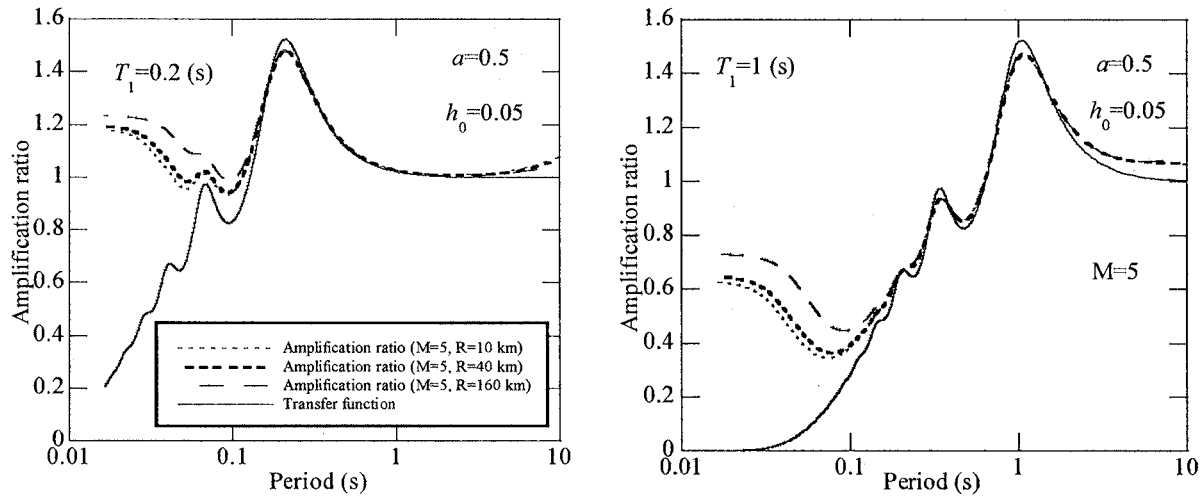

(a) Site-1 (b) Site-2

Fig. 2-3-6 Variation of the second term in Eq. (2-3-18) depending on the closest distance

In order to investigate the reason for dependence of the second term on input motions, values of the weight function $W(\omega,\bar{\omega})$ corresponding to the three levels of input motions used in Fig.2-3-5 are calculated, and some represented results are shown in Fig.2-3-7. It can be noted that, the values at large period band increase as the magnitude increase; contrary, the values at small period band decrease as the magnitude increase. The reason is because that, long-period contents of the input motion increases with increasing of magnitude. As the second term is calculated by weighted averaging the FSR, and the weight function is affected by input motions, thus the second term is dependent on input motions.

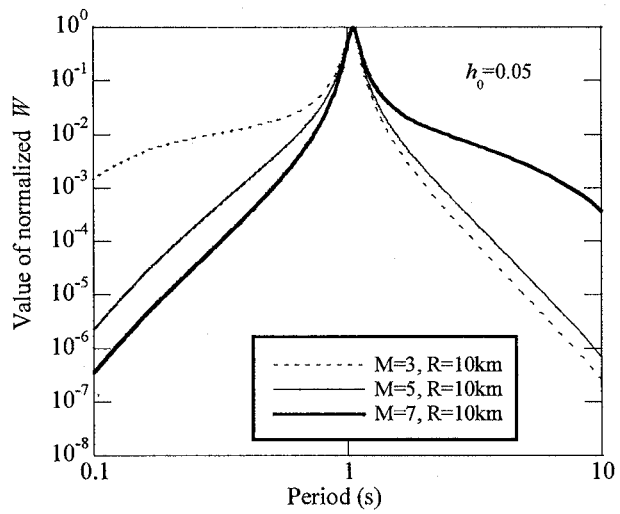

Fig. 2-3-7 Dependence of the weight function on bedrock motion

2.3.5 Conclusion

This section theoretically investigates the relationship between RSR and FSR based on the RVT. The content of this section and the main conclusions are summarized as follows:

(1) An equation expressing the relationship between the RSR and the FSR is derived based on the RVT.

(2) According to the derived equation, the relationship between the RSR and the FSR is investigated. It is found that, the shape of RSR is nearly consistent with the one of FSR, and maximum value of FSRs and RSRs occur at about the same period; the maximum value of FSRs is found systematically exceed that of RSRs, and the shape of RSR is relatively gentler.

(3) The dependence of the relationship on magnitude and epicentral distance is examined using several examples. It is found that, at period band longer than the site's fundamental period, difference between RSRs and FSRs decreases with increasing magnitude and epicentral distance.

2.4 Construction of site amplification function

As the seismic load for structural design is commonly given in the form of response spectrum, site effects are typically characterized as ratio of response spectrum at ground surface against the one specified at outcrop bedrock in seismic codes. In this section, a simple function for estimation of the response spectral ratio (RSR) is proposed. The equation for RSR is called site amplification function in this study.

In order to construct the function for the RSR, a single-layer soil profile on bedrock, is considered. But as introduced in section 2.2, even for such a simple soil model, there is not a closed form equation for the RSR in theory. To obtain the RSR, site response analysis has to be conducted in frequency or time-history domain. Analyses in sections 2.2 and 2.3 suggest that, (1) the shape of RSR is nearly consistent with the one of Fourier spectral ratio (FSR), (2) maximum value of FSRs and RSRs occur at about the same period, and the one of FSRs systematically exceed that of RSRs, (3) values of RSRs are nearly same with those of FSRs at period band longer than the site's fundamental period, especially for earthquake with large magnitude and long epicentral distance. Therefore, it is conservative to construct the function for the RSR using the FSR for most period bands.

The simple function for the RSR is constructed to envelope the transfer function of the simple soil model. Three critical point: first peak value at fundamental period, second peak value at second natural period, and the minimum value between the two peaks are used to control the function, as depicted in Fig.2-4-1. The equation for the RSR is expressed as:

$$Gs = \begin{cases} Gs_0 + \dfrac{Gs_2 - Gs_0}{T_2} T & T \le T_2 \\ Gs_2 & T_2 < T \le T_{1/2} \\ \dfrac{Gs_1 - Gs_2}{0.9T_1 - T_{1/2}} (T - T_{1/2}) + Gs_2 & T_{1/2} < T \le 0.9T_1 \\ Gs_1 & 0.9T_1 < T \le 1.1T_1 \\ \dfrac{Gs_1 - 1}{\dfrac{1}{1.1T_1} - 0.1} \left(\dfrac{1}{T} - \dfrac{1}{1.1T_1}\right) + Gs_1 & 1.1T_1 < T \end{cases} \quad (2\text{-}4\text{-}1)$$

where T_2 ($=T_1/3$) and Gs_2 are, respectively, the second natural period and corresponding peak value. Gs_2 can be estimated approximately by:

$$Gs_2 = \frac{1}{4.71h + a_G} \quad (2\text{-}4\text{-}2)$$

$T_{1/2}$ is the period corresponding to minimum value between first and second peak, as shown in Fig. 2-4-1. To obtain an equation for the $T_{1/2}$, the transfer function of the linear single-layer soil profile on bedrock is calculated and expressed as:

$$T(\omega) = \frac{1}{\cos A + ia \sin A} \tag{2-4-3}$$

where

$$A = \frac{\omega T}{4} \tag{2-4-4}$$

It can be noted from Eq. (2-4-4), when $A=n\pi$, value of the transfer function is minimum, thus $T_{1/2}$ can be obtained as:

$$T_{1/2} = \frac{T_1}{2} \tag{2-4-5}$$

As maximum values of FSRs and RSRs occur at about the same period, and the one of FSRs systematically exceed that of RSRs, thus using the peaks at natural periods to construct the amplification function Gs, is conservative for seismic design. In addition, for conservation in seismic design, the values of Gs are defined equal Gs_2 at period $T_{1\text{-}2}$ and not less than 1 at periods band, $T< T_2$.

Simple functions for estimation of the RSR have also been developed in the Japanese seismic code [20] and many studies [54]. The biggest difference between these functions with the proposed one is that, the value of Gs between Gs_1 and Gs_2 are approximated by a straight line by connecting Gs_1 and Gs_2 in the code method as shown in Fig.2-4-2, which is found overestimates the RSR significantly [54]. The proposed function introduces a new parameter $T_{1\text{-}2}$, and uses a fold line to estimate the value of Gs between Gs_1 and Gs_2 as shown in Fig. 2-4-2, which is clearly more reasonable.

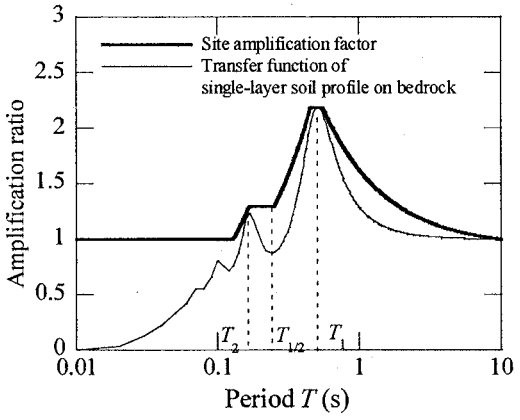

Fig. 2-4-1 Illustration of the proposed site amplification function

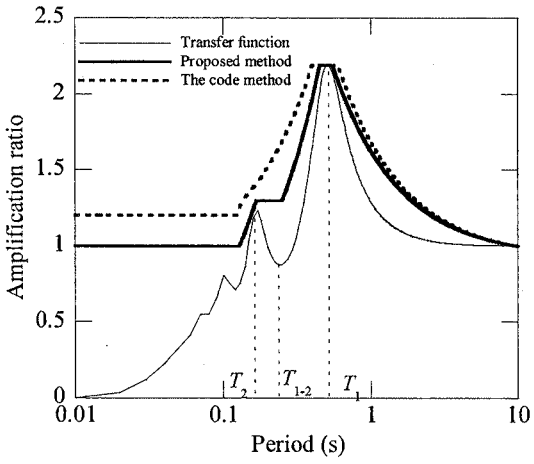

Fig. 2-4-2 Comparison of the proposed site amplification function with the one used in the Japanese seismic code

Chapter 3

First resonance peak of layered soil profiles

3.1 Introduction

According to Chapter 2, there are five parameters affecting the site amplification function Gs. They are, respectively, the fundamental period T_1, the first resonance peak Gs_1, the second natural period T_2, the second resonance peak Gs_2 and the period $T_{1/2}$. As the parameters T_2, Gs_2 and $T_{1/2}$ can be expressed by T_1 and Gs_1; thus, once T_1 and Gs_1 are obtained, the site amplification function Gs can be determined. This chapter focuses on methods for estimation of the first resonance peak Gs_1.

Many studies have focused on assessment of Gs_1 of layered soil profiles [27, 28]. In theory, the Gs_1 can be accurately obtained by calculating the site transfer function using matrix method proposed by Thomson WT [55] and Haskell NA [56] or directly using the program SHAKE [57], although this procedure is cumbersome. To avoid the complicated procedure of the direct method, a simple method for practical engineering is included in the Japanese Seismic Code. In this method, Gs_1 is evaluated by approximating a multi-layer soil profile as an equivalent single-layer profile by weighted averaging the soil shear wave velocity and density. However, this method significantly underestimates Gs_1 when the impedance contrast of the soil layers is large [27- 29]. Although some improvements have been proposed by Kehji K *et al.* [28], the accuracy of this methods remains unacceptable for engineering design [29]. Therefore, new methods for evaluating the Gs_1 of layered soil profiles that is both simple and highly accurate needs to be developed for practical engineering.

This chapter tries to develop new simple methods for estimations of the first resonance peak Gs_1. This chapter is organized as follows. First, in Section 3.2, the current methods for estimating Gs_1 are reviewed. Next, three simple methods for estimating the Gs_1 of layered soil profiles are, respectively, presented in Sections 3.3, 3.4 and 3.5. The method developed in Section 3.3 calculates the Gs_1, by replacing the layered shear wave velocity profile with an equivalent linearly varying profile. The method in Section 3.4 calculates the Gs_1, by replacing the multiple soil layers with equivalent two layers. The method in Section 3.5 calculates the Gs_1, by successively replacing the top two layers with an equivalent single layer.

3.2 Review of current methods for calculating Gs_1

Many studies have focused on determining the first resonance peak, Gs_1, of layered soil profiles. For the simplest soil model (i.e., a single-layer soil profile on bedrock), simple equations for Gs_1 and fundamental period, T_1, are given by:

$$Gs_1 = \frac{1}{1.57h + a_G} \tag{3-2-1}$$

$$T_1 = \frac{4H}{V} \tag{3-2-2}$$

where H is the soil thickness, V is the soil shear wave velocity, h is the soil damping ratio, and a_G is the impedance ratio of the soil layer with respect to the bedrock, which is defined as:

$$a_G = \frac{\rho V}{\rho_B V_B} \tag{3-2-3}$$

where V_B and ρ_B are the shear wave velocity and density of the bedrock, respectively.

For a multi-layer soil profile on bedrock, the most widely used method for determining the Gs_1 and fundamental period, T_1, is to replace multiple soil layers with an equivalent single layer by calculating the weighted averages of soil shear wave velocity and density as:

$$V = \frac{\sum_{m=1}^{N} V_m H_m}{\sum_{m=1}^{n} H_m} \tag{3-2-4}$$

$$\rho = \frac{\sum_{m=1}^{N} \rho_m H_m}{\sum_{m=1}^{n} H_m} \tag{3-2-5}$$

where m is soil layer number, each soil layer has finite thickness H_m, shear wave velocity V_m, and density ρ_m, and N is the number of soil layers. And, the damping ratio h is also calculated as the weighted average of all soil layers [58, 59] as follows:

$$h = \frac{\sum_{m=1}^{N} h_m E_m}{\sum_{i=1}^{m} E_m} \tag{3-2-6}$$

where E_m is the energy stored in mth layer [20, 58]. For linear analysis, the soil damping ratio of each layer, h_m, is constant, and is generally considered equal to 0.02. For nonlinear analysis, the damping ratio of each layer is dependent on the shaking level, and can be approximately estimated using the equivalent-linear method.

It should be noted that replacing a multi-layer soil profile with an equivalent single-layer soil profile using Eqs. (3-2-4) and (3-2-5) does not guarantee that the T_1 and Gs_1 of the equivalent single-layer soil profile are equal to those of the original multi-layer soil profile. As mentioned earlier, this method is known to underestimate Gs_1, especially when the impedance contrast of the soil layers is large [27-29].

Then, another approximate method for estimating Gs_1 of a multi-layer soil profile on bedrock is proposed by Kehji K *et al.* [28], and the equation is expressed as:

$$Gs_1 = \prod_{m=1}^{N} \frac{1}{1.57h'_m + a_m} \tag{3-2-7}$$

where h'_m is the equivalent damping ratio of the mth soil layer, a_m is the impedance ratio of mth soil layer with respect to the $(m+1)$ th soil layer. Kehji K *et al.* [28] assumes that, for a multi-layer soil profile, Gs_1 of each soil layer can be calculated by Eq. (3-2-1), and Gs_1 of the total soil profile is equal to the product of that of each soil layer. However, even for the same soil profile, the Gs_1 calculated by this method differs depending on how the soil profile is discretized [28]. Therefore, a practical method that is both simple and highly accurate is required.

3.3 linear equivalence

3.3.1 Introduction

As introduced in 3.2, most simple methods estimate the Gs_1 of multi-layer soil profiles by replacing the multiple soil layers with an equivalent single layer. And the shear wave velocity for the equivalent single layer is calculated by weighted averaging those of each soil layer. But, for actual soil profiles, shear wave velocity generally increases along with the depth. Thus, it is more reasonable to replace the layered shear wave velocity with one varying linearly than with the one being constant. Based on this consideration, a method for estimation of the Gs_1 is developed in section 3.3 by replacing the multiple soil layers with an equivalent single layer with shear wave velocity varying linearly.

The section 3.3 is organized as follows. Firstly, for a single layer soil with shear wave velocity varying linearly on bedrock, an equation for Gs_1 is derived, in section 3.3.2. Then, for multi-layer soil profiles, a method to replace multiple soil layers with an equivalent single layer soil with shear wave velocity varying linearly is developed, in section 3.3.3. Then, 67 representative soil profiles are used to investigate the accuracy of the proposed method.

3.3.2 Gs_1 of a single layer soil profile on bedrock with shear wave velocity varying linearly

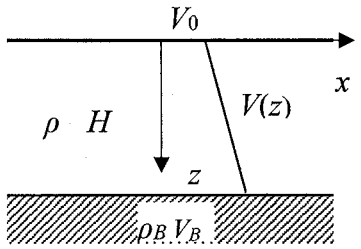

Fig.3-3-1 Single layer soil on bedrock with linearly varying shear wave velocity profile

A single layer soil on bedrock with shear wave velocity varying linearly, as shown in Fig. 3-3-1, is considered. The equation for soil shear wave velocity, $V(z)$, is expressed as:

$$V(z) = V_0(1 + k'\frac{z}{H}) \tag{3-3-1}$$

where, V_0 is value of the soil shear wave velocity at ground surface, H is height of the soil layer, and k' represents variation degree of the soil shear wave velocity along with depth.

To obtain the equation for Gs_1, the transfer function of the soil profiles shown in Fig.3-3-1 needs be derived. For vertically propagating shear waves, the equilibrium equation can be written as:

$$\rho\frac{\partial^2 u}{\partial t^2} = \frac{\partial}{\partial z}(G(z)\frac{\partial u}{\partial z}) \tag{3-3-2}$$

where ρ is soil density, u is soil displacement, and $G(z)$ is soil shear modular defined as:

$$G(z)=\rho V(z)^2 \tag{3-3-3}$$

For harmonic seismic waves, Eq. (3-3-2) can be solved, the transfer function can be obtained as [60]:

$$Tr(\omega)=\frac{1}{\frac{2\overline{m}\cos\theta+\sin\theta}{2\overline{m}\sqrt{1+k'}}+\frac{ia\omega H\sqrt{1+k'}}{kV_0\overline{m}}\sin\theta} \tag{3-3-4}$$

where

$$\overline{m}=\sqrt{(\frac{\omega H}{k'V_0})^2-0.25} \tag{3-3-5}$$

$$\theta=\overline{m}\ln(1+k') \tag{3-3-6}$$

$$a=\frac{\rho V_0}{\rho_B V_B} \tag{3-3-7}$$

ρ_B, V_B ,respectively, are density and shear wave velocity of bedrock.

First peak of the transfer function corresponding to the fundamental period, i.e. Gs_1, can be obtained by submitting value of the fundamental period into Eq. (3-3-4). For the soil profile shown in Fig.3-3-1, on rigid bedrock, the fundamental period, T_0 can be obtained by [60]:

$$2\overline{m}_0\cos\theta_0+\sin\theta_0=0 \tag{3-3-8}$$

where

$$\overline{m}_0=\sqrt{(\frac{\omega_0 H}{k'V_0})^2-0.25} \tag{3-3-9}$$

$$\theta_0=\overline{m}_0\ln(1+k') \tag{3-3-10}$$

ω_0 is the fundamental frequency.

As the effect of bedrock rigidity on site fundamental period is considered negligible [61, 62], Eq. (3-3-8) is also available to calculate the fundamental period for soil profiles on elastic bedrock. Substituting Eq. (3-3-8) into Eq. (3-3-4), the real part of the denominator in Eq. (3-3-4) becomes zero, and the first resonance peak, Gs_1, can be given by:

$$Gs_1=\frac{1}{\frac{a\omega_0 H\sqrt{1+k'}\sin\theta_0}{k'V_0\overline{m}_0}} \tag{3-3-11}$$

Equation (3-3-11) is derived by disregarding the soil damping. However, soil damping has been shown to significantly affect the site amplification; thus, the soil damping ratio should be parameterized in the equation for Gs_1. For a single-layer soil profile on bedrock, the soil damping ratio is considered approximately by the term $1.57h$ in Eq. (3-2-1). Based on this consideration, the equation for Gs_1 considering soil damping for the soil profile shown in Fig. 3-3-1 is approximated as:

$$Gs_1 = \frac{1}{1.57h + \dfrac{a\omega_0 H\sqrt{1+k'}\sin\theta_0}{kV_0\overline{m}_0}} \tag{3-3-12}$$

For a uniform soil profile, i.e. k'=0, Eq. (3-3-12) identically reverts to Eq. (3-2-1).

Accuracy of the derived equation

In order to investigate the accuracy of the derived Eqs. (3-3-11) and (3-3-12), a wide range of values for the parameters affecting the amplification ratio are considered. According to Eq. (3-3-4), there are five parameters, namely H, V_0, k, a and h, that control the amplification ratio. As H and V_0 always appear in form of H/V_0 in Eq. (3-3-4), thus the H/V_0 can be considered as a single parameter. In addition, as shear wave velocity of bedrock is generally larger than that of soil, thus only soil profiles meeting the condition $V_B > V_0(1+k)$, are considered.

Firstly, to investigate the accuracy of Eq. (3-3-11), results estimated by Eq. (3-3-11) are compared with accurate results obtained by Eq. (3-3-4). The comparison are shown in Fig.3-3-2, the real line represents the results by Eq. (3-3-4), and the dotted line represents the results by Eq. (3-3-11). Fig. 3-3-2 indicates that results by proposed equation agree very well with those accurate results. Accuracy of Eq. (3-3-12) is also investigated in Fig. 3-3-3. To consider the soil damping, theoretical results are calculated by replacing the shear wave velocity, $V(z)$, with $V(z)\sqrt{1+2hi}$. It can be found that, error in results by Eq. (3-3-12) increases as soil damping ratio increases; however, the maximum relative error is approximately 4.5% when the damping ratio is as much as16%. Thus, the accuracies of the two equation are considered excellent for engineering use.

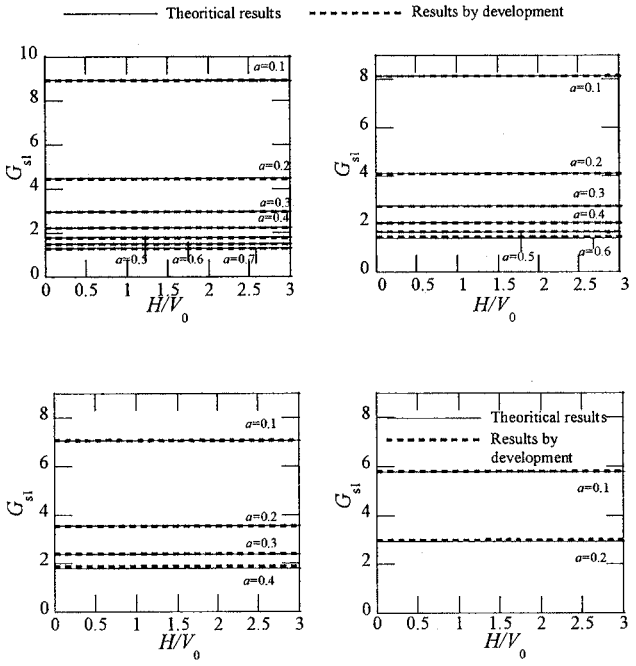

Fig. 3-3-2 Verification of the Eq. (3-3-11) for undamped Gs_1 of the soil profile of Fig.3-3-1

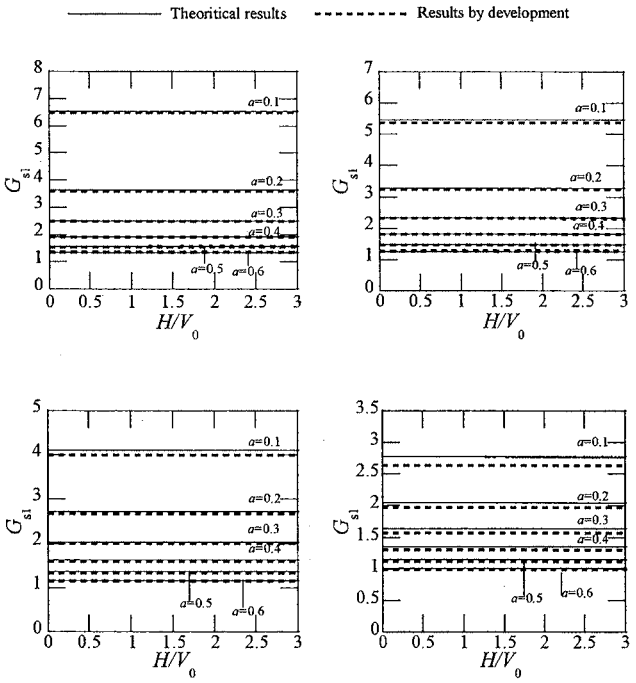

Fig. 3-3-3 Verification of the Eq. (3-3-12) for damped Gs_1 of the soil profile of Fig.3-3-1

3.3.3 Gs_1 of multi-layer soil profiles on bedrock

Many studies estimate the Gs_1 by replacing the layered shear wave velocity with constant one, as introduced in section 3.2. But, for actual soil profiles, shear wave velocity generally increases along with the depth. Thus, it is more reasonable to replace the layered shear wave velocity with the one varying linearly, as shown in Fig. 3-3-4 (b). In this section, a method to replace the layered shear wave velocity with one varying linearly is developed.

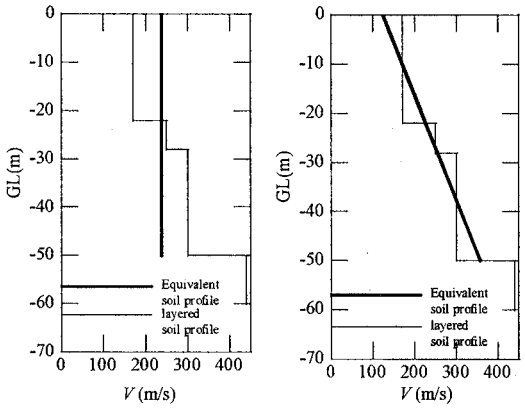

(a) (b)

Fig. 3-3-4 Illustration of the concept of replacing layered shear wave velocity profile, (a) with an equivalent constant profile, (b) with an equivalent lineally varying profile.

To replace the layered shear wave velocity with one varying linearly, regression analysis is used here. Specifically, values of depth and shear wave velocity at midpoint of each soil layer, (z_i, V_i) are considered as regression point, and the function for shear wave velocity expressed as Eq. (3-3-1) is considered as regression function. Based on the least squares method, the coefficient k and V_0 in Eq. (3-3-1) can be obtained by minimizing the sum of squared residuals between an observed value, (z_i, V_i), and the fitted value (z_i, $V(z_i)$). The residual of ith regression point is expressed as:

$$\overline{D_i} = V_i - V_0(1 + k'z_i) \tag{3-3-13}$$

and, the sum of squared residuals is calculated by:

$$\overline{D} = \sum_{i=1}^{N} \overline{D_i}^2 \tag{3-3-14}$$

To minimize the sum of squared residuals, the gradient respect to k and V_0 are set to 0, expressed as:

$$\frac{\partial \overline{D}}{\partial k} = 0 \quad \frac{\partial \overline{D}}{\partial V_0} = 0 \tag{3-3-15}$$

According to Eq. (3-3-15) equation for k and V_0 can be given by:

$$k' = \frac{(\overline{m}_3 - \overline{m}_1\overline{m}_2)H}{\overline{m}_2\overline{m}_4 - \overline{m}_1\overline{m}_3} \tag{3-3-16}$$

$$V_0 = \frac{\overline{m}_3}{\overline{m}_1 + \overline{m}_4 k'/H} \tag{3-3-17}$$

where

$$\overline{m}_1 = \sum_{i=1}^{N} z_i \Big/ N \quad \overline{m}_2 = \sum_{i=1}^{N} V_i \Big/ N \quad \overline{m}_3 = \sum_{i=1}^{N} z_i V_i \Big/ N \quad \overline{m}_4 = \sum_{i=1}^{N} {z_i}^2 \Big/ N .$$

Using Eqs. (3-3-1), (3-3-16) and (3-3-17), layered shear wave velocity can be replaced with one varying linearly.

The density ρ_{eq} and damping ratio h_{eq} of the equivalent single layer soil can be simply estimated by Eqs. (3-2-5) and (3-2-6).

3.3.4 Numerical examples using the proposed method

In order to investigate the accuracy of the proposed method, 67 representative soil profiles selected from Strong-motion Seismograph Networks (K-NET, KIK-net) are used. According to JARA [63], these soil profiles are divided into three site classes, and the shear wave velocity profiles above the engineering bedrock of each site classification are presented in Fig. 3-3-5. According to Japanese Seismic Code, engineering bedrock is defined as the layer where the shear wave velocity is greater than approximately 400 m/s [59]. The unit weights are not given for some sites; these weights are

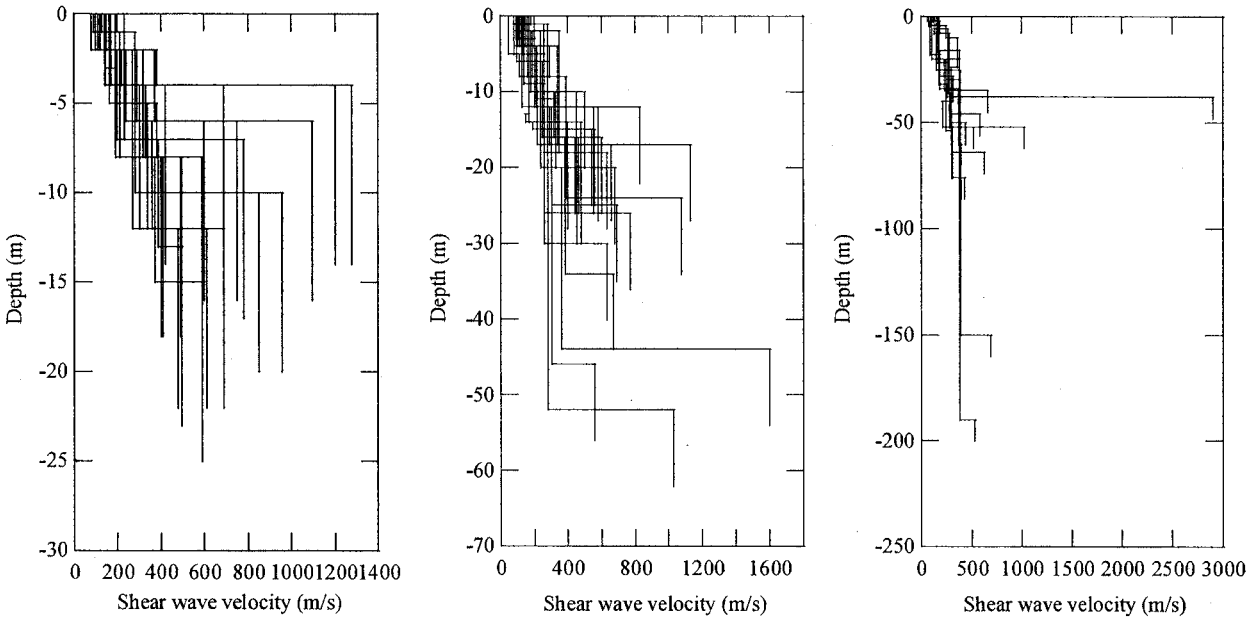

Fig. 3-3-5 Shear wave velocity profiles above engineering bedrock used for analyses: (a) first site class, (b) second site class, and (c) third site class.

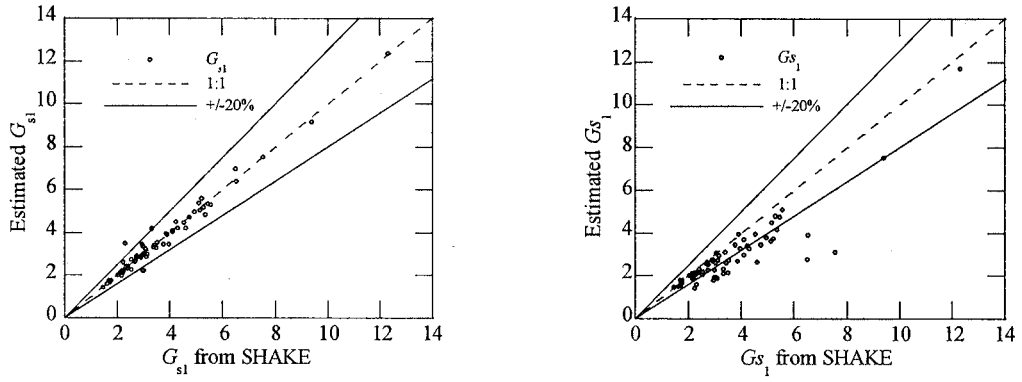

(a) Comparison of results calculated by proposed method with those by SHAKE

(b) Comparison of results calculated by Code method with those by SHAKE

Fig. 3-3-6 Verification of the proposed method for G_{s1} of multi-layer soil profile on bedrock

empirically determined according to Yuki S *et al.* [64] as 15.68 KN/m^3 for clay, 18.62 KN/m^3 for sand, 19.60 KN/m^3 for engineering bedrock with shear wave velocity in the range of 400~800 m/s, and 21.56 KN/m^3 for engineering bedrock with shear wave velocity greater than 800 m/s. The initial fundamental periods of the selected soil profiles are calculated by the SHAKE program, and the results vary widely from 0.05 to 1.72 s.

The Gs_1 of the 67 soil profiles are estimated by the proposed procedure and compared with those

obtained using the SHAKE program. Fig. 3-3-6 (a) shows that, the Gs_1 obtained by the proposed method are remarkably accurate; 91% of estimated values for the linear analysis are within 20% of the SHAKE results. The average error in Gs_1 is only 9.7%, which is considered sufficient for engineering calculation. In addition, the Gs_1 is also estimated using the method in the Japanese Seismic Code and compared with those obtained using the proposed method and the SHAKE program. Fig. 3-3-6 (b) shows that most of the Gs_1 estimated by the code method are underestimated by over 20% compared to the SHAKE results, which is consistent with previous studies [27- 29]. The average error in Gs_1 estimated by the code method is as large as 17.2%, which is much greater than that for the proposed method. Generally speaking, the proposed procedure produces accurate estimates of Gs_1 and is much more accurate than the method used in the Japanese Seismic Code.

3.3.5 Conclusions

The section 3.3 proposes a simple method for estimation of the Gs_1 of multi-layer soil profiles. The main conclusions are summarized as follows:

(a) An equation for the Gs_1 of a single layer soil profile on bedrock with the shear wave velocity varying linearly, is derived. Accuracy of the derived equation is found be very good by investing a wide range of values for the parameters affecting the Gs_1.

(b) For multi-layer soil profiles, a method to replace the layered shear wave velocity with one varying linearly is developed. By further using the derived equation for the Gs_1, results for multi-layer soil profiles can be obtained.

(c) To investigate the accuracy of the proposed method, 67 actual sites are used. It is found that, the proposed procedure produces accurate estimates of Gs_1, and results by the proposed method are more accurate than those by the method used in Japanese Seismic Code.

3.4 Two-layer equivalence

3.4.1 Introduction

As introduced in section 3.2, the method used in the Japanese code estimates the Gs_1 of multi-layer soil profiles by replacing the multiple soil layers with an equivalent single layer. The shear wave velocity and density for the equivalent single layer are calculated by weighted averaging those of every soil layers. As weighted average ignores distribution of soil impedance along depth; it can be easily infer that, the larger the variation degree of soil impedance are, the larger the error in estimation of the Gs_1 will be. Many studies [27-29] have pointed out that, this method underestimates Gs_1 significantly, when the impedance contrast of the soil layers is large.

In this section, in order to avoid averaging the soil layers with large impedance contrast and obtain more accurate results; the multiple soil layers are divided into two parts at the interface where impedance contrast of the soil layers is largest, and the two parts are, respectively, replaced by two equivalent soil layers. Then, the $Gs_1$is estimated by an equation for two-layer soil profiles on bedrock.

The section 3.4 is organized as follows. Firstly, an equation for Gs_1 of two-layer soil profiles on bedrock, is derived in section 3.4.2. Then, for multi-layer soil profiles, a method to replace multiple soil layers with an equivalent two soil layers is developed, in section 3.4.3. Then, the 67 representative soil profiles selected in section 3.3.4 are used to investigate the accuracy of the proposed method.

3.4.2 Gs_1 of a two-layer soil profile on bedrock

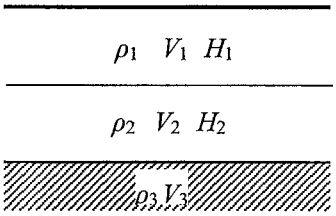

Fig. 3-4-1 Two-layer soil profile on bedrock

To derive the expression for Gs_1, a two-layer soil profile on bedrock, as shown in Fig. 3-4-1, is considered. For vertically propagating shear waves, the equilibrium equation can be written as:

$$\rho_m \frac{\partial^2 y_m}{\partial t^2} = G_m \frac{\partial^2 y_m}{\partial x^2} \tag{3-4-1}$$

where

$$G_m = G_{mo}(1+2ih_m) \tag{3-4-2}$$

m is the layer number (m = 1, 2, 3); ρ_m, h_m, G_{m0}, and y_m are the density, damping ratio, shear modulus and displacement of mth layer, respectively; x is the depth below the surface of each layer; t is time; and i is the complex number ($i^2 = -1$).

For harmonic seismic waves, Eq. (3-4-1) can be solved, and the displacement y_m and shear strength τ_m of the mth layer can be respectively given by:

$$y_m(x,t) = U_m e^{i\omega(t+x/V_m)} + D_m e^{i\omega(t-x/V_m)} \tag{3-4-3}$$

$$\tau_m(x,t) = i\omega\rho_m V_m\left(U_m e^{i\omega(t+x/V_m)} - D_m e^{i\omega(t-x/V_m)}\right) \tag{3-4-4}$$

where ω is the angular frequency of the harmonic wave; U_m and D_m are the amplitudes of waves traveling upwards and downwards in the mth layer, respectively; and V_m is the shear wave velocity of the mth layer, which is defined as:

$$V_m = \sqrt{\frac{G_m}{\rho}} \tag{3-4-5}$$

According to the boundary condition that shear stress at the ground surface is equal to 0 [i.e., $\tau_1(0,t) = 0$], the amplitudes of waves traveling upwards and downwards at the ground surface are equal,

$$U_1 = D_1 \tag{3-4-6}$$

According to two additional boundary conditions, (1) relative displacement at the interface between two adjacent layers is zero and (2) shear stress at the interface between two adjacent layers is continuous, expressed as:

$$\begin{cases} y_m(H_m,t) = y_{m+1}(0,t) \\ \tau_m(H_m,t) = \tau_{m+1}(0,t) \end{cases} \tag{3-4-7}$$

the amplitudes of waves traveling upwards and downward (U_m and D_m, respectively) in each layer are given by:

$$\begin{cases} U_{m+1} = \dfrac{1}{2}[(1+a_m)U_m e^{i\omega H_m/V_m} + (1-a_m)D_m e^{-i\omega H_m/V_m}] \\ D_{m+1} = \dfrac{1}{2}[(1-a_m)U_m e^{i\omega H_m/V_m} + (1+a_m)D_m e^{-i\omega H_m/V_m}] \end{cases} \tag{3-4-8}$$

where H_m is the thickness of the mth soil layer.

Using Eqs. (3-4-6) and (3-4-8), the wave amplitude traveling upwards at the bedrock, U_3, can be given by:

$$U_3 = U_1((\cos C_1 \cos C_2 - a_1 \sin C_1 \sin C_2) + i(a_1 a_2 \sin C_1 \cos C_2 + a_2 \cos C_1 \sin C_2)), \tag{3-4-9}$$

where

$$C_m = \frac{\pi T_{(m)}}{2T\sqrt{1+2ih_m}}, \qquad T_{(m)} = \frac{4H_m}{V_m}, \qquad T = \frac{2\pi}{\omega},$$

and a_m is the impedance ratio between adjacent layers, which is defined as:

$$a_m = \frac{\rho_m V_m}{\rho_{m+1} V_{m+1}} \tag{3-4-10}$$

Then, the transfer function for the seismic motions at outcrop bedrock can be obtained as:

$$H_2(\omega) = \frac{U_1 + D_1}{2 \times U_3} = \frac{1}{(\cos C_1 \cos C_2 - a_1 \sin C_1 \sin C_2) + i(a_1 a_2 \sin C_1 \cos C_2 + a_2 \cos C_1 \sin C_2)} \tag{3-4-11}$$

Using Eq. (3-4-11), the first peak of the transfer function corresponding to the fundamental period can be obtained by making the period T equal to the fundamental period of the two-layer soil profile. For two undamped soil layers ($h_m = 0$) on rigid bedrock ($V_B = \infty$), the equation for $T_{1\text{-}2L}$ has been derived by Madera GA [65] and is given by:

$$\tan\frac{\pi T_{(1)}}{2T_{1-2L}} \tan\frac{\pi T_{(2)}}{2T_{1-2L}} = \frac{\rho_2 H_2 T_{(1)}}{\rho_1 H_1 T_{(2)}} \tag{3-4-12}$$

As the effect of bedrock rigidity on site fundamental period is considered negligible [61, 62], Eq. (3-4-21) is also available to calculate the fundamental period for the two-layer soil profile on elastic bedrock. Soil damping is first disregarded. Substituting Eq. (3-4-12) into Eq. (3-4-11), the real part of the denominator in Eq. (3-4-11) becomes zero, and the undamped first resonance peak ($h_m = 0$) of the two-layer soil profile can be given by:

$$Gs_1 = \frac{1}{\left| a_1 a_2 \sin\frac{\pi T_{(1)}}{2T_{1-2L}} \cos\frac{\pi T_{(2)}}{2T_{1-2L}} + a_2 \cos\frac{\pi T_{(1)}}{2T_{1-2L}} \sin\frac{\pi T_{(2)}}{2T_{1-2L}} \right|} \tag{3-4-13}$$

Equation (3-4-13) is derived by disregarding the soil damping. However, soil damping has been shown to significantly affect the site amplification; thus, the soil damping ratio should be parameterized in the equation for $Gs_{1\text{-}2L}$. For a single-layer soil profile on bedrock, the soil damping ratio is considered approximately by the term $1.57h$ in Eq. (3-2-1). Based on this consideration, the equation for $Gs_{1\text{-}2L}$ considering soil damping for the two-layer soil profile is approximated as:

$$Gs_1 = \frac{1}{\left| a_1 a_2 \sin\frac{\pi T_{(1)}}{2T_{2L-1}} \cos\frac{\pi T_{(2)}}{2T_{2L-1}} + a_2 \cos\frac{\pi T_{(1)}}{2T_{2L-1}} \sin\frac{\pi T_{(2)}}{2T_{2L-1}} \right| + 1.57 h_{eq}} \tag{3-4-14}$$

where h_{eq} is the equivalent damping ratio calculated by Eq. (3-2-6).

It should be noted that Eq. (3-4-14) is consistent with Eq. (3-2-1) when $V_1 = V_2$, $\rho_1 = \rho_2$ and $h_1 = h_2$.

Validity of the derived equation

To investigate the accuracy of Eq. (3-4-14), a series of two-layer soil profiles on bedrock are considered. It can be known from Eq. (3-4-11), parameters including: impedance ratio α_m, damping ratio h_m and fundamental period T_m, affect the results of Gs_1. A wide range of values for these parameters are considered as shown in Figs. 3-4-2 and 3-4-3. For simplify, damping ratios of the two soil layers are considered equal, and the one of bedrock is considered equals 0. Then, Gs_1 of all considered two-layer soil profiles are calculated by the derived equation, obtained results are compared with those obtained by wave propagation theory (Eq. (3-4-11)) in Figs. 3-4-2 and 3-4-3. Fig. 3-4-2 shows the results obtained by disregarding the soil damping ratio, and Fig. 3-4-3 shows those obtained considering a wide range of soil damping ratios. In Figs. 3-4-2 and 3-4-3, the results

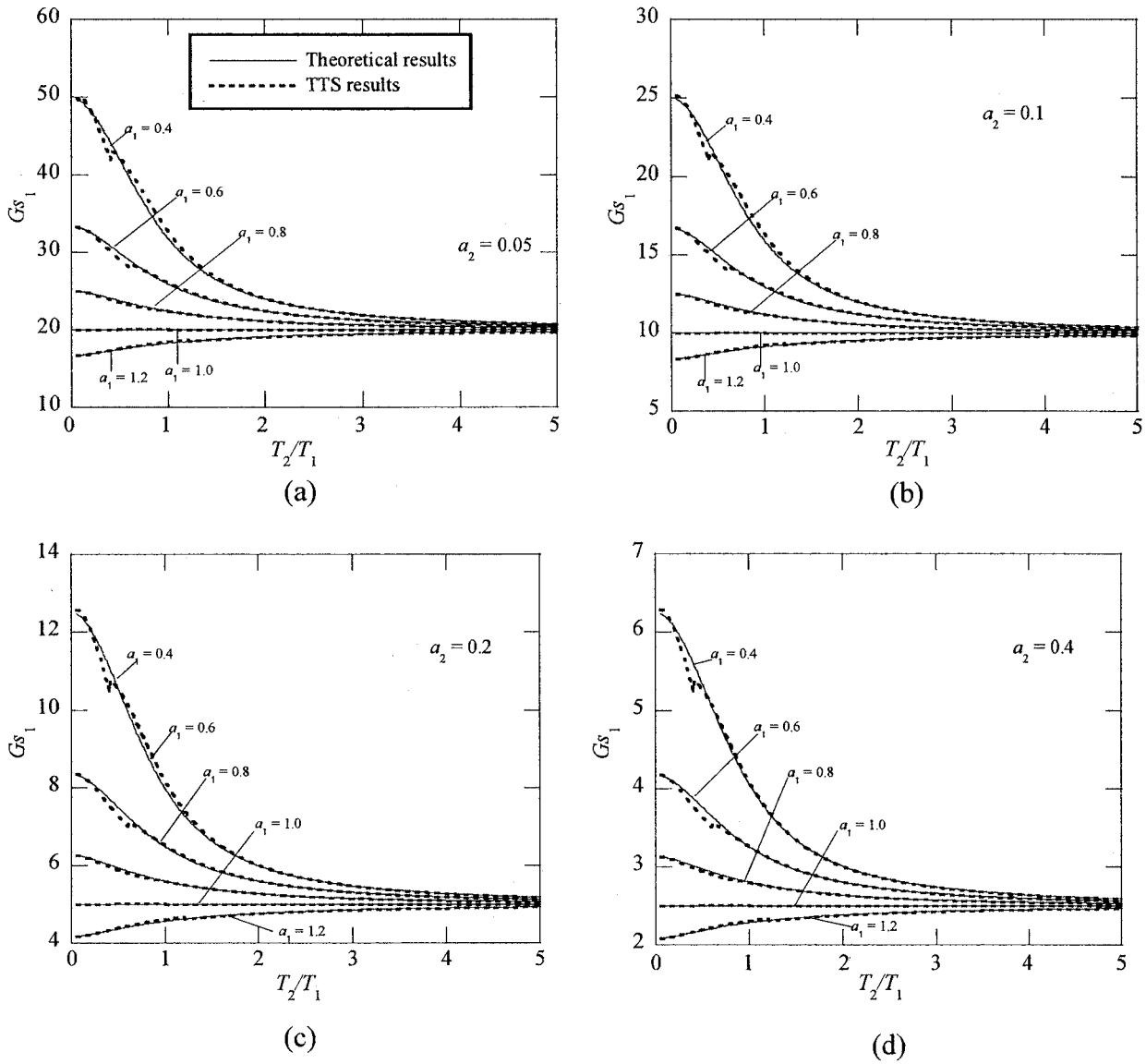

Fig. 3-4-2 Comparison of undamped Gs_1 calculated using the developed TTS procedure and wave propagation theory: (a) impedance ratio $\alpha_2 = 0.05$, (b) $\alpha_2 = 0.1$, (c) $\alpha_2 = 0.2$, and (d) $\alpha_2 = 0.4$.

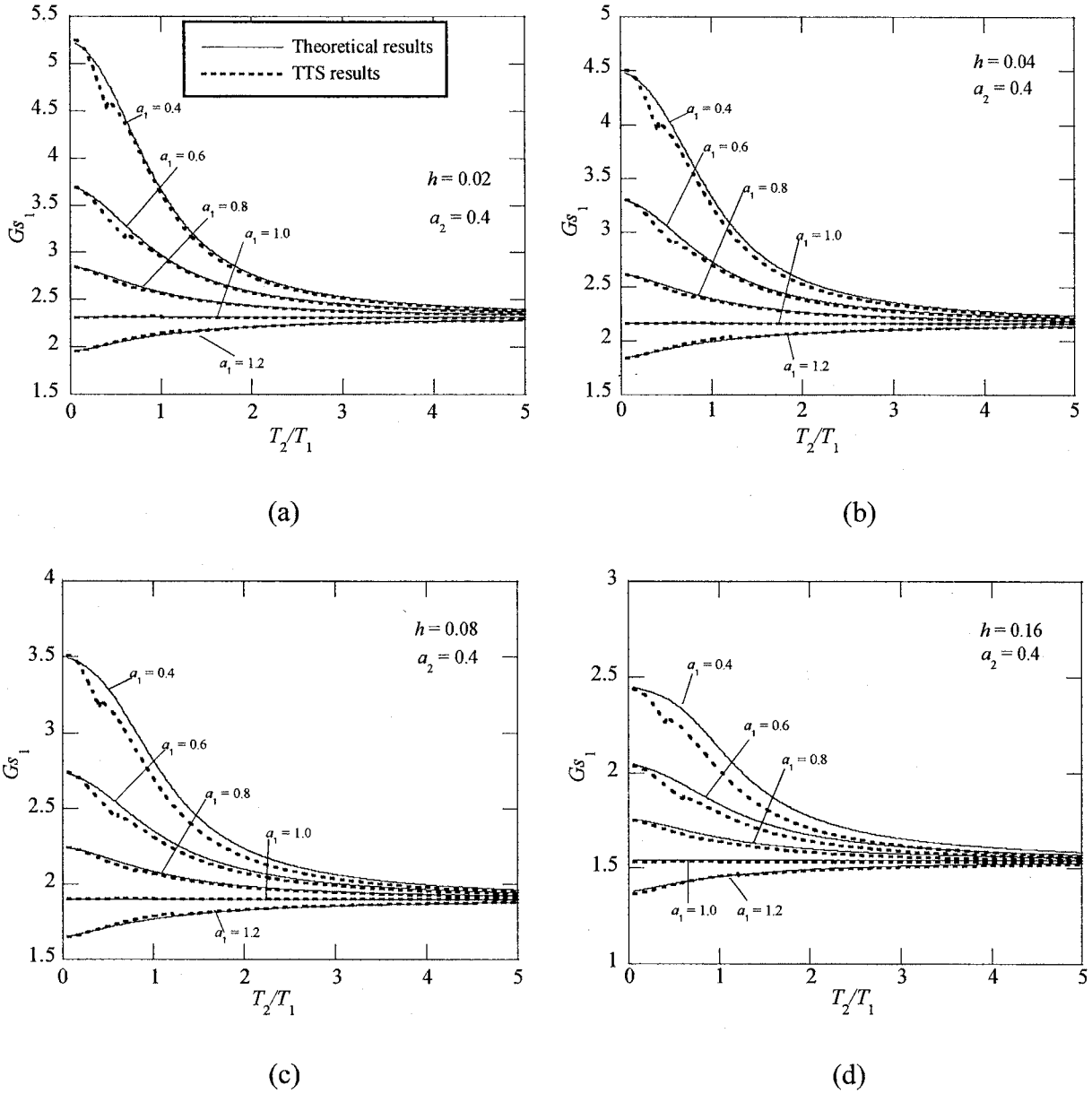

Fig. 3-4-3 Comparison of damped Gs_1 calculated using the developed TTS procedure and wave propagation theory: (a) damping ratio $h = 0.02$, (b) $h = 0.04$, (c) $h = 0.08$, and (d) $h = 0.16$.

obtained by wave propagation theory, referred to as theoretical results, are represented by thin solid lines, and the results by the derived equation are shown by thick dotted lines.

Fig. 3-4-2 indicates good agreement between the results by the derived equation and wave propagation theory. The maximum relative error in the analyzed soil profiles is approximately 1%. Fig. 3-4-3 indicates that the error by the derived equation increases as soil damping ratio increases; however, the maximum relative error is approximately 5% when the damping ratio is as much as16%. Thus, the accuracy of the derived equation is considered excellent for engineering use.

3.4.3 Gs_1 of multi-layer soil profiles on bedrock

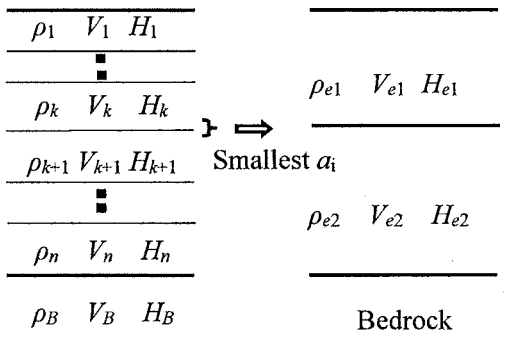

Fig. 3-4-4 Illustration of the concept of replacing a multi-layer soil profile on bedrock by an equivalent two-layer soil profile.

In this section, a method to replace multiple soil layers with an equivalent two soil layers is developed. In order to avoid averaging the soil layers with large impedance contrast; the multiple soil layers are divided into two parts at the interface where impedance contrast of the soil layers is largest as shown in Fig.3-4-4. Then the two parts are, respectively, replaced by two equivalent soil layers using following equations

$$V_{e1} = \frac{\sum_{m=1}^{k} V_m H_m}{\sum_{m=1}^{k} H_m} \tag{3-4-15}$$

$$V_{e2} = \frac{\sum_{m=k+1}^{n} V_m H_m}{\sum_{m=k+1}^{n} H_m} \tag{3-4-16}$$

$$\rho_{e1} = \frac{\sum_{m=1}^{k} \rho_m H_m}{\sum_{m=1}^{k} H_m} \tag{3-4-17}$$

$$\rho_{e2} = \frac{\sum_{m=k+1}^{n} \rho_m H_m}{\sum_{m=k+1}^{n} H_m} \tag{3-4-18}$$

where V_{e1} and ρ_{e1} are, respectively, shear wave velocity and density of the upper equivalent soil layer, V_{e2} and ρ_{e2} are, respectively, shear wave velocity and density of the lower equivalent soil layer.

3.4.4 Numerical examples using the proposed method

In order to investigate the accuracy of the proposed method, the 67 representative soil profiles selected in section 3.3.4 are used. The Gs_1 of the 67 soil profiles are estimated by the proposed procedure and compared with those obtained using the SHAKE program. Fig. 3-4-5 (a) shows that, the Gs_1 obtained by the proposed method are remarkably accurate; 94% of estimated values for the linear analysis are within 20% of the SHAKE results. The average error in Gs_1 is only 5.7%, which is considered sufficient for engineering calculation. In addition, the Gs_1 is also estimated using the method in the Japanese Seismic Code and compared with those obtained using the proposed method and the SHAKE program. Fig. 3-4-5 (b) shows that most of the Gs_1 estimated by the code method are underestimated by over 20% compared to the SHAKE results, which is consistent with previous studies [27-29]. The average error in Gs_1 estimated by the code method is as large as 17.2%, which is much greater than that for the proposed method. Generally speaking, the proposed procedure produces accurate estimates of Gs_1 and is much more accurate than the method used in the Japanese Seismic Code.

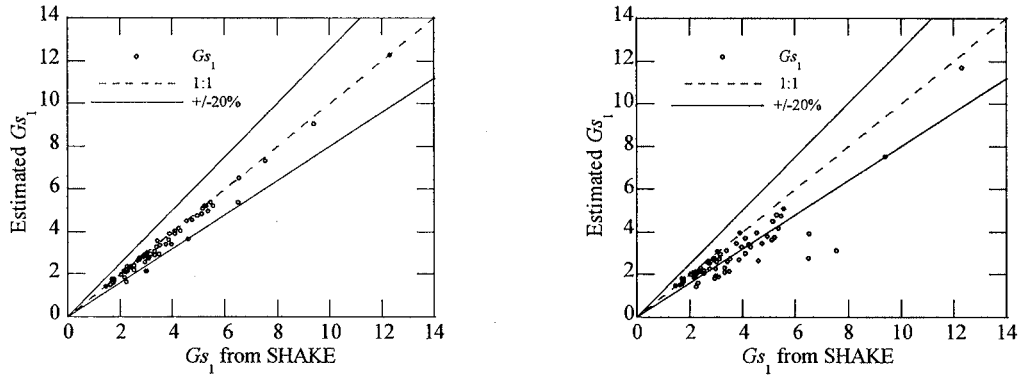

(a)Comparison of results calculated by proposed method and SHAKE

(b) Comparison of results calculated by Code method and SHAKE

Fig. 3-4-5 Verification of proposed method of Gs1 for multi-layer soil profiles on bedrock

3.4.5 Conclusions

The section 3.4 proposes a simple method for estimation of Gs_1 of multi-layer soil profiles. The main conclusions are summarized as follows:

(a) An equation for Gs_1 of a two-layer soil profile on bedrock is developed, according to the derived transfer function. Accuracy of the derived equation is found be very good by investing a wide range of values for the parameters affecting the Gs_1.

(b) For multi-layer soil profiles, a method to replace the multiple soil layers with two equivalent

soil layers is developed. By further using the derived equation for the Gs_1, results for multi-layer soil profiles can be obtained.

(c) To investigate the accuracy of the proposed method, 67 actual sites are used. It is found that, the proposed procedure produces accurate estimates of Gs_1, and results by the proposed method are more accurate than those by the method used in Japanese Seismic Code.

3.5 Successive use of two-layer equivalence

3.5.1 Introduction

As introduced in section 3.2, replacing a multi-layer soil profile with an equivalent single-layer soil profile by roughly weighted averaging the shear wave velocity and density can't guarantee that the fundamental period and the first resonance peak, Gs_1, of the equivalent single-layer soil profile are equal to those of the original multi-layer soil profile.

In this section, another simple method for determining the Gs_1 of layered soil profiles is developed. This method tries to replace the multi-layer soil profile with an equivalent one-layer soil profile, and make the two soil profiles have same fundamental period and Gs_1.Then the Gs_1 along with the fundamental period can be easily obtained. To realize this one-layer equivalence, a procedure to replace a two-layer soil profile on bedrock by an equivalent single-layer soil profile, which is called the two-to-single (TTS) procedure, is derived in section 3.5.2. Then, by successively applying the TTS procedure, a multi-layer soil profile on bedrock can be replaced by an equivalent single-layer profile. In this procedure, the top two layers are assumed overlie bedrock and are replaced by an equivalent single layer using the derived TTS procedure. The equivalent single layer and the third layer can be treated as a new two-layer soil, which is also replaced by an equivalent single layer. By applying the TTS procedure successively to the remaining lower layers, the multiple soil layers are finally replaced by an equivalent single layer. The fundamental period and Gs_1 can then be easily obtained. In section 3.5.4, to demonstrate the validity of the proposed method, Gs_1 of 67 representative soil profiles are evaluated by the proposed method, and the results are shown to agree well with those obtained by the wave propagation method.

3.5.2 Development of the TTS procedure

Fig. 3-5-1 schematically shows the procedure developed to replace a two-layer soil profile on bedrock (a) with an equivalent single-layer soil profile (b) with the same fundamental period and Gs_1. To develop this procedure, the fundamental parameters including shear wave velocity V_{eq}, thickness H_{eq}, density ρ_{eq} and damping ratio h_{eq} of the equivalent single-layer soil profile should be expressed in terms of those of the two-layer soil profile based on the following two equivalence equations:

$$T_{1\text{-}2L} = T_{1\text{-}eq} \tag{3-5-1}$$

$$Gs_{1\text{-}2L} = Gs_{1\text{-}eq} \tag{3-5-2}$$

where $T_{1\text{-}2L}$ and $Gs_{1\text{-}2L}$ represent the fundamental period and first resonance peak of the two-layer soil profile, respectively; $T_{1\text{-}eq}$ and $Gs_{1\text{-}eq}$ represent the fundamental period and first resonance peak of the equivalent single-layer soil profile, respectively.

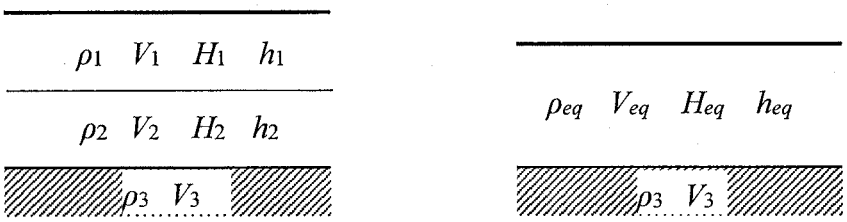

(a) (b)

Fig. 3-5-1 Illustration of the concept of replacing a two-layer soil profile on bedrock with an equivalent single-layer soil profile.

However, it is theoretically impossible to solve two equations containing four unknown parameters. For this reason, additional two equivalence equations are introduced: (1) as soil destiny generally does not exhibit large variations, the destiny of the equivalent single-layer soil, ρ_{eq}, is considered approximately equal to the weighted-average density calculated by Eq. (3-2-5); and (2) the damping ratio of the equivalent single-layer soil, h_{eq}, is considered approximately equal to the weighted-average damping ratio calculated by Eq. (3-2-6). Thus, the remaining two parameters (shear wave velocity V_{eq} and thickness H_{eq}) of the equivalent single layer can be determined using Eqs. (3-5-1) and (3-5-2).

Substituting Eqs. (3-2-1) and (3-4-14) into Eq. (3-5-2), the shear wave velocity V_{eq} of the equivalent single layer can be obtained as:

$$V_{eq} = \left| \frac{V_1 \rho_1}{\rho_{eq}} \sin\frac{\pi T_{(1)}}{2T_{1-2L}} \cos\frac{\pi T_{(2)}}{2T_{1-2L}} + \frac{V_2 \rho_2}{\rho_{eq}} \cos\frac{\pi T_{(1)}}{2T_{1-2L}} \sin\frac{\pi T_{(2)}}{2T_{1-2L}} \right| \tag{3-5-3}$$

Next, according to Eq. (3-5-1) [i.e., $T_{1\text{-}2L} = 4H_{eq} / V_{eq}$], the thickness H_{eq} of the equivalent single-layer soil can be given by:

$$H_{eq} = \frac{T_{1-2L} V_{eq}}{4} \tag{3-5-4}$$

As introduced above, the fundamental period $T_{1\text{-}2L}$ in the Eqs. (3-5-3) and (3-5-4), can be obtained using the charts given by Madera GA [65] or using the following approximated equations by Hadjian AH [66]:

$$\frac{T_{1-2L}}{T_{(1)}} = \sqrt{\frac{\pi^2}{8}\left[0.75 + \left(\frac{T_{(2)}}{T_{(1)}}\right)^2 \left(1 + 2\frac{H_1\rho_1}{H_2\rho_2}\right)\right]}, \quad \text{for } H_1/H_2 > 1 \tag{3-5-5}$$

$$\frac{T_{1-2L}}{T_{(1)}} = \left[1 + \beta\left(\frac{T_{(2)}}{T_{(1)}}\right)^{\bar{n}} \left(1 + \frac{H_1\rho_1}{H_2\rho_2}\right)^{\bar{n}}\right]^{\frac{1}{\bar{n}}}, \quad \text{for } H_1/H_2 \le 1 \tag{3-5-6}$$

where

$$\overline{n} = 4 - 1.8\frac{H_1\rho_1}{H_2\rho_2} \quad \text{and} \quad \beta = 1 - 0.2(\frac{H_1\rho_1}{H_2\rho_2})^2$$

Hence, using Eqs. (3-2-5), (3-2-6), (3-5-3) and (3-5-4), an equivalent single-layer soil profile that has the same fundamental period and first resonance peak as the two-layer soil profile can be obtained.

3.5.3 Gs_1 of multi-layer soil profiles on bedrock

Method for calculating Gs_1

This section presents a simple procedure for determining the Gs_1 of multi-layer soil profiles on bedrock by successively applying the TTS procedure developed in section 3.5.2. Specifically, for a multi-layer soil on bedrock [Fig. 3-5-2 (a)], the top two layers are assumed to overlie bedrock and are replaced by an equivalent single layer using the TTS procedure. Subsequently, the equivalent single layer and the third layer can be treated as a new top two-layer soil and can also be replaced by an equivalent single layer. By applying the TTS procedure successively to the remaining lower layers of the soil profile, the multiple soil layers can finally be replaced by an equivalent single layer, and the fundamental period and Gs_1 of the total soil profile can be obtained. The concept of this procedure is illustrated in Fig. 3-5-2 and involves the following steps:

(a) For a multi-layer soil on bedrock [Fig. 3-5-2 (a)], the top two soil layers are assumed to overlie bedrock and can be replaced with an equivalent soil layer using the TTS procedure [i.e., Eqs. (3-2-5), (3-2-6), (3-5-3) and (3-5-4)]. Next, a new multi-layer soil [Fig. 3-5-2 (b)] is formed.

(b) For the new multi-layer soil shown in Fig. 3-5-2 (b), the top two layers are again assumed to overlie bedrock and are replaced by another equivalent single layer using the TTS procedure. Another new multi-layer soil [Fig. 3-5-2 (c)] is then formed.

(c) By successively applying the TTS procedure until the last soil layer is considered, a final equivalent single-layer soil is obtained, as shown in Fig. 3-5-2 (d).

(d) Finally, the Gs_1 and fundamental period for the final single-layer soil can be readily obtained using Eqs. (3-2-1) and (3-2-2), respectively.

The proposed procedure seems more complicated than the current methods introduced in Section 3.2 at first glance. In reality, comparing with the simplest weighted-average method, the proposed procedure just replaces Eq. (3-2-4) by Eq. (3-5-3), adds a simple Eq. (3-5-4), and uses these equations more times. As these equations can be easily implemented in a spreadsheet, the proposed method can be simply used in practical engineering.

In addition, it should be noted that, the developed procedure for Gs_1 is applicable for not only linear analysis but also the equivalent-linear analysis considering soil nonlinearity. For the equivalent-linear analysis, the proposed procedure is applied just using the final strain-compatible shear modulus and damping ratios after the iteration. Many simple equivalent-linear methods have been developed for estimation of soil nonlinearity (i.e. strain-compatible shear modulus and damping ratio) using bedrock

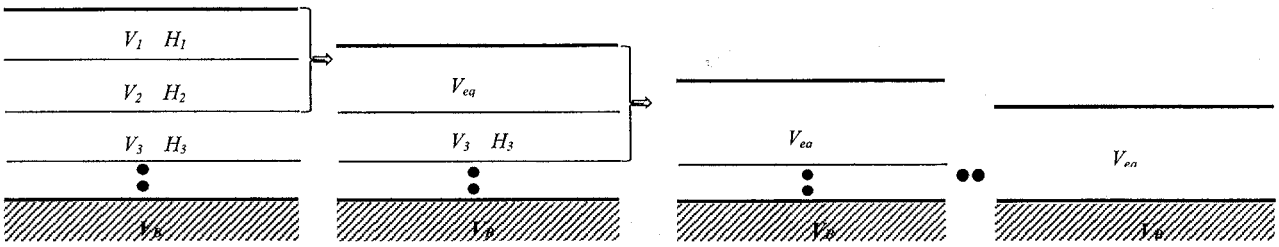

Fig. 3-5-2 Illustration of the concept of replacing a multi-layer soil profile on bedrock with an equivalent single-layer soil profile.

response spectrum directly [29, 67]. The method by Kenji M *et al.* [67] has been introduced in the Japanese seismic code. Here, any one of these simple methods can be used to consider soil nonlinear in estimation of Gs_1.

Application of the proposed method

This section presents an example calculation in which the proposed procedure is applied to a multi-layer soil profile selected from the Strong-motion Seismograph Networks (K-NET, KIK-net) of Japan. The shear wave velocity of this soil profile is shown in Fig. 3-5-3, and the soil data for each layer are listed in Table 3-5-1. For simplicity, nonlinear behavior is not considered here, and the damping ratios of all layers are set to 2%. Each step of the calculation is detailed below, and the results of each step are given in Table 3-5-2.

Step 1: Assuming that the top two soil layers overlie bedrock and since the thickness of the first layer (2 m) is smaller than that of the second layer (3 m), the fundamental period $T_{1\text{-}2L}$ can be calculated using Eq. (3-5-6) as $T_{1\text{-}2L} = 0.102$ s. Using Eqs. (3-2-5), (3-5-3) and (3-5-4), the destiny, shear wave velocity, and thickness of the equivalent single layer can then be obtained as $\rho_{eq} = 1.724$ tf/m^3, $V_{eq} = 181.2$ m/s, and $H_{eq} = 4.616$ m, respectively.

Step 2: The top two layers are replaced by the new layer obtained in Step 1, and the new layer and the third layer are considered as a new two-layer soil profile. As $H_1 < H_2$ (4.616 m < 7 m), $T_{1\text{-}2L}$ can again be calculated using Eq. (3-5-6) as 0.350 s. The destiny, shear wave velocity, and thickness of the new equivalent single layer can then be obtained using Eqs. (3-2-5), (3-5-3) and (3-5-4) as $\rho_{eq} = 1.685$ tf/m^3, $V_{eq} = 141.0$ m/s, and $H_{eq} = 12.34$ m, respectively.

Step 3: The new top two layers are replaced by the single layer obtained in Step 2, and the new layer and the fourth layer are considered as a new two-layer soil profile. This time, as $H_1 > H_2$ (12.34 m > 5 m), $T_{1\text{-}2L}$ can be calculated using Eq. (3-5-5) as $T_{1\text{-}2L} = 0.385$ s. The destiny, shear wave velocity, and thickness of the final single layer can then be calculated using by Eqs. (3-2-5), (3-5-3) and (3-5-4) as $\rho_{eq} = 1.707$ tf/m^3, $V_{eq} = 144.2$ m/s, and $H_{eq} = 13.88$ m, respectively.

Step 4: As nonlinear soil behavior is not considered in this calculation, the equivalent damping ratio is considered to be equal to 2%. Finally, the Gs_1 of the multi-layer soil profile can be calculated

from the Gs_1 of the final equivalent single layer obtained in Step 3 using Eq. (3-2-1). For this example, $Gs_1 = 5.353$.

Using the proposed procedure, the calculations in each step can be easily implemented using spreadsheet software. To verify the accuracy of the Gs_1 obtained above by the new procedure, the transfer function of the example soil profile is calculated by the SHAKE program, and the resulting

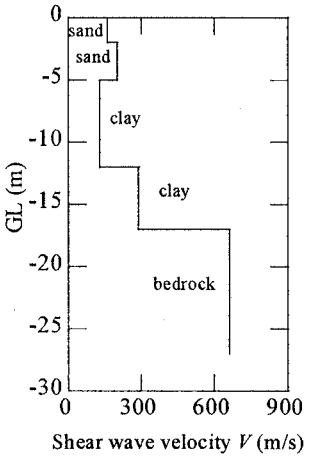

Fig. 3-5-3 Shear wave velocity of the example soil profile.

Table 3-5-1 Soil data for the example soil profile

Layer No.	H_m (m)	V_m (m/s)	ρ_m (tf/m^3)	h_m
1	2	160	1.82	2%
2	3	200	1.66	2%
3	7	130	1.66	2%
4	5	290	1.76	2%
5	10	660	2.40	2%

Table 3-5-2 Results of the example soil profile at each step by the proposed procedure

Step	$T_{1\text{-}2L}$ (s)	ρ_{eq} (tf/m^3)	V_{eq} (m/s)	H_{eq} (m)	Gs_1
1.	0.102	1.724	181.2	4.616	--
2.	0.350	1.685	141.0	12.34	--
3.	0.385	1.707	144.2	13.88	--
4.	0.385	--	--	--	5.353

Table 3-5-3 Comparison of results obtained using different methods

Method	Estimated fundamental period	Estimated Gs_1
1. Code Method	0.352	4.176
2. Proposed Method	0.385	5.353
3. SHAKE	0.394	5.354

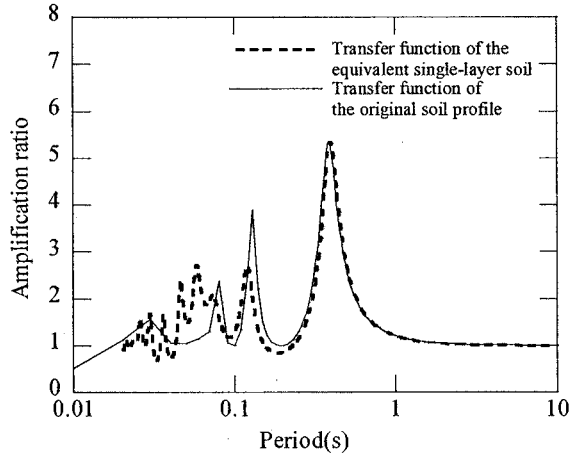

Fig. 3-5-4 Comparison of the transfer function of the equivalent single-layer soil profile with that of the original soil profile.

Gs_1 and fundamental period are listed in Table 3-5-2. The results obtained using the proposed method show good agreement with those obtained using the SHAKE program. The results produced by the method in the Japanese Seismic Code are also listed in Table 3-5-3. Compared to the SHAKE program, the Japanese Seismic Code method underestimates the Gs_1. In addition, the transfer function of the equivalent single-layer soil profile generated using the proposed procedure is compared with that of the original soil profile in Fig. 3-5-4. Fig. 3-5-4 also indicates good agreement in the first resonance peak. The proposed method is further verified in the next section.

3.5.4 Numerical examples using the proposed method

In order to investigate the accuracy of the proposed method, the 67 representative soil profiles selected in section 3.3.4 are used.

The fundamental periods and Gs_1 of the 67 soil profiles are estimated by the proposed procedure and compared with those obtained using the SHAKE program, in Fig.3-5-5. The Gs_1 obtained by the

proposed method are remarkably accurate; 94% of estimated values are within 15% of the SHAKE results. The average error in Gs_1 is only 4.6%, which is considered sufficient for engineering calculation. The accuracy in fundamental period is also remarkably good; 85% of the estimates are within 15% of SHAKE results.

In addition, the fundamental periods and Gs_1 are also estimated using the method in the Japanese Seismic Code and compared with those obtained using the proposed method and the SHAKE program, in Fig.3-5-6. In Figs.3-5-6 (b), most of the Gs_1 estimated by the code method are underestimated by over 15% compared to the SHAKE results, which is consistent with previous studies [27-29]. The average error in Gs_1 estimated by the code method is as large as 17.2%, which is much greater than that for the proposed method. Fig.3-5-6 (b) shows that the errors in fundamental period obtained by

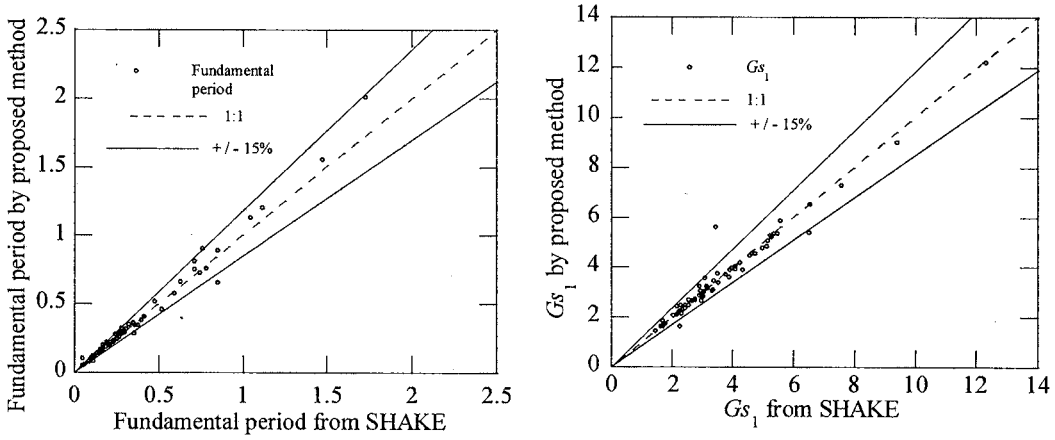

Fig. 3-5-5 Comparisons of fundamental period and Gs_1 calculated using the proposed method and SHAKE program.

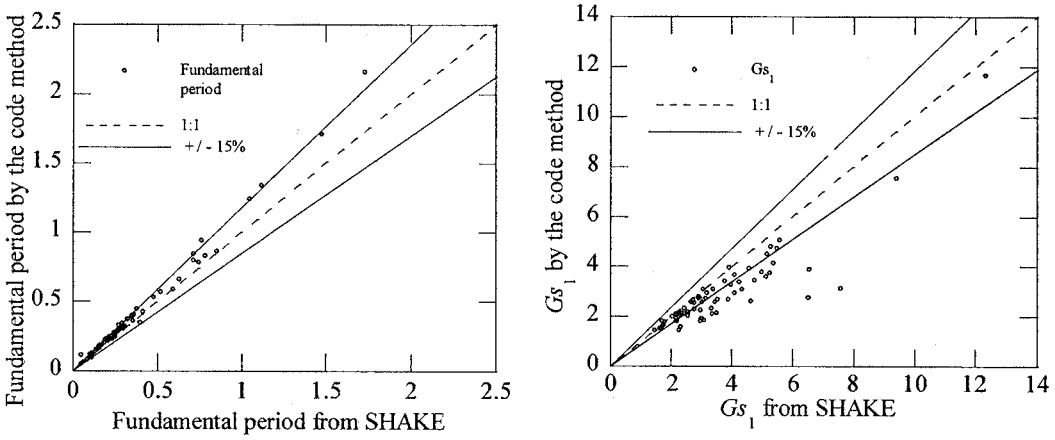

Fig. 3-5-6 Comparisons of fundamental period and Gs_1calculated by the code method and SHAKE program.

the code method are also large, 37% of the results having errors greater than 15%. Generally speaking, the proposed procedure produces accurate estimates of both fundamental period and Gs_1 and is much more accurate than the method used in the Japanese Seismic Code.

3.5.5 Conclusion

The section 3.5 proposes a simple method for estimation of Gs_1 of multi-layer soil profiles. The main conclusions are summarized as follows:

(a) A procedure to replace a two-layer soil profile on bedrock with an equivalent single-layer soil profile with the same Gs_1 and fundamental period is developed.

(b) Based on the developed TTS procedure, a simple procedure for estimating the Gs_1 of a multi-layer soil profile is proposed. The proposed procedure is applied in an example calculation. It is found that the procedure can be easily implemented in a spreadsheet, and the estimated results are highly accurate.

(c) To investigate the validity of the proposed method, the Gs_1 and fundamental periods of 67 representative soil profiles are estimated. The proposed method shows remarkably good accuracy in estimating both the Gs_1 and fundamental period and is clearly more accurate than the current code method.

Chapter 4

Evaluation of soil nonlinear behavior in estimation of site effects

4.1 Introduction

In chapter 3, the methods for estimation of the first resonance peak are developed without considering soil nonlinear behavior. Actually, soil behaves nonlinearly even at small shear-strain level, and the soil nonlinearity can significantly influence the site response. Thus, it is necessary to take into account the nonlinear effect in estimation of site effects.

In this chapter, a simple procedure is developed to consider the soil nonlinear behavior in estimation of site effects. This chapter is organized as follows. Firstly, a response spectrum method is developed to estimate the soil nonlinear behavior, in Section 4.2. During the application of this method, as the first mode shape is necessary; in Section 4.3, a simple method for estimating the first mode shape of layered soil profiles is proposed,. Then, the validity of the proposed method for soil nonlinear behavior is investigated using many actual soil profiles, in Section 4.4. In addition, in Section 4.5, the validity of the total proposed method for site effects are demonstrated by estimating response spectra of several actual reprehensive soil profiles.

4.2 Estimation of soil nonlinear behavior

4.2.1 Soil shear modulus degradation and damping

Nonlinear behavior of soil is often characterized as shear modulus degradation and energy dissipation (damping) depending on the shear strains. And, the soil shear strain is in turn dependent on intensity of bedrock motion that is generally represented by a design response spectrum in seismic codes. In this section, a simple procedure is developed to estimate the soil shear modulus degradation and damping according to the bedrock response spectrum.

To incorporate the strain-dependent soil properties in site response analysis, the equivalent-linear approach implemented in the popular SHAKE program [57] is used in this study. The equivalent-linear approach is based on the assumption that the nonlinear soil response can be simulated by a linear elastic mode with damping, provided that its constants are assigned according to the average strain level achieved. The average shear strain, γ_{eq}, is assumed to be constant throughout the excitation and is typically taken to be 0.65 times the maximum strain, γ_{max}, expressed as:

$$\gamma_{eq} = 0.65\gamma_{\max} \tag{4-2-1}$$

Then, to calculate the maximum shear strain of soil γ_{max} according to the bedrock response spectrum, the response spectrum method is adopted in this work. The method uses the bedrock response spectrum directly instead of transforming it to time-history accelerations or power spectrum density. Furthermore, as site response is dominated by the first vibration mode for most cases [68], for simplify, soil response is considered approximately equal with that of the first vibration mode. Thus, maximum soil displacement profile, $u(z)$, can be approximately calculated as:

$$u(z) = \left(\frac{T_1}{2\pi}\right)^2 S_{a0}(T_1)F(h')p_1X_1 \tag{4-2-2}$$

where S_{a0} is 5% damped acceleration response spectrum at bedrock; p_1 and X_1, respectively, are the fundamental mode shape and corresponding participation factor. And, F is damping modification factor (DMF) to adjust elastic response spectral values corresponding to 5% of damping to other damping levels. Many simple equations for DMF are proposed and introduced into different seismic codes [69]. And recently, a number of more rational empirical equations are developed using recorded ground motion, considering the structural period-, magnitude-, site condition- and source distance-dependent properties [70-73]. Nevertheless, for simplify, the simple equation in Japanese seismic code [59] is used to estimate values of DMF, expressed as:

$$F(h') = \frac{1.5}{1+10h'} \tag{4-2-3}$$

In this equation, h' is an equivalent damping estimated by:

$$h' = h + \xi_1 \tag{4-2-4}$$

In this study, the h' is defined to account for not only the soil material damping but also the radiation damping. The radiation damping representing the wave energy reflected back into the bedrock half-space is converted approximately into an equivalent material damping ratio ξ_1, which will be introduced in detail in section 4.2.2. And, the soil material damping that is different for each soil layer is accounted for by an equivalent damping ratio for the first mode, h. For the unclassical damped soil system, the damping ratio h is evaluated, as suggested by [58] for system composed of elements with different damping, by considering a weighted value of the material damming of each layer according to the following formula:

$$h = \frac{\sum_{i=1}^{n-1} h_i E_i}{\sum_{i=1}^{n-1} E_i} \tag{4-2-5}$$

where E_i, is the weight that represents the normalized elastic energy stored in ith layer for a deformed shape corresponding to first mode, and can be approximately estimated by:

$$E_i = \frac{G_i (u_i - u_{i+1})^2}{2H_i} \tag{4-2-6}$$

u_i and u_{i+1} are, respectively, the value of maximum soil displacement at upper and lower boundary of ith layer soil, G_i ($= \rho_i V_i^2$) is shear modulus of ith layer soil, H_i is thickness of ith layer soil. And, h_i is the material damping of the ith layer associated with the degradation in the shear modulus and is represented by a strain-dependent equation [59]:

$$h_i = h_{\max}(1 - G_i/G_{i0}) \tag{4-2-7}$$

where $h_{\max}$ is the maximum damping ratio defined at the hypothetical limiting condition where the secant shear modulus approaches zero. In Eq. (4-2-7), only the shear strain dependent hysteretic component of material damping is considered, to simply take account of the viscous component, h_i is defined not less than 0.2%. The G_i / G_0 ratio defining the strain dependent degradation of the soil shear modulus has been generalized by the hyperbolic relationship of Eq. (4-2-8) as proposed originally by Hardin and Drnevich [74],

$$\frac{G_i}{G_{0i}} = \frac{1}{1 + \gamma_{ieq}/\gamma_r} \tag{4-2-8}$$

here, γ_{ieq} is the average shear strain of ith soil layer. γ_r is reference shear strain of soil, the value can be determined according to Japanese seismic code [59]: 0.18% for cohesive soil, and 0.1% for sandy soil. The models of strain-dependent shear modulus and damping are shown in Fig.4-3-1.

Using Eqs. (4-2-2) - (4-2-4), soil maximum displacement profile, $u(z)$, can be obtained. Then, maximum shear strain of ith soil layer, $\gamma_{i\max}$, can be approximately calculated, by assuming values of displacement within every soil layer approximately vary linearly,

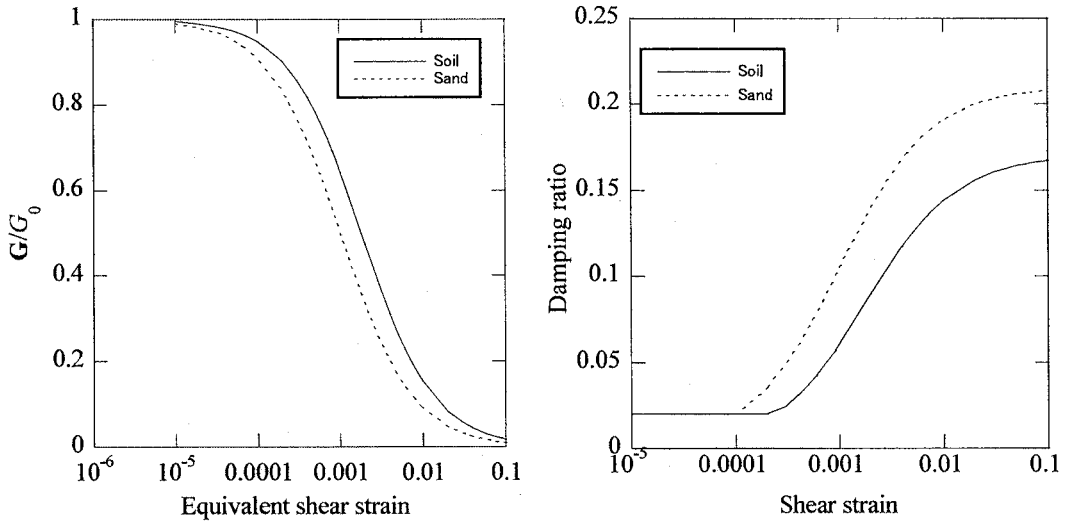

(a) Degradation of the soil shear modulus (b) Soil damping

Fig.4-2-1 Shear modulus degradation and soil damping depending on the shear strains

$$\gamma_{i\max} = \frac{u_i - u_{i+1}}{H_i} \tag{4-2-9}$$

Then, average shear strain, γ_{ieq}, of each soil layer can be obtained using Eq. (4-2-1), and in turn, soil shear modulus degradation and damping can be calculated using the Eqs. (4-2-8) and (4-2-7), respectively.

It should be noted that the developed method is an iterative procedure, since the damping, h, (and hence $F(h')$) is not known *a priori*. The solution start by considering the initial values at low strain level, and the iteration will stop when the difference in the values of shear strain between two successive iterations is less than some specified value. Finally, using the soil properties after convergence, the fundamental period and the first resonance peak considering nonlinear behavior of soil can be obtained by the procedure introduced in section 3.5.

4.2.2 Effect of bedrock rigidity

For layered soil profiles on rigid bedrock half-space, modal analysis (and hence response spectrum analysis of Eq. (4-2-2)) can be used for site response analysis. But, in reality, the bedrock has finite rigidity, energy losses known as radiation damping can be caused by refraction and reflection of seismic waves at the soil-bedrock interface. For this case, modal analysis and thus the response spectrum analysis of Eq. (4-2-2) cannot be used, in theory. In this study, to make the model analysis available, the radiation damping is converged to equivalent material damping ξ_1 as introduced in section 4.2.1, so that a system of layered soil profile on a flexible half space can be replaced by an

equivalent layered soil profile on a rigid half space. And, the equation for the equivalent material damping ξ_1 is derived, in this section.

For modal analysis, if a linear hysteretic damping mechanism can be assumed for the equivalent modal damping, the transfer function of the layered soil system on a rigid half-space can be written as:

$$H(\omega)=\sum_{k=1}^{N_M}\frac{1+2\xi_k(\omega/\omega_k)i}{1-(\omega/\omega_k)^2+2\xi(\omega/\omega_k)i}P_k \tag{4-2-10}$$

where ω_k is the modal frequency, ξ_k is the equivalent material modal damping ratio, P_k is the effective modal participation factor at the ground surface for the kth mode and N_M is the total number of modes used in the analysis. For simplify, assume only the first mode exist, then the transfer function can be simplified as:

$$H(\omega)=\sqrt{\frac{1+4\xi_1^2(\omega/\omega_1)^2}{\left[1-(\omega/\omega_1)^2\right]^2+4\xi_1^2(\omega/\omega_1)^2}} \tag{4-2-11}$$

In order to convert the radiation damping into equivalent modal damping ratio, value of $H(\omega)$ in Eq. (4-2-11) at the fundamental frequency is approximated by first resonance peak obtained using the procedure introduce in section 3.5, i.e.

$$Gs_1=\sqrt{\frac{1+4\xi_1^2}{4\xi_1^2}} \tag{4-2-12}$$

Then, the equivalent damping ratio can be solved from

$$\xi_1=\frac{1}{2\sqrt{Gs_1^2-1}} \tag{4-2-13}$$

The consideration of converting the radiation damping into equivalent modal damping ratio to make modal analysis available has been used by studies [60, 75], and also equations for the equivalent material damping ratios of each mode were derived by [75]. But, obviously, the simple Eq. (4-2-13) using result of Gs_1 obtained by the procedure introduce in section 3.5, is more compatible for this work.

4.3 Fundamental mode shape and participation factor

4.3.1 Introduction

It is noted that, to calculate the maximum displacement using Eq. (4-2-2), the fundamental mode shape and corresponding participation factor must be estimated firstly. In principle, the fundamental mode shape and corresponding participation factor can be exactly obtained by solving equilibrium equations of free vibration, or accurately estimated using an eigenvalue analysis by discretizing the continuous soil profile into lumped-parameter multi-degree-of-freedom (MDOF) model. But, implementation of these methods is generally too complicated for practical engineering.

Numerous studies focused on simple approaches for the fundamental period of layered soil profiles [62, 66, 76], but there are still few studies about simple approaches for the fundamental mode shape. Dobry et al. [76] concluded that the Simplified Version of Rayleigh Procedure [76] can give accurate solution of both the fundamental period and mode shape. The simplified Rayleigh procedure is iterative [66]. Subsequently, Hadjian [66] developed another direct approach to calculate the fundamental mode shape. Using the Hadjian method, values of the fundamental mode shape are assumed to vary linearly along with depth within each soil layer. For soil profiles with high soil layers, to reduce the error caused by the 'linearly vary' assumption, the high layers are generally further discretized into thinner layers. However, contrarily, the more layers the soil profile be discretized, the larger the error in estimation of the fundamental mode shape will be. The reason is as follows. The Hadjian method estimates the fundamental mode shape using results of the fundamental period calculated by the Successive Use of Two-Layer Solution Procedure by Madera [65]. During the application of the Madera procedure [65], at each step of replacing the top two layers with an equivalent single layer, the top two layers are assumed to lie on a rigid rock, when in fact they lie on a soil layer with limited stiffness. And, the times of the rigid-rock assumption be used are positively correlated to the number of soil layers. Thus, the more layers the soil profile be discretized, the more the assumptions used. The errors in estimation of the fundamental period can accumulate along with the times of the assumption be used, and the accumulated error will be transmitted to the fundamental mode shape. So, the more layers results in the larger error in estimation of the fundamental mode shape. Therefore, for the soil profiles with high soil layers, it is difficult to use the Hadjian method to give accurate estimation of the fundamental mode shape.

In this section, a simple method is developed to estimate the fundamental mode shape of layered soil profiles. The rest of this section is organized as follows. Firstly, a new equation for analysis of the natural frequencies and mode shapes of layered soil profiles is derived, in section 4.3.2. Then, in Section 4.3.3, by conjunctively using the derived equation and the procedure developed in section 3.5, a new approach is developed to estimate the fundamental mode shape. In Section 4.3.4, the accuracy of the proposed procedure is investigated and compared with that of the Hadjian method, using 67 representative layered soil profiles. It is found that, results by the proposed method agree

very well with accurate results, and the accuracy of the proposed method is better than those of the Hadjian method especially for soil profiles with high soil layers.

4.3.2 An equation for natural frequencies and mode shapes

To develop a method for estimation of the fundamental mode shape of layered soil profiles, an equation for estimation of the natural frequencies and mode shapes is derived, in this section. To derive the equation, a multi-layer soil profile on rigid bedrock as shown in Fig. 4-3-1 is considered. The layered soil profile is considered to vibrate freely in the natural mode. Then, according to the equilibrium between inertia force and elastic force at any *i*th interface, inertia force of the soil layers above *i*th interface, $F(z_i)$, is equal to elastic force, $T(z_i)$, acting at the *i*th interface,

$$F(z_i) = T(z_i) \tag{4-3-1}$$

where, z_i is the depth of the *i*th interface. Inertia force of the soil layers above the *i*th interface is calculated by:

$$F(z_i) = \int_{z_1}^{z_2} -\rho(z)\frac{\partial^2 u}{\partial t^2}dz + \int_{z_2}^{z_3} -\rho(z)\frac{\partial^2 u}{\partial t^2}dz + \ldots + \int_{z_{i-1}}^{z_i} -\rho(z)\frac{\partial^2 u}{\partial t^2}dz \tag{4-3-2}$$

here, u is displacement of soil layers given by:

$$u(z,t) = X(z)\sin(\omega t + \varphi) \tag{4-3-3}$$

and, ω represents the natural frequency of the layered soil profile, X represents the corresponding mode shape. Submitting Eq. (4-3-3) into Eq. (4-3-2), $F(z_i)$, can be expressed as:

$$F(z_i) = \left(\int_{z_1}^{z_2} \rho(z)\omega^2 X(z)dz + \int_{z_2}^{z_3} \rho(z)\omega^2 X(z)dz + \ldots + \int_{z_{i-1}}^{z_i} \rho(z)\omega^2 X(z)dz\right)\sin(\omega t + \varphi) \tag{4-3-4}$$

For simplify, value of the mode shape, X, is assumed vary linearly with depth within each soil layer, then Eq. (4-3-4) can be simplified as:

$$F(z_i) = \frac{1}{2}\omega^2 \sin(\omega t + \varphi)\sum_{j=1}^{i-1}\rho_j(X(z_j) + X(z_{j+1}))H_j \tag{4-3-5}$$

Similarly, elastic forces acting at the *i*th interface is simply calculated by:

$$T(z_i) = \sin(\omega t + \varphi)\frac{G_i}{H_i}(X(z_i) - X(z_{i+1})) \tag{4-3-6}$$

where G_i is the shear modulus of *i*th layer soil, $G_i = \rho_i V_i^2$, and V_i is the shear wave velocity. Then, submitting Eqs. (4-3-5) and (4-3-6) into Eq. (4-3-1),

$$\frac{G_i}{H_i}(X(z_i) - X(z_{i+1})) = \frac{1}{2}\omega^2 \sum_{j=1}^{i-1}\rho_j(X(z_j) + X(z_{j+1}))H_j \tag{4-3-7}$$

From Eq. (4-3-7), the following equation can be obtained:

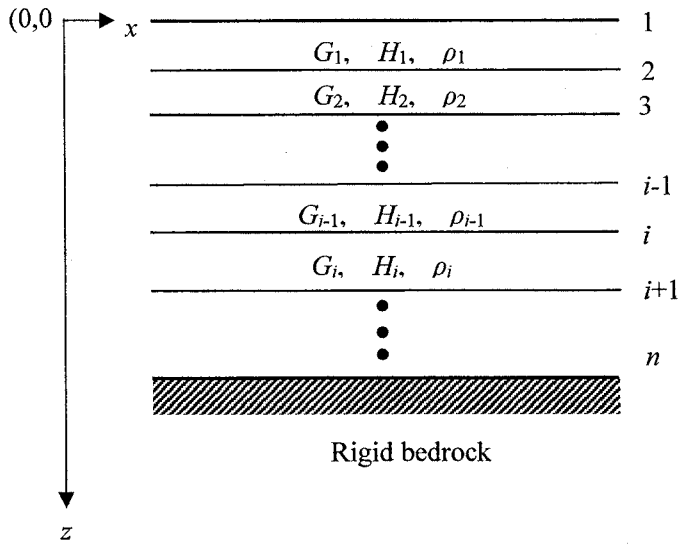

Fig.4-3-1 A multi-layer soil profile on rigid bedrock

$$X(z_{i+1}) = X(z_i) - \frac{H_i K_i}{G_i} \tag{4-3-8}$$

$$K_i = \frac{1}{2}\omega^2 \sum_{j=1}^{i-1} \rho_j (X(z_j) + X(z_{j+1})) H_j \tag{4-3-9}$$

In Eqs. (4-3-8) and (4-3-9), as both the fundamental frequency, ω, and mode shape, X, are unknown; in theory, the equation can't be solved directly. The fundamental frequency, ω, and the mode shape, X, can be obtained by following steps:

(1) Assume a value for frequency, ω, then all values of the fundamental mode shape, $X(z_i)$, can be recursively calculated by stetting the value at surface as 1, i.e. $X(z_1)$=1.

(2) As is well known that, the value of the fundamental mode shape at base, $X(z_n)$, equals 0 for natural vibration, thus, if $X(z_n)$ is equal to zero, the initial assumption of ω is the correct natural frequency of vibration, otherwise, the assumed value of ω is adjusted.

(3) Repeat the steps (1) and (2), until obtained $X(z_n)$ equals 0. Then, the natural frequencies and mode shapes can be obtained.

To illustrate how to adjust the assumed value of frequency, ω, according to the calculated value of $X(z_n)$, an example calculation using Eqs. (4-3-8) and (4-3-9) is conducted. Shear wave velocity profile of the used example site is shown in Fig. 4-3-2. And, obtained results are shown in Fig. 4-3-3. In this figure, horizontal ordinate represents the assumed frequency ω, and longitudinal coordinates represents the calculated value of $X(z_n)$. It can be known that, if estimated value of $X(z_n)$ is positive, the assumed ω is smaller than the true frequency in the case of odd modes, or the assumed frequency is larger than the true frequency in case of even modes. Similarly, if estimated value of $X(z_n)$ is

negative, the assumed ω is larger than the true frequency in the case of odd modes, or the assumed frequency is smaller than the true frequency in case of even modes. Based on this law, any natural periods and mode shapes can be found gradually.

In principle, the developed method can give any natural frequencies and mode shapes with any desired degree of accuracy. Since values of the fundamental mode shape between two adjacent soil interfaces are assumed vary linearly during the derivation of Eqs. (4-3-5) and (4-3-6); accuracy of the obtained result by Eqs. (4-3-8) and (4-3-9) totally depends on the soil-layer height be discretized.

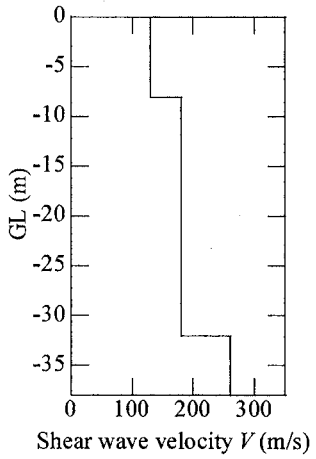

Fig.4-3-2 Shear wave velocity of an example soil profile

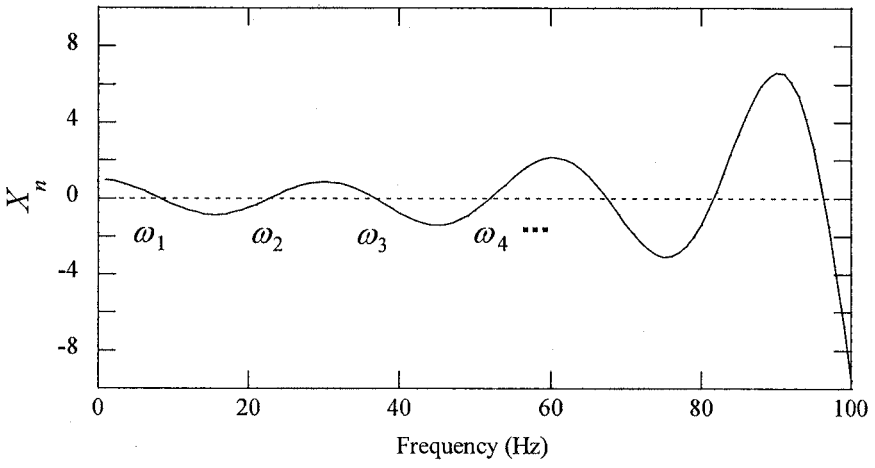

Fig.4-3-3 Relationship between estimated values of the fundamental mode shape at base with assumed frequencies

4.3.3 A method for the fundamental mode shape and participation factor

Although the method developed in the Section 4.3.2 can give any natural frequencies and mode

shapes with any desired degree of accuracy, the repeated assumption and judgment make this method difficult used in practical engineering. It is noted that, if exact value of the fundamental frequency is given, Eqs. (4-3-8) and (4-3-9) can directly give results of the fundamental mode shape with any desired degree of accuracy. The proposed procedure in section 3.5 was found can predict the fundamental frequency accurately and easily [65, 66, 76]. Thus, if the proposed procedure in section 3.5 and Eqs. (4-3-8) and (4-3-9) are conjunctively used, both the fundamental frequency and mode shape can be calculated easily and accurately.

Estimation of the fundamental mode shape

By conjunctively using the proposed procedure in section 3.5 and Eqs. (4-3-8) and (4-3-9), a procedure including the following steps can be proposed to estimate the fundamental period and mode shape of layered soil profiles.

(1) Estimate the fundamental period using the proposed procedure in section 3.5.

(2) Submit the obtained result of the fundamental period into Eqs. (4-3-8) and (4-3-9), the fundamental mode shape can be given directly.

(3) As the fundamental period estimated by the proposed procedure in section 3.5 is not totally exact, error of the fundamental period, in turn, error of the fundamental mode shape will be in existent. In order to reduce the error, the obtained fundamental mode shape is further modified simply. As value of the fundamental mode shape at base, $X(z_n)$, should equal 0 for natural vibration in theory, the obtained values of the fundamental mode shape are modified by:

$$X_1^m(z_i) = X_1(z_i) - X_1(z_n) \tag{4-3-10}$$

where $X_{1\text{-}i}^m$ is the modified value of the fundamental mode shape at ith soil interface.

In addition, a simple equation for estimation of the participation factor corresponding to the first mode of layered soil profiles is also derived. As is well known, for a lamped-parameter system, the participation factor, p, is estimated by:

$$p = \frac{\phi^T \{m_i\}}{\phi^T [M] \phi} \tag{4-3-11}$$

where, $\{m_i\}$ is the vector of masses, and $[M]$ is the associated diagonal mass matrix, ϕ is the mode shape. For a layered soil profile, masses are considered concentrate at the layer interface, mass m_i at ith interface is estimated by $m_i = 0.5(\rho_{i-1}H_{i-1} + \rho_i H_i)$. Then, according to Eq. (4-3-12), an equation for the participation factor of layered soil profiles, p_L, can be derived as:

$$p_L = \frac{X_1^m(z_1)\rho_1 H_1 + \sum_{i=2}^{n-1}(\rho_{i-1}H_{i-1} + \rho_i H_i)X_1^m(z_i)}{(X_1^m(z_1))^2 \rho_1 H_1 + \sum_{i=2}^{n-1}(\rho_{i-1}H_{i-1} + \rho_i H_i)(X_1^m(z_i))^2} \tag{4-3-12}$$

4.3.4 Numerical examples and discussions

Numerical examples

In order to investigate the accuracy of the proposed method, 4 representative soil profiles of the selected 67 soil profiles selected from Strong-motion Seismograph Networks (K-NET, KIK-net) [35] are used. The soil data for the four sites are listed in Table 4-3-1. Then, the fundamental mode shape is estimated by discretizing the soil profiles into a number of 1 m-height soil layers. The results obtained by the proposed method are compared with those obtained using the exact Rayleigh Procedure [76], in Fig. 4-3-4. In Figs. 4-3-4(a)-(b), horizontal ordinate represents the estimated values of the fundamental mode shape with the one at ground surface normalized to 1, and longitudinal coordinates represents the depth. It is found that, results by the proposed method agree very well with those obtained using the Rayleigh Procedure. The fundamental mode shapes are also estimated by the Hadjian method [66], the obtained results are compared with those obtained using the proposed method and the Rayleigh Procedure in Fig. 4-3-4. Fig. 4-3-4 shows that, the fundamental mode shapes estimated by the proposed method are much closer to exact values than those by the Hadjian method.

In order to further compare the accuracies of the proposed method and the Hadjian method in estimation of the fundamental mode shape, other 63 representative soil profiles are further selected from Strong-motion Seismograph Networks (K-NET, KIK-net) [35]. In addition, a parameter r is introduced to measure the accuracy in estimation of the fundamental mode shape, equation for r is expressed as

$$r = \sum_{i=1}^{n} \frac{(X_{1-i}^{EV} - X_{1-i}^{ES})^2}{X_{1-i}^{ES}} \tag{4-3-13}$$

where $X^{EV}{}_{1\text{-}i}$, $_1X^{ES}{}_{1\text{-}i}$, respectively, represent the evaluated and exact value of the fundamental mode

Table 4-3-1 Soil data of the four representative soil profiles

Site No.	Layer No. i	Thickness H_i (m)	Shear wave velocity V_i (m/s)	Density ρ_i (KN/m^3)
Site-1	1	8	130	18.62
	2	24	180	18.62
	3	6	260	18.62
Site-2	1	22	170	18.62
	2	6	250	18.62
	3	22	300	18.62
Site-3	1	6	136	15.68
	2	30	267	18.62
	3	16	292	18.62
Site-4	1	20	110	15.68
	2	170	380	18.62

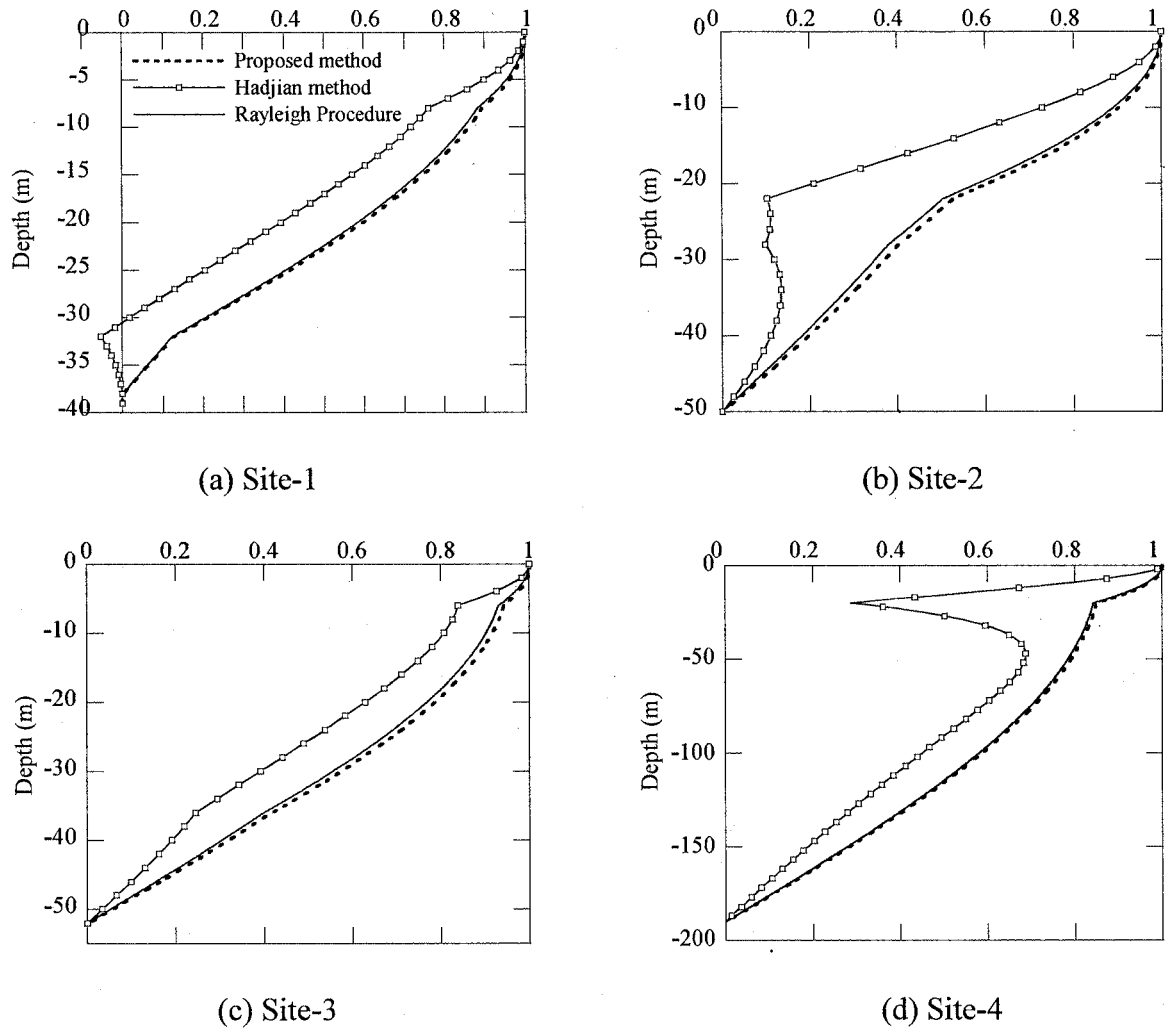

Fig.4-3-4 Fundamental mode shapes of four representative soil profiles estimated by different methods

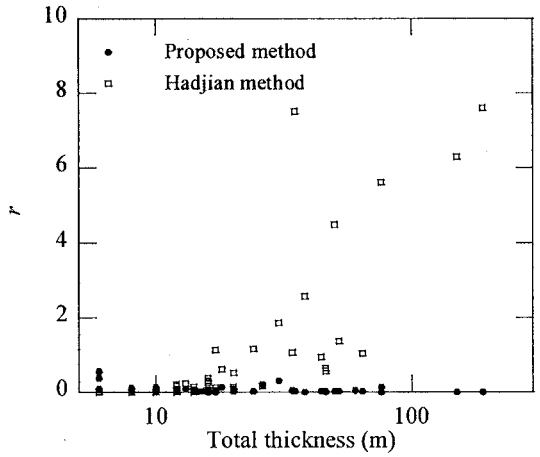

Fig.4-3-5 Values of *r* for the 67 soil profiles

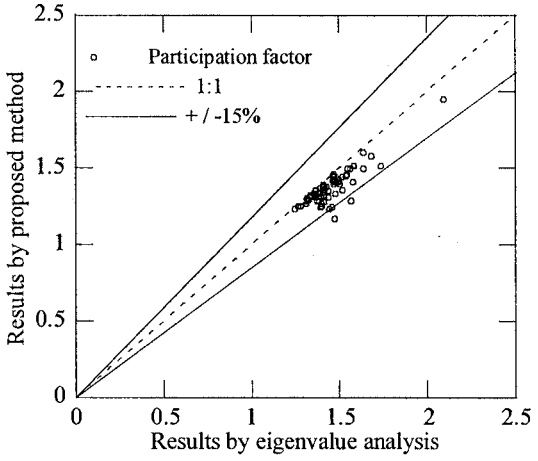

Fig.4-3-6 Comparisons of participation factors calculated by the proposed method and eigenvalue analysis

shape at *i*th soil interface. It can be known from Eq. (4-3-13) that, the closer to 0 the value r is, the more accurate the calculated results are.

Values r of the total 67 soil profiles corresponding to the two simple methods are calculated by Eq. (4-3-13), and obtained results are shown in Fig.4-3-5. The horizontal ordinate represents the total thickness of estimated soil profiles, and the longitudinal coordinates represents calculated value of r. For the soil profiles with total thickness less than about 20 m, values of r corresponding to the two methods have no obvious difference, which means that the accuracy of the two methods are nearly same. For the soil profiles with total thickness larger than about 20 m, values of r corresponding to the proposed method are obviously less than those corresponding to the Hadjian method, which means that results estimated by the proposed method are more accurate. In addition, it can be seen that, with the total thickness of soil profiles become thicker, values of r of the Hadjian method become larger. This means that errors by the Hadjian method are larger for higher soil profiles.

In addition, participation factors corresponding to the first mode of the 67 soil profiles are estimated by the simple Eq. (4-3-12). In Fig. 4-3-6, the obtained results are compared with those estimated by an eigenvalue analysis by discretizing the continuous soil profile into lumped-parameter MDOF model. The obtained modal participation factors are remarkably accurate; 97% of the estimated values are within 15% of the results by eigenvalue analysis. In other words, ± 15% can be regarded as the limits of the 97% confidence level.

Discussions

In the previous section, a part of values of the fundamental mode shape estimated by the Hadjian method are found deviate significantly from exact ones, especially for high soil profiles. In following, the reason for the deviation as well as area of application of the Hadjian method is clarified.

The Hadjian method [66] estimates the fundamental mode shape, $X_1(z)$, of layered soil profiles, by following equation:

$$X_1(z_i) = \cos(\frac{\pi}{2}\frac{T_{1-i}}{T_{1-n}}) \tag{4-3-14}$$

where, $X_1(z_i)$ is the value of the fundamental mode shape at ith soil interface as shown in Fig. 4-3-1. And, T_{1-i} represents the decoupled fundamental period of the soil layers from the first interface (ground surface) to the ith interface, T_{1-n} represents the fundamental period of the total soil profile. The Hadjian method estimates the fundamental mode shape using results of the fundamental period calculated by the Madera method [65]. And, all values of T_{1-i} (i=1~n) are obtained during the application of the Madera procedure.

Eq. (4-3-14) gives results of the fundamental model shape at the soil interfaces, for values between two adjacent interfaces, values of the fundamental mode shape are assumed vary linearly along with depth. For soil profiles with high soil layers, to reduce the error caused by the 'linearly vary' assumption, the high layers need be discretized into thinner layers. But, during the application of the Madera procedure, at each step of replacing the top two layers with an equivalent single layer, the top two layers are assumed to lie on rigid rock, when in fact they lie on a soil layer with limited stiffness. In addition, the times of the rigid-rock assumption be used are positively correlated to the number of soil layers. Thus, the more layers the soil profile be discretized, the more the rigid-rock assumptions will be used. The errors in estimation of the fundamental period can accumulate along with the times of the assumption be used, and the accumulated error will be transmitted to the fundamental mode shape. So, the more layers results in the larger error in estimation of the fundamental mode shape. And therefore, for the soil profiles with high soil layers in the previous section, errors of the fundamental mode shape are significant.

To verify the above inference, the 67 soil profiles are discretized into different thickness, then fundamental periods are calculated by the Madera procedure. The obtained results are compared with those obtained by the Rayleigh Procedure in Fig. 4-3-7. As shows in Fig. 4-3-7 (a), accuracies of results corresponding to the soil profiles without be discretized are remarkably good. But, error of the fundamental period increases with number of soil layers be discretized as shown in Fig. 4-3-7 (b). This observation supports the inference that error of the fundamental period accumulates with times of the rigid-rock assumptions be used. In addition, fundamental mode shapes of the four representative soil profiles in Fig.4-3-4 without be discretized, are recalculated by the Hadjian method, and results are shown in Fig. 4-3-8. The results can be found are more accurate than those of soil profiles be discretized, although the errors for high soil layers are still significant. This observation supports the inference that, error of the fundamental period can be transmitted to the fundamental mode shape.

Thus, for soil profiles with high soil layers, such as the four soil profiles used pre, it is difficult to use the Hadjian method to calculate the fundamental mode shape accurately. Because, to reduce the

error cause by the 'linearly vary' assumption, soil layers should be discretized into thinner layers; but unfortunately, error of estimated results will become much bigger due to the accumulation of error by using the rigid-rock assumption more times. But for estimation of the fundamental period only, as soil layers need not be discretized into thinner soil layers, and original numbers of soil layers are not that much for general soil profiles; the Madera procedure can give accurate estimation of the fundamental period as shown in Fig. 4-3-7 (a).

Actually, same with the Hadjian method, the proposed method also assumes that values of the fundamental mode shape between two adjacent soil interfaces vary linearly along with depth. Thus, for soil profiles with high soil layers, to reduce the error caused by the 'linearly vary' assumption, the high layers also need be discretized into thinner layers. But, it should be noted that, Eqs. (4-3-8) and (4-3-9) only need the final result of the fundamental period by the Madera procedure, instead of all results of the decoupled fundamental period, $T_{1\text{-}i}$ corresponding to every analyzed interfaces as the Hadjian method (Eq. (4-3-14)). This means that, although the soil layers are discretized into thinner layers during the estimation of the fundamental mode shape, during the estimation of the fundamental period they needn't be discretized thinner. Thus, the proposed method can avoid using the rigid-rock assumption more times, in turn, accumulation of the error.

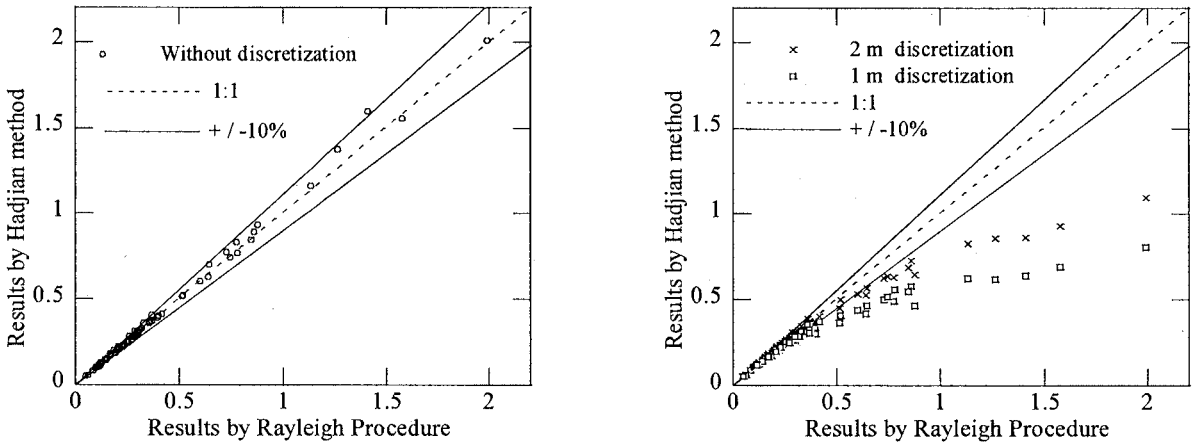

Fig.4-3-7 Fundamental periods of the 67 soil profiles with soil layers be discretized into different thickness by the Madera procedure using the approximate equations by Hadjian

4.3.5 Conclusions

In this section, a simple method is developed to calculate the fundamental mode shape of layered soil profiles. On the basis of the preceding discussion, one can draw the following conclusions:

(1) A new equation is derived for estimation of the natural frequencies and mode shapes of layered soil profiles.

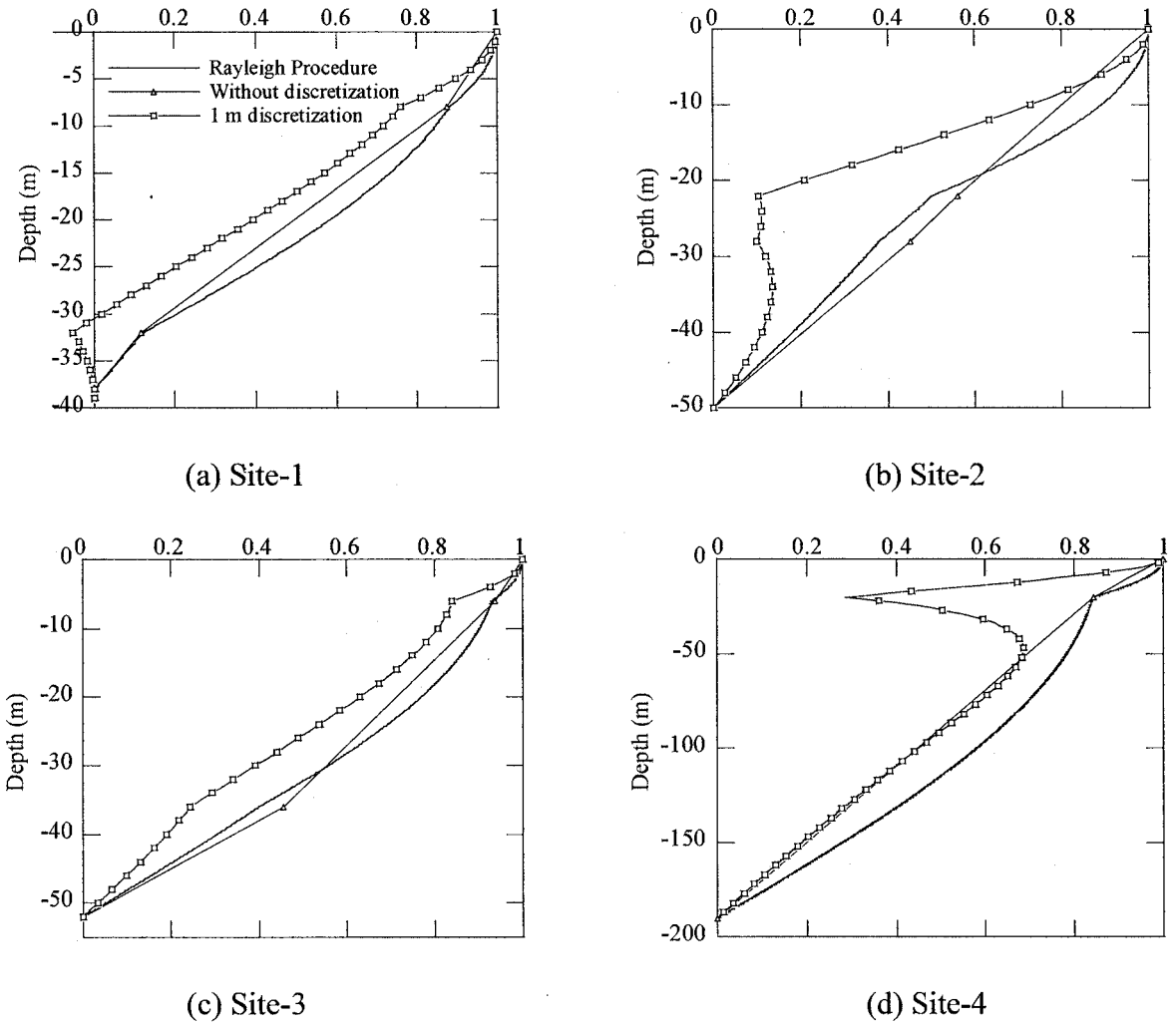

Fig.4-3-8 Fundamental mode shapes of the four soil profiles with soil layers be discretized into different thickness by the Hadjian method

(2) By conjunctively using the derived equation and the proposed procedure in section 3.5, a simple approach is developed to estimate the fundamental mode shape. The proposed approach can be conveniently implemented in simple spreadsheets and easily used by practicing engineers.

(3) The accuracy of the proposed approach is investigated using a lot of representative layered soil profiles. Results by the proposed method are found agree very well with accurate results.

(4) Using the approximate equations proposed by Hadjian, for the estimation of the fundamental mode shape, the Hadjian method is difficult used for analysis of soil profiles with high soil layers.

4.4 Validation of the proposed method

In order to investigate the accuracy of the proposed method for estimation of nonlinear effect of soil, the 67 representative soil profiles selected from Strong-motion Seismograph Networks (K-NET, KIK-net) [35] are used. Two levels of input motions, level 1 and level 2, defined in Japanese seismic code are considered in the accuracy investigation. For the proposed method, the acceleration response spectra specified at engineering bedrock are used directly. For the SHAKE program used for calibration, the bedrock response spectra are converted to corresponding time-history motions. And, duration of the level-1 and level-2 time-history motion are respectively, 60s and 120s. The proposed method in section 3.5 are used to calculate the fundamental period and first resonance peak.

The fundamental periods and first resonance peaks of the 67 soil profiles under the two levels of seismic motions, are estimated by the proposed procedure and compared with those obtained using

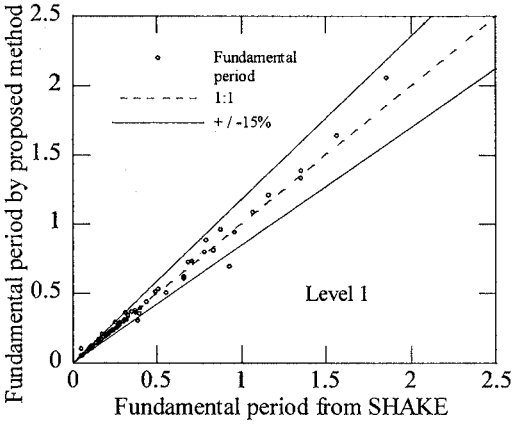

(a) Fundamental periods for the level-1 motion

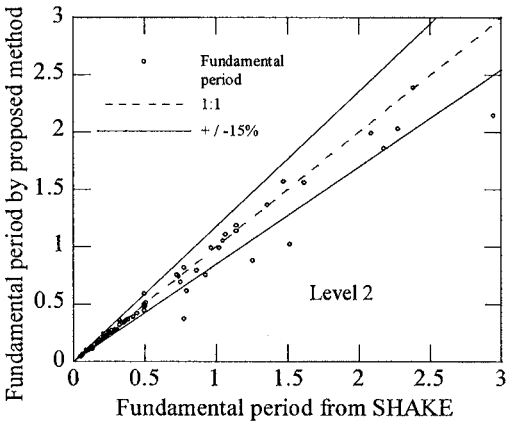

(b) Fundamental periods for the level-2 motion

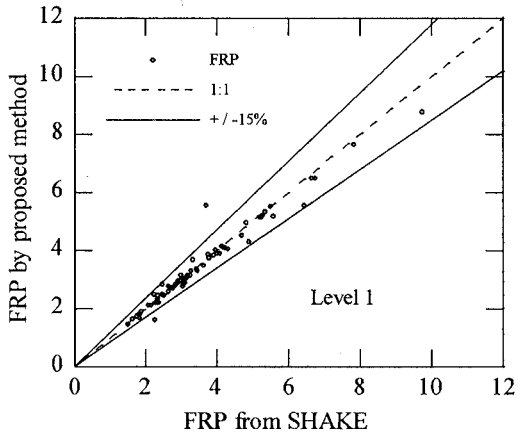

(c) First resonance peaks for the level-1 motion

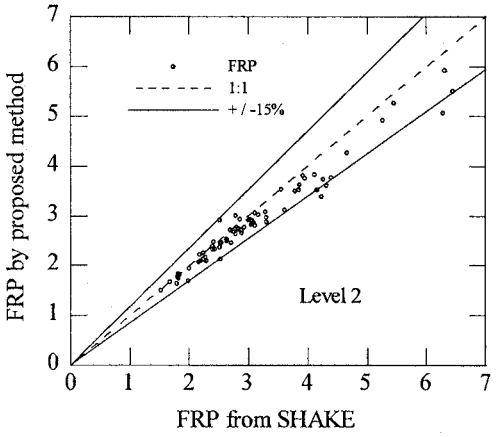

(d) First resonance peaks for the level-2 motion

Fig. 4-4-1 Comparisons of fundamental period and FRP calculated using the proposed method and SHAKE program.

the SHAKE program (Fig. 4-4-1). Figs. 4-4-1(a) - (d) show that, the obtained fundamental periods and first resonance peak under seismic motion of each level are remarkably accurate. 93% of the estimated fundamental period and 97% of the estimated first resonance peaks for the level-1 seismic motion, are within 15% of the SHAKE results. And. 88% of the estimated fundamental period and 94% of the estimated first resonance peaks for the level-2 seismic motion, are within 15% of the SHAKE results. In addition, the average error in both fundamental period and first resonance peak are less than 6.7%, for each level of seismic motions. The accuracy is considered sufficient for engineering calculation.

The good accuracy in every levels of motions indicates that, not only (1) the procedure introduced in section 3.5 gives accurate estimation of fundamental period and first resonance peak, which has been validated for linear analysis, but also (2) the developed procedure in Chapter 4 estimates nonlinear effect of soil accurately.

4.5 Free-field response spectra by the proposed method

In order to investigate the accuracy of the proposed method for estimating nonlinear site effects, 4 actual sites with detail data be surveyed by PS logging are used [28]. The shear wave velocity profiles and soil properties of each sites are presented in Fig. 4-5-1. For simplify, only the level-2 input motions defined in Japanese seismic code are considered in this section, and 10 time-history motions used for the SHAKE analysis are converted from the bedrock response spectrum.

RSRs of the four sites are calculated by the proposed methods, then response spectra at ground surface of each site are obtained. Then, the calculated results by the proposed method are compared with those obtained using the SHAKE program, in Fig. 4-5-2. It can be found that, results of each site by the proposed method agree very well with those by the SHAKE program. To see clearly, only values of response spectra for periods between 0~5s are shown in the figure, in fact values of response spectra for periods between 5~10s also agree very well with those by the SHAKE program. In addition, response spectra at ground surface of each site are also calculated by the method in Japanese seismic code, and the results are also shown in Fig.4-5-2. Same with the conclusion of previous studies [27-29], values of response spectra at fundamental periods are underestimated by the code

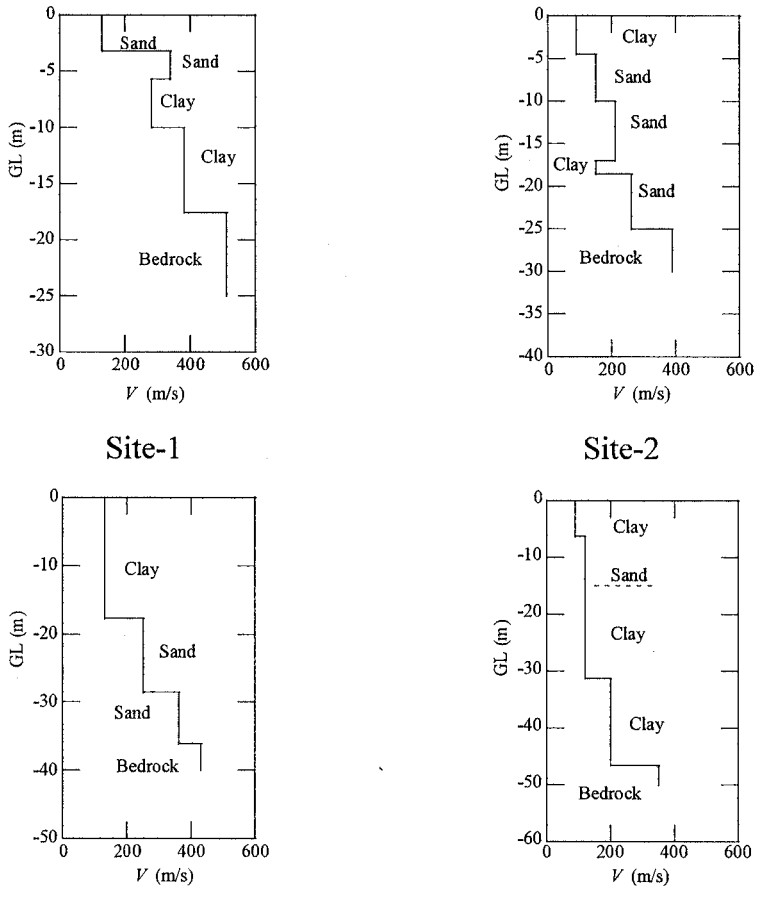

Fig. 4-5-1 Shear wave velocity profiles and soil properties of the four actual sites used for analysis

method, especially for the site-1, site-2 and site-3, in which impedance contrast of the soil layers are large.

For the site-4 that has long fundamental period, values of response spectrum between fundamental period and second natural period are overestimated by the code method; and, the results by the proposed method can be seen clearly agree better with those by the SHAKE. For the other three sites that have short fundamental period, as the space between fundamental period and second natural period is very short, results by the proposed method have no obvious difference with those by the code method.

Although Gs_2 are estimated in different ways, by the proposed method and the code method, values of response spectrum at second natural by the two methods have no obvious difference. This observation indicates that the accuracy of Gs_2 of both the two methods are sufficient for engineering use.

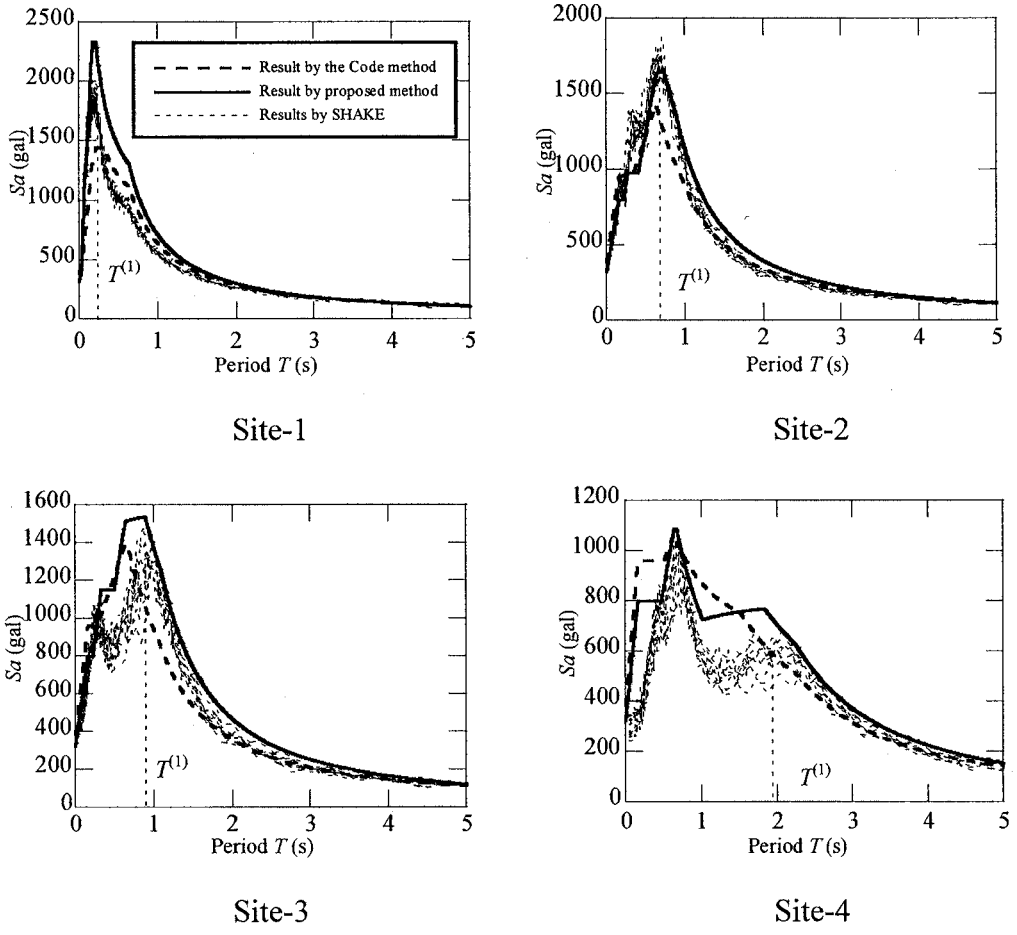

Fig. 4-5-2 Comparison of acceleration response spectra at ground surface of the multi-layer soil profiles calculated by different methods

4.6 Conclusions

In this chapter, a simple procedure for estimation of the soil nonlinear behavior is developed. On the basis of the preceding discussion, one can draw the following conclusions:

(1) A simplified response spectrum method is developed to estimate the soil nonlinear behavior. To make the response spectrum method available, radiation damping caused by refraction and reflection of seismic waves at the soil-bedrock interface, is converged to equivalent material damping.

(2) A simple method is developed to calculate the fundamental mode shape and corresponding participation factor used for calculation of the maximum displacement. The accuracy of the proposed approach is investigated using a lot of representative layered soil profiles. Results by the proposed method are found agree very well with accurate results.

(3) The accuracy of the proposed approach for estimation of soil nonlinear behavior is investigated using a lot of representative layered soil profiles. Results by the proposed method are found agree very well with accurate results.

(4) The accuracy of the proposed method for estimating nonlinear site effects is investigated by calculating free-field response spectra of four example sites. Results by the proposed method are found agree very well with accurate results.

Chapter 5

Fundamental period of MDOF structures

5.1 Introduction

In this chapter, the consideration of estimating the first resonance peak in Chapter 3 is extended to calculate the fundamental period of multiple-degree-of-freedom (MDOF) system.

The fundamental period is a key parameter for the seismic design of a building structure using the equivalent-lateral-force procedure; in principle, it can be accurately evaluated by means of an eigenvalue analysis [77] on a structural model. In most building-design projects, since the building's period cannot be analytically calculated before it has been designed, accurate computation is generally not possible in the preliminary design stage, and, typically, simple formulae for the fundamental period are used to initiate the design process. These simple formulae also serve as a basis for limiting the period from a finite-element model by applying the upper-bound factor suggested in the 2003 NEHRP Recommended Provisions for Seismic Regulations for New Buildings and subsequently in ASCE 7-05 [15]. Therefore, at present, simple formulae for estimating the fundamental period with good accuracy play an important role in structural design [78, 79].

Many researchers have previously proposed such formulae for this purpose. Generally, there are two kinds of simple formulae for the fundamental period: empirical [79-91] and analytical [92-98, 11, 59). A lot of empirical formulae have been developed. Asteris *et al* [80, 81] give an extensive review of these formulae. Empirical formulae adopted in most codes are simply expressed in terms of the height of buildings [98, 11]. Some researchers take into account other parameters apart from the height of building. Kose [84] takes into account the presence of infill walls and frame type. Hatzigeorgiou and Kanapitsas [86] proposed an expression considering the soil flexibility, the influence of shear walls, and the external and internal infill wall. Asteris *et al* [80, 81] proposed a more accurate formula that takes into account the number of stories, the number of span, the span length, the infill wall panel stiffness and the percentage of openings within the infill wall. Further, Asteris *et al* [83] recognized that the vertical geometric irregularity significantly influences the fundamental period, and proposed a reduction factor to quantify this effect.

Analytical formulae also have been adopted in many codes [11, 59, 98]. This chapter focus on the analytical ones, which have generally been developed based on vibration theory for a multiple-

degree-of-freedom (MDOF) system. Among these, Rayleigh's method, Geiger's method, and Dunkerley's method are the three most widely used; the first two of which were specified in the 1997 Uniform Building Code [11], the Japanese seismic code [59], respectively.

In this chapter, the consideration of estimating site effects in Chapter 3 is extended to calculate the fundamental period of MDOF. The rest of this chapter is organized as follows. Firstly, several most widely used simple formulae for estimating the fundamental period are briefly reviewed in Section 5.2. Then, in Section 5.3, the new method is described. In this method, the fundamental period is estimated by replacing the complicated MDOF system with an equivalent single-degree-of-freedom (SDOF) system. Then, to investigate the accuracy of the proposed method, the fundamental periods of numerous MDOF models are estimated by the proposed method in Section 5.4 and compared to their accepted values. Finally, the main results of this study are concluded in Section 5.5.

5.2 Review of the current methods

Many studies have contributed calculation methods for estimating the fundamental period of MDOF systems. This section reviews several most widely used methods briefly.

The first one, Rayleigh's method, is a simple theoretical technique based on energy principles, which was specified in the 1997 Uniform Building Code [11]. To introduce the basic consideration of Rayleigh's method for the fundamental period, consider a MDOF system undergoing free harmonic motion with a fundamental frequency ω_1. The displacement vector $\{x(t)\}$ and velocity vector $\{x'(t)\}$ of the MDOF system corresponding to fundamental vibration are given by

$$\{x(t)\} = \{u\}\sin(\omega_1 t + \varphi_1) \tag{5-2-1}$$

$$\{x'(t)\} = \{u\}\omega_1 \cos(\omega_1 t + \varphi_1) \tag{5-2-2}$$

where $\{u\}$ is a displacement vector representing the fundamental mode shape corresponding to fundamental vibration and φ_1 is the phase angle of the harmonic vibration.

Then, the maximum kinetic energy, *KE*, of the system can be expressed as

$$KE = \frac{1}{2}\{u\}^T[M]\{u\}\omega_1^2 \tag{5-2-3}$$

where $[M]$ is the mass matrix of the MDOF system, and the maximum strain energy, *SE*, of the system can be expressed as

$$SE = \frac{1}{2}\{u\}^T[K]\{u\} \tag{5-2-4}$$

where $[K]$ is the stiffness matrix of the MDOF system.

It is known that when the kinetic energy of the system is maximal, the strain energy will be zero; on the contrary, when the strain energy of the system is maximal, kinetic energy will be zero. Then, based on the principle of conservation of energy (i.e., total mechanical energy is constant), the *KE* is equal to the *SE*. Accordingly, the fundamental frequency ω_1 is given by

$$\omega_1^2 = \frac{\{u\}^T[K]\{u\}}{\{u\}^T[M]\{u\}} \tag{5-2-5}$$

As shown in Eq. (5-2-5), before calculating the fundamental period using Rayleigh's method, the fundamental mode shape $\{u\}$ should be determined. For simplicity, instead of using an accurate eigenvalue analysis, the fundamental mode shape is always determined based on some assumption. Thus, the accuracy of Rayleigh's method depends entirely upon the assumed fundamental mode shape. A widely used estimate for the fundamental mode shape is the static displacement resulting from subjecting the masses in the system to forces proportional to their weights. Based on this assumption, the fundamental period, T_R, is given by

$$T_R = 2\pi\sqrt{\frac{\sum_{i=1}^{n} G_i u_i^2}{g\sum_{i=1}^{n} G_i u_i}} \tag{5-2-6}$$

where $G_i = gm_i$, m_i is the mass of the ith degree of freedom, and n is the number of total degrees of freedom.

The second technique, Geiger's method, is also a widely used approximation method for estimating the fundamental period of a MDOF system. This method was specified in the Japanese seismic code [59]. To introduce the basic consideration of this method, consider an SDOF system with mass m and lateral stiffness k. Then, the fundamental period T_G of the SDOF system can be given by

$$T_G = 2\pi\sqrt{\frac{m}{k}} = 2\pi\sqrt{\frac{mg}{kg}} \tag{5-2-7}$$

By defining $\delta = mg/k$ and $C = \sqrt{g}/2\pi$, T_G can be expressed as

$$T_G = \frac{\sqrt{\delta}}{C} \tag{5-2-8}$$

where δ represents the top lateral displacement resulting due to the weight of the system.

When Eq. (5-2-8) is applied to estimating the fundamental period of an MDOF system, the top displacement (in cm) is estimated by

$$\delta = \sum_{i=1}^{n} \frac{\sum_{j=i}^{n} m_j g}{k_i} \tag{5-2-9}$$

In Japanese seismic code [59], C is determined empirically according to the number of stories n and equals 5.4 when $n = 2$ and 5.7 when $n > 2$.

Eurocode 8 [98] also uses Eq. (5-2-8) to estimate the fundamental period, but C is adopted as 5.

Note that, as with Rayleigh's method, when Eq. (5-2-8) is used to calculate the fundamental period, the top displacement should be estimated.

Another method, Dunkerley's method, is based on the flexibility of the system-eigenvalue problem and provides an "upper-bound" estimation of the fundamental period. The basic premise of this method is to reduce the actual system into a number of simple subsystems; then, the square of the fundamental period, T_D^2, equals the sum of that of each subsystem. Dunkerley's equation can be expressed as

$$T_D^2 = T_{11}^2 + T_{22}^2 + \ldots + T_{nn}^2 \tag{5-2-10}$$

where T_{ii} is the natural period of an SDOF system with mass "m_i" acting alone at state i.

Unlike the previous two methods, Dunkerley's method considers only the mass and stiffness of the analyzed MDOF system, without mode shape or top displacement. However, it has been reported that this method is not as accurate as the others [97].

5.3 Method for estimating the fundamental period

A simple method for estimating the fundamental period of an MDOF system is proposed in this section. The basic principle is to replace a complicated MDOF system with an equivalent SDOF system for which the fundamental period can be easily obtained. To realize the SDOF-system equivalence, a procedure to replace a two-degree-of-freedom (2-DOF) system with an SDOF system having the same fundamental period, called the two-to-single (TTS) procedure, is developed firstly; then, using the TTS procedure successively, the MDOF system can be replaced with an equivalent SDOF system having approximately the same fundamental period.

A procedure to replace a 2-DOF system with an SDOF system

In order to develop the TTS procedure to reduce a 2-DOF system to an SDOF system with the same fundamental period, a 2-DOF system and an equivalent SDOF system are considered, as shown in Fig. 5-3-1. In essence, developing the TTS procedure means expressing parameters including mass, m_{eq}, and stiffness, k_{eq}, of the equivalent SDOF system in terms of the parameters of the 2-DOF system. For this purpose, the following two equivalent equations are considered

$$m_{eq} = m_1 + m_2 \tag{5-3-1}$$

$$T_{eq} = T_{2-DOF} \tag{5-3-2}$$

here, m_i, $i = 1, 2$, is mass of the ith degree of freedom and $T_{2\text{-}DOF}$ is the fundamental period of the 2-DOF system; T_{eq} is the fundamental period of the equivalent SDOF system. In order to determine the stiffness, k_{eq}, of the equivalent SDOF system using Eq. (5-3-2), the fundamental period, $T_{2\text{-}DOF}$, of the 2-DOF system should be derived firstly.

Consider the 2-DOF system in free harmonic vibration. The basic eigen problem for this system is represented as

$$(\omega_i^2[M]-[K])\{u\} = 0 \tag{5-3-3}$$

where ω_i, $i = 1, 2$, are the free-vibration frequencies, $[M]$ and $[K]$ are the mass and stiffness matrices of the 2-DOF system, respectively, and are expressed as

$$[M]=\begin{bmatrix} m_1 & 0 \\ 0 & m_2 \end{bmatrix}, [K]=\begin{bmatrix} k_1 & -k_1 \\ -k_1 & k_1+k_2 \end{bmatrix}$$

and k_i, $i = 1, 2$, is the stiffness of the ith degree of freedom.

By eigenvalue analysis, the fundamental frequency ω_1 can be given by

$$\omega_1^2 = \frac{1}{2}\left[\frac{k_1+k_2}{m_2}+\frac{k_1}{m_1}-\sqrt{(\frac{k_1+k_2}{m_2}-\frac{k_1}{m_1})^2+4\frac{k_1^2}{m_1 m_2}}\right] \tag{5-3-4}$$

As $T_{2\text{-}DOF} = 2\pi/\omega_1$, according to Eq. (5-3-2), the stiffness, k_{eq}, of the SDOF system is given by

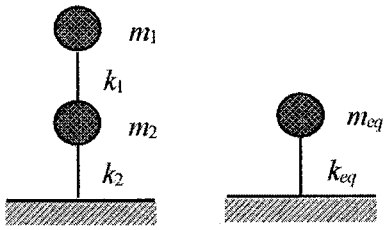

Fig. 5-3-1 Illustration of the concept of replacing a 2-DOF system with an equival ent SDOF system

$$k_{eq} = \frac{1}{2}(m_1 + m_2)\left[\frac{k_1 + k_2}{m_2} + \frac{k_1}{m_1} - \sqrt{(\frac{k_1 + k_2}{m_2} - \frac{k_1}{m_1})^2 + 4\frac{k_1^2}{m_1 m_2}}\right] \tag{5-3-5}$$

Using Eqs. (5-3-1) and (5-3-5), an equivalent SDOF system having the same fundamental period as the 2-DOF system can be obtained.

A procedure for estimating the fundamental period of an MDOF system

Successively using the procedure for replacing a 2-DOF system with an equivalent SDOF system as described above, a procedure for finding the fundamental period of an MDOF system can be developed. The concept of this procedure is illustrated in Fig. 5-3-2. And, the procedure includes following steps:

1. For the MDOF system shown in Fig. 5-3-2(a), the top two masses m_1 and m_2 are assumed to lie on rigid ground and can be considered as a 2-DOF system. Then, based on the TTS procedure (i.e., Eq. (5-3-1) and (5-3-4)), an equivalent SDOF system having the same fundamental period as the top 2-DOF system can be obtained, forming a new MDOF system as shown in Fig. 5-3-2(b).
2. Then, as in step (1), the top two masses of the new MDOF system as shown in Fig. 5-3-2(b) are considered as a new 2-DOF system lying on rigid ground and can be replaced with another equivalent SDOF system using Eqs. (5-3-1) and (5-3-4) again, forming another new MDOF system, as shown in Fig. 5-3-2(c).
3. By application of the TTS procedure successively to the remaining lower masses, finally, the MDOF system is replaced with an equivalent SDOF system, as shown in Fig. 5-3-2(d). Then, the fundamental period can be readily obtained.

Validation of the rigid-ground assumption

In the procedure for replacing an MDOF system with an equivalent SDOF system described in the previous section, at each step of replacement, the top two masses are always considered as a 2-DOF

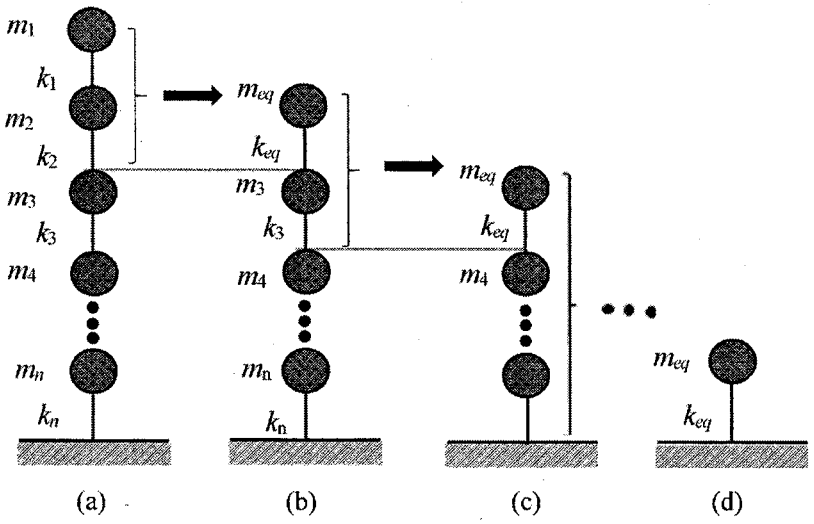

Fig. 5-3-2 Illustration of the concept of replacing an MDOF system with an equivalent SDOF system

system lying on rigid ground. However, except at the final step, the 2-DOF system lies on a floor with limited stiffness. In order to validate the rigid-ground assumption, the fundamental periods of a large number of MDOF structures are computed using the procedure described above and compared with those obtained using an eigenvalue analysis.

The analyzed MDOF structures are divided into two major categories: MDOF structures with floor stiffness varying with height and those with only one special floor with different stiffness from the others. As the mass of the actual structure generally varies less significantly as a function of height than does stiffness, the mass, m_0, of the analyzed structures is considered constant.

In the first category, the variation of stiffness with height is expressed as

$$k_i = r^{i-1} k_0 \tag{5-3-6}$$

where k_i is the stiffness of the ith mass point, as shown in Fig. 5-3-2(a), k_0 is a constant value, and factor r represents the variation degree of stiffness along height. Eq. (5-3-6) means that, the stiffness of the top story equals k_0, and stiffness of any lower ith story is r times as large as that of the upper i-1th story. Generally, as the stiffness of the actual structure increases from the top to the bottom, factor r is considered to vary from 1 to 1.5.

In the second category, the stiffness of only a special floor, k_i, is considered variable, and the others are constant and equal to k_0. The variation of the stiffness of this special floor is expressed as

$$k_i = r k_0 \tag{5-3-7}$$

Eq. (5-3-7) means that, stiffness of the special story is r times as large as that of other stories equaling k_0. In this case, factor r is considered to vary from 0.5 to 1.5, and i varies from 1 to n, where n the number of stories.

It can be easily shown that, in these designed MDOF structures, the parameters controlling the fundamental period are the factor r, the ratio between stiffness and mass, k_0/m_0, and the number of stories n. Thus, the error in the estimated fundamental period caused by the rigid-ground assumption is also considered to be affected by these three parameters. The variation ranges of the parameter r have been introduced above, for the parameter k_0/m_0, two values, 10,000 (kN/cm)/6 (t) and 10,000 (kN/cm)/60 (t), are considered in the following calculation. The value, 10,000 (kN/cm)/6 (t), is determined according to an actual structure constructed in Japan [99]. To observe the possible effect of the parameter k_0/m_0 on the error clearly, another extreme value, 10,000 (kN/cm)/60 (t), is assumed. The extreme range assumed for the parameter k_0/m_0 is to observe the possible effect clearly instead of representing actual condition. And number of stories n is considered to vary from 3 to 10.

The fundamental periods of these MDOF structures are calculated using the previously developed procedure and compared against those obtained using an eigenvalue analysis. The errors are expressed by ratios of the fundamental periods calculated by the previous developed procedure, T_p, with those by an eigenvalue analysis, T_e. Fig. 5-3-3(a) shows the results of the first category of MDOF structures. For the second category of MDOF structures, results are very similar regardless of the value of i expressed in Eq. (5-3-7); for simplicity, only representative results when $i = n$ are shown in Fig. 5-3-3(b). In these figures, the horizontal coordinate is the factor r, representing the variation degree of stiffness, and the longitudinal coordinate represents the error.

It is observed that, for both subcategories in which there is error in the estimated fundamental period, the maximum relative error is less than 8%. The errors are dependent on the factor r and the number of stories n, but not on the ratio k_0/m_0. The errors increase with increasing r for the first category but do not change noticeably for the second category. For both subcategories, the errors increase with n. Comparing the effects of n and r on the errors, that of n is clearly more prominent.

The reason for the dependence on the number of stories is that, when replacing an MDOF system with an equivalent SDOF system, the top 2-DOF system at each step is assumed to lie on rigid ground, when in fact it lies on a floor with limited stiffness; thus, the more stories the analyzed MDOF system has, the more the assumptions used, resulting in a larger error.

Generally speaking, the rigid-bedrock assumption used in the previously developed procedure can cause a calculation error in the fundamental period, but the maximum relative error of the analyzed MDOF structures is below about 8%. The errors are affected by the number of stories n and the variation degree of the stiffness with height, although the former effect is more significant.

Correction factor

Based on the analysis in the previous subsection, the prediction of the fundamental period using the previously developed procedure is improved with the appropriate introduction of a correction factor.

The fact that the error in the fundamental period obtained using the previously developed procedure is affected by the number of stories and the variation degree of the stiffness along height

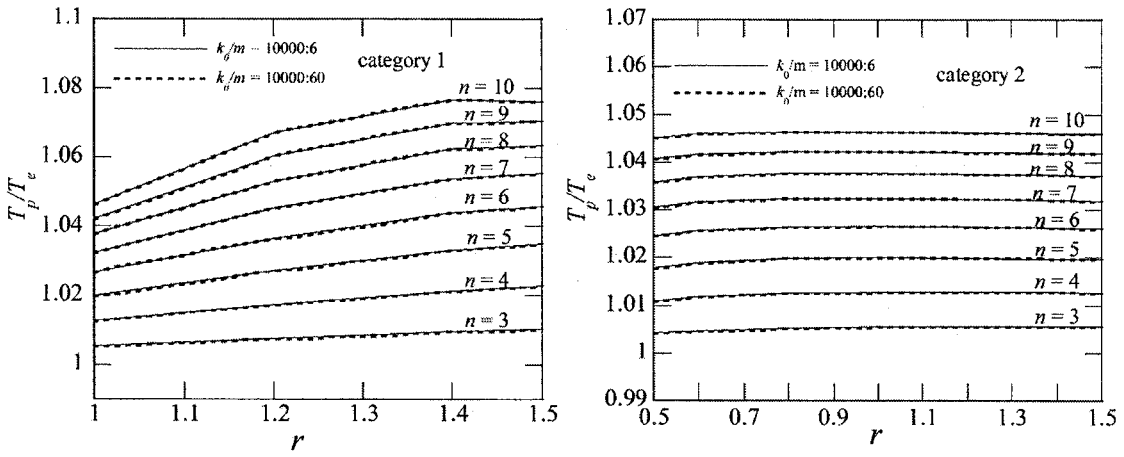

(a) Results for structures in the first category (b) Results for structures in the second category

Fig. 5-3-3 Comparison of the fundamental periods obtained by the procedure described in the previous Section with those obtained by eigenvalue analysis

leads us to conclude that the correction factor should be expressed in terms of the number of stories, n, and a factor representing the variation degree of stiffness. However, since the variation degree ofthe stiffness of an actual building cannot be expressed as a single factor like the idealized one, r, used previously, and since an increase in the number of stories affects the error more significantly than variation of the stiffness, the correction factor is expressed only in terms of n.

To isolate the effects of variations of stiffness and mass, MDOF structures with constant mass and stiffness with height are used to conduct the correction. MDOF structures composed of 3–20 stories are used for the correction. Then, a correction factor R is introduced, defined as the ratio between the fundamental periods obtained by an eigenvalue analysis and by the previous developed procedure. To determine the correction factor R, the fundamental ratios of the exact and predicted periods of all analyzed MDOF structures are computed, and the results are shown in Fig. 5-3-4. By trial-and-error analysis of a large number of functional forms, a very simple function is adopted for the correction factor R, given by

$$R = (0.4n)^{-1/30} \tag{5-3-8}$$

The accuracy of this function can also be found very well from Fig. 5-3-4. The standard deviation of residuals expressing the random variability of results by Eq. (5-3-8) is almost equal to 0.001.

Finally, considering the correction factor, the fundamental period of an MDOF structure can be estimated as

$$T_{Pr} = 2\pi R\sqrt{\frac{m_{eq}}{k_{eq}}} \tag{5-3-9}$$

where m_{eq} and k_{eq} are the mass and stiffness, respectively, of the final equivalent SDOF system

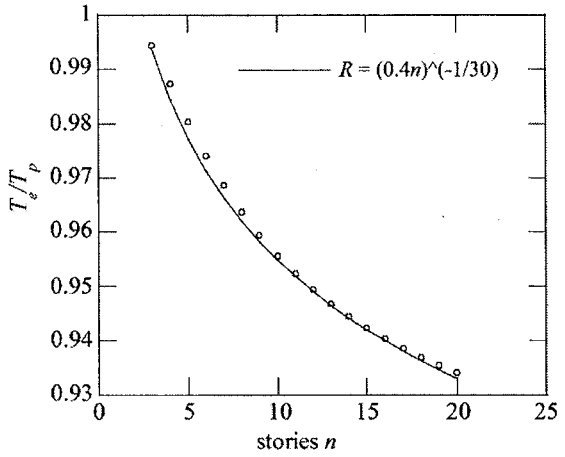

Fig. 5-3-4 Ratios between the fundamental periods obtained by eigenvalue analysis and by the method described in the previous section

obtained by the previous developed procedure.

The proposed method is composed of three equations (i.e., Eqs. (5-3-1), (5-3-5), and (5-3-8)), of which the second equation seems more complicated than the current methods introduced in Section 5.2 at first glance. In Rayleigh's method, the mode shape should be determined first; and, in Geiger's method, the top displacement should be estimated. As Eq. (5-3-5) is expressed in terms of only mass and stiffness without any other additional parameters, the proposed method is considered simpler and more direct than any presented in Section 5.2.

It should be noted that, the proposed method is developed for estimation of the fundamental period of the widely used MDOF structural model. This means that, for an actual structure, it must be simplified as an MDOF model before applying the proposed method. During the simplification, besides the structural elements, the infill walls also should be properly considered in the model, since contribution of the infill walls to the fundamental period may be also crucial [80,81].

In addition, as the proposed method considers variations of mass and stiffness with height, thus the method is available for structures with vertical irregularity. For structures with plan irregularities, torsion may be caused to the building, thus torsional stiffness should be considered in the model of the structure. However, during the derivation of the proposed method, only lateral stiffness is considered. Thus, the proposed method is only available for the shear-type MDOF system. Improving the proposed method to analyze structures with plan irregularities is necessary in the further study.

5.4 Examples using the proposed method

Designed MDOF structures

In order to investigate the accuracy of the proposed method, a recalculation of the fundamental periods of the two categories of MDOF structures introduced in Section 5.3 is performed, and fundamental period ratios between the predicted periods, T_{pr}, and the exact ones are shown in Fig. 5-4-1. It is observed that errors are very low for both categories, with the maximum relative error below 3%. Although the error increases with the number of stories for the first category of MDOF structures, the error level (3%) is considered acceptable for engineering use.

In addition, in order to compare the accuracy of the proposed method with those of the methods introduced in Section 5.2, the fundamental periods of the two categories of MDOF structures are also estimated by the current methods. MDOF structures with as many as 60 stories are considered for comparison. Representative results are shown in Figs. 5-4-2 (a)–(d). In these figures, the horizontal coordinate is n and the longitudinal coordinates are the fundamental periods calculated by different methods.

It can be noted that all results obtained by the proposed method are much more accurate than those obtained by Dunkerley's method, the Eurocode 8 method and Geiger's method adopted in Japanese code. Indeed, the accuracy of the proposed method is nearly equivalent to that of Rayleigh's method adopted in UBC 1997. Further comparisons of the average relative errors of the results estimated by different methods are conducted. The corresponding results of those MDOF structures used in Fig. 5-4-2 are listed in Table 5-4-1. The average relative errors by the proposed method are smaller than those of the current methods.

Generally speaking, the accuracy of the proposed method is very good and is much better than that of Dunkerley's method and the Eurocode 8 method. For most of the estimated structures, the accuracy of the proposed method is better than those of Rayleigh's method adopted in UBC 1997

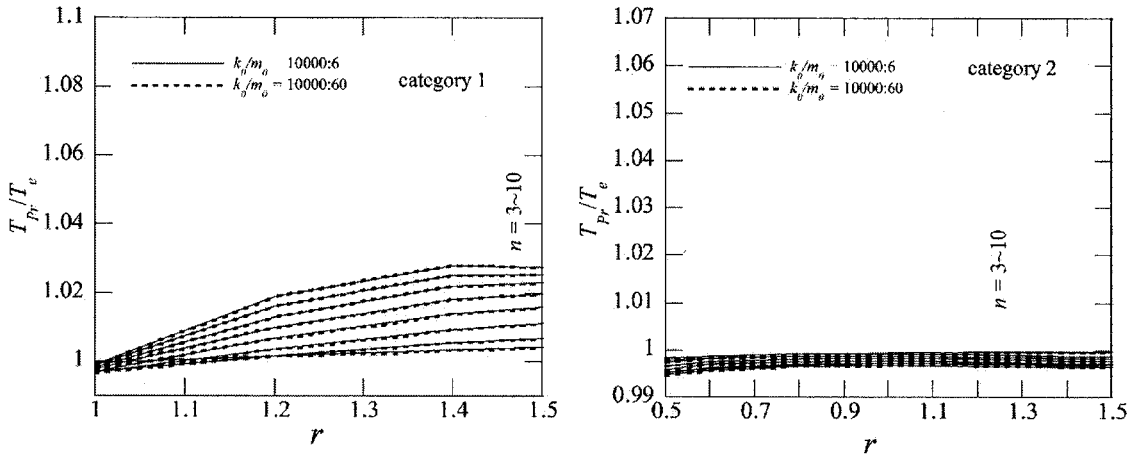

(a) Results for structures in the first category (b) Results for structures in the second category

Fig. 5-4-1 Comparison between fundamental periods obtained by the proposed method and by eigenvalue analysis

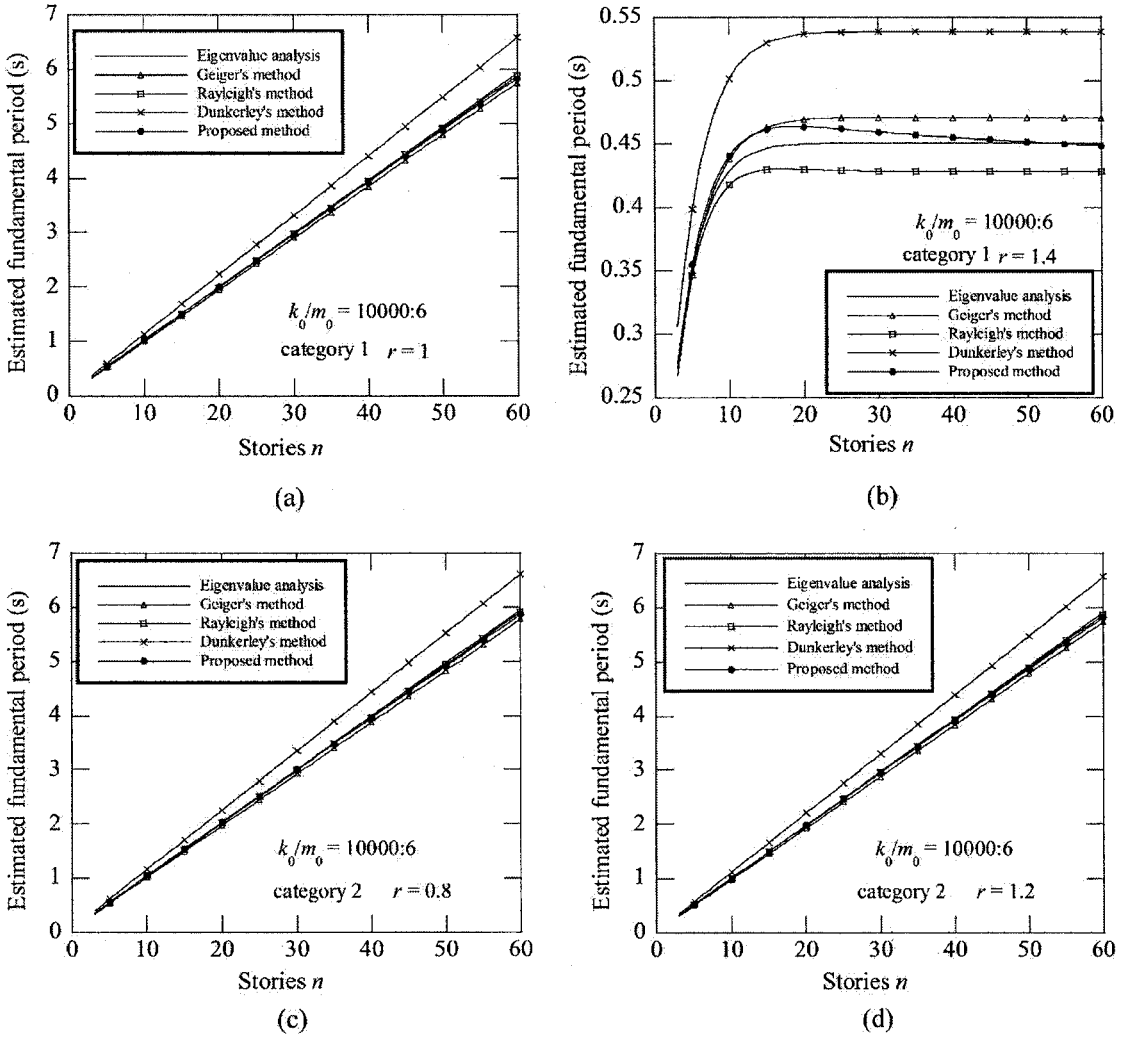

Fig. 5-4-2 Fundamental periods calculated by different methods. (a) Results for structures in the first category when $r = 1$. (b) Results for structures in the first category when $r = 1.4$. (c) Result for structures in the second category when $r = 0.8$. (d) Results for structures in the second category when $r = 1.2$

Table 5-4-1 Average relative error in the estimation results

--	Fig.5-4-2 (a) (%)	Fig.5-4-2 (b) (%)	Fig.5-4-2 (c) (%)	Fig.5-4-2 (d) (%)
Proposed method	0.617	1.542	0.616	0.624
UBC 1997	0.643	4.298	0.623	0.655
Japanese code	3.032	3.890	3.084	3.000
Dunkerley's method	10.935	18.615	10.876	10.967
Eurocode 8	10.543	18.196	10.484	10.575

and Geiger's method adopted in Japanese code.

MDOF models of actual structures

Further accuracy investigations are performed by estimating the fundamental periods of 19 MDOF models of actual structures [99-104]. Parameters of these MDOF models are listed in Table 5-4-2. A wide range of structures with 3–36 stories are considered. Most of these structures are in Japan, and others are found in unknown locations. The fundamental periods of the 19 MDOF models are calculated by the proposed method and the current methods; the obtained results are listed in Table 5-4-3, and the corresponding relative errors are also estimated and listed in brackets. It can be seen that the average relative error by the proposed method equals 1.098% and that the maximum relative error equals 2.828%. For 79% of the estimated MDOF models, relative error is less than 2%. This accuracy is encouraging, and results by the proposed method are considered to agree very well with those obtained by eigenvalue analysis.

Comparing the results of the various methods, it can be seen that, for all estimated models, the relative error of the proposed method is much lower than that of Dunkerley's method and the Eurocode 8 method; for 84% of the estimated models, the proposed method also obtains a smaller relative error than Rayleigh's method adopted in UBC 1997. In addition, the average and maximum relative errors by the proposed method are the lowest, meaning the accuracy of this method is the highest.

Generally speaking, the accuracy of the proposed method is reasonably good, with a maximum relative error below 2.828%. The accuracy is much better than that of Dunkerley's method and the Eurocode 8 method, and is better than that of Geiger's method adopted in Japanese code or Rayleigh's method adopted in UBC 1997 for most of the structures considered.

Table 5-4-2 Parameters of the analyzed actual structures

Model No.	Structure Location	Structure Stories	Direction
01	Wakayama-Ken of Japan	3	X
02			Y
03	Tochigi-ken of Japan	4	X
04			Y
05	Ibaraki-ken of Japan	5	X
06			Y
07	Ibaraki-ken of Japan	7	X
08			Y
09	Tokyo of Japan	23	X
10			Y
11	Tokyo of Japan	36	X

12			Y
13	--	5	X
14			Y
15	--	5	--
16	Tokyo of Japan	3	X
17			Y
18	--	8	NS
19			EW

Table 5-4-3 Fundamental periods and corresponding relative errors of the analyzed MDOF models calculated by different methods

Model No.	Theoretical method (s)	Dunkerley's method (s)	UBC 1997 (s)	Japanese code (s)	Proposed method (s)	Eurocode 8 (s)
01	0.213	0.258 (20.069)	0.211 (0.850)	0.205 (3.417)	0.213 (0.236)	0.234 (10.105)
02	0.122	0.148 (20.059)	0.121 (0.833)	0.118 (3.326)	0.122 (0.323)	0.134 (10.209)
03	0.313	0.406 (27.236)	0.307 (1.850)	0.314 (0.295)	0.314 (0.420)	0.358 (14.336)
04	0.392	0.527 (31.768)	0.383 (2.322)	0.394 (0.458)	0.394 (0.448)	0.449 (14.522)
05	0.139	0.207 (43.524)	0.137 (1.603)	0.140 (0.578)	0.141 (1.337)	0.159 (14.659)
06	0.139	0.207 (43.524)	0.137 (1.603)	0.140 (0.578)	0.141 (1.337)	0.159 (14.659)
07	0.713	1.061 (42.435)	0.704 (1.239)	0.704 (1.314)	0.720 (0.911)	0.802 (12.501)
08	0.696	1.038 (41.781)	0.686 (1.422)	0.692 (0.653)	0.707 (1.591)	0.789 (13.256)
09	1.026	1.673 (48.196)	1.012 (1.362)	1.043 (1.682)	1.049 (2.242)	1.189 (15.917)
10	1.047	1.811 (56.246)	1.032 (1.385)	1.074 (2.558)	1.076 (2.828)	1.224 (12.916)
11	2.084	3.081 (33.481)	2.051 (1.557)	2.089 (0.266)	2.112 (1.368)	2.382 (14.303)

12	2.170	3.180 (32.368)	2.138 (1.508)	2.172 (0.067)	2.198 (1.283)	2.467 (14.076)
13	0.150	0.187 (21.487)	0.149 (0.892)	0.147 (1.992)	0.150 (0.044)	0.168 (11.730)
14	0.139	0.206 (43.525)	0.137 (1.604)	0.140 (0.583)	0.141 (1.338)	0.159 (14.665)
15	0.691	0.816 (15.463)	0.686 (0.754)	0.669 (3.126)	0.691 (0.013)	0.763 (10.437)
16	5.491	8.094 (43.031)	5.346 (2.638)	5.520 (0.531)	5.625 (2.441)	6.897 (25.625)
17	5.933	8.881 (45.817)	5.760 (2.919)	5.954 (0.352)	6.053 (2.032)	7.469 (25.900)
18	0.342	0.403 (13.273)	0.339 (0.904)	0.335 (2.023)	0.343 (0.287)	0.382 (11.694)
19	0.355	0.429 (15.822)	0.352 (0.973)	0.349 (1.818)	0.356 (0.391)	0.397 (11.927)
Error (Avg.)	--	33.637	1.485	1.348	1.098	14.602
Error (Max.)	--	56.246	2.919	3.417	2.828	25.900

5.5 Conclusions

On the basis of the preceding discussion, one can draw the following conclusions:

1. A simple method of evaluating the fundamental period by replacing the complicated MDOF system with an equivalent SDOF system is proposed. The proposed method is available for shear-type MDOF system. As the proposed method is composed of three simple explicit formulae, it can be conveniently implemented in simple spreadsheets. In addition, the application of the proposed method does not require expert knowledge concerning eigenvalue analysis; thus, the proposed method is thought can be used by practicing engineers conveniently. Moreover, as simple formulae are expressed in terms of the mass, stiffness, and number of stories directly without the mode shape or top displacement, the proposed method is a simpler and a more direct method.

2. The accuracy of the proposed method is investigated by estimating a series of designed MDOF structures and 19 MDOF models of actual structures, and is found to be reasonably good. The accuracy of the proposed method is much better than that of Dunkerley's method and the Eurocode 8 method, and is better than that of Rayleigh's method adopted in UBC 1997 and Geiger's method adopted in Japanese code for most of the analyzed structures.

Chapter 6

Conclusions

In this study, a new simple site-specific method for estimating site effects of layered soil profiles is proposed. The proposed method takes into account properties of every soil layers, frequency dependent properties of the site effects, and the soil nonlinear behavior. The contents of this study are summarized as follows.

(1) Site amplification function

As the seismic motion for structural design is usually given in the form of response spectrum, the site effects are typically characterized as ratio of response spectrum at ground surface against the one specified at outcrop bedrock in seismic codes. In Chapter 2, an equation for estimating the response spectral ratio (RSR) is developed.

1. To develop a function for estimating the RSR, RSR and Fourier spectral ratio (FSR) are compared based on ground-motion records, in Section 2.2. It is found that, (1) the shape of RSR is nearly consistent with the one of FSR, the shape of RSR is relatively gentler; (2) maximum value of FSRs and RSRs occur at about the same period, and the one of FSRs systematically exceed that of RSRs; (3) at period band longer than the site fundamental period, difference between RSRs and FSRs decreases as magnitude and epicentral distance increase.
2. Comparison between RSR and FSR are also conducted based on random vibration theory (RVT), in Section 2.3. An equation expressing the relationship between the RSR and the FSR is derived based on the RVT. According to the derived equation, the relationship between the RSR and the FSR is investigated. Nearly same findings with those based on statistical analysis in section 2.2 are obtained.
3. Based on the comparisons between RSR and FSR, a site amplification function representing the RSR is constructed in Section 2.4.

(2) First resonance peak

The developed equation for RSR in Chapter 2 consists of two basic parameters, namely the fundamental period and first resonance peak. In Chapter 3, three simple methods for estimation of the first resonance peak of layered soil profiles are developed.

1. In section 3.3, a simple method for estimation of the Gs_1 of layered soil profiles is developed. The

method calculates results of Gs_1, by replacing the layered shear wave velocity with an equivalent linearly varying profile. The equivalent shear wave velocity profile is determined by regressing the values at midpoint of each soil layer. The validity of the proposed method is demonstrated by evaluating 67 representative sites. The results obtained using the proposed procedure agree well with those produced by the wave propagation method.

2. In section 3.4, another simple method for estimation of the Gs_1 of layered soil profiles is developed. The method calculates the Gs_1, by replacing the multiple soil layers with equivalent two layers. The interface of the equivalent two layers locates between two adjacent soil layers whose impedance contrast is largest among all soil layers. The validity of the proposed method is demonstrated by evaluating 67 representative sites. The results obtained using the proposed procedure agree well with those produced by the wave propagation method.
3. In section 3.5, another simple method for estimation of the Gs_1 of layered soil profiles is developed. This method calculates the Gs_1, by successively replacing the top two layers with an equivalent single layer using the TTS procedure. The validity of the proposed method is demonstrated by evaluating 67 representative sites. The results obtained using the proposed procedure agree well with those produced by the wave propagation method, and the accuracy of this method is better than those of the two proposed methods above.

(3) Soil nonlinear behavior

As the soil nonlinearity significantly influences the site response, a simple procedure to consider the soil nonlinear behavior in estimation of the site effects is developed in Chapter 4.

1. In Section 4.2, a simple procedure to consider the soil nonlinear behavior in estimation of the site effects is developed.
2. During the application of this method, the first mode shape is necessary. A simple method for estimating the first mode shape of layered soil profiles is proposed, in Section 4.3. The validity of the proposed method is demonstrated by evaluating 67 representative sites. The results obtained using the proposed procedure agree well with those produced by the exact Rayleigh Procedure.
3. The accuracy of the proposed method for nonlinear soil behavior is investigated using the 67 soil profiles, and considering two levels of input motions, in section 4.4. The results obtained using the proposed procedure agree well with those by SHAKE using both two levels of inputs. In addition, the validity of the total proposed method for site effects are demonstrated by estimating ground-surface response spectra of several actual reprehensive soil profiles in Section 4.5. The results obtained using the proposed procedure agree well with those produced by the equivalent linear method.

(4) Fundamental period of MDOF structures

In Chapter 5, the consideration of estimating site effects in Chapter 3 is extended to calculate the

fundamental period of a multiple-degree-of-freedom (MDOF) system.

1. The proposed method is composed of three simple explicit formulae, it can be conveniently implemented in simple spreadsheets. In addition, the application of the proposed method does not require expert knowledge concerning eigenvalue analysis; thus, the proposed method is thought can be used by practicing engineers conveniently. Moreover, as simple formulae are expressed in terms of the mass, stiffness, and number of stories directly without the mode shape or top displacement, the proposed method is a simpler and a more direct method.
2. The accuracy of the proposed method is investigated by estimating a series of designed MDOF structures and 19 MDOF models of actual structures, and is found to be reasonably good. The accuracy of the proposed method is much better than that of Dunkerley's method and the Eurocode 8 method, and is better than that of Rayleigh's method adopted in UBC 1997 and Geiger's method adopted in Japanese code for most of the analyzed structures.

Appendices

Appendix 1: Current methods for site effects in seismic codes

A1.1 1994 and 1996 NEHRP, ASCE/SEI 7-05, ASCE/SEI 7-10, 1997 UBC, 2003, 2012 and 2015 IBC

The method for site effects in seismic codes including, ASCE/SEI 7-05 [15], ASCE/SEI 7-10 [16], 1997 UBC [11], 2003 [12], 2012 [13] and 2015 IBC [14], is based on earlier works in 1994 National Earthquake Hazard Reduction Program (NEHRP) [17] and the later revision in 1996 [106]. In 1994 NEHRP, site effects are reflected by two site coefficients F_a and F_v of five site classes. The values of the site coefficients F_a and F_v for five site classes are listed in Tables 1-1-1 and 1-1-2, respectively. The site classes are divided in terms of a representative average shear wave velocity, V_{30}, as shown in Table 1-1-3. The F_a and F_v, respectively, represent response spectral ratios for short period and long period (1s), expressed as:

$$S_{MS} = F_a S_s \tag{A1-1-1}$$

$$S_{M1} = F_v S_1 \tag{A1-1-2}$$

where S_s and S_1 are, respectively, rock-site maximum considered earthquake (MCE) spectral response acceleration at short period and at a period of 1s; S_{MS} and S_{M1} are, respectively, free-field MCE spectral response acceleration at short period and at a period of 1s.

The values for the F_a and F_v are based on results derived from both empirical studies of recorded motions and numerical site response analysis [18]. The empirical studies included studies of strong-motion recordings of the Loma Prieta earthquake in 1989 and those comparison with those obtained in previous earthquakes. These data are generally associated with low rock accelerations equal or less than about 0.1g, because results at higher rock motions were not available. The values of site coefficient in Tables 1-1-1 and 1-1-2 for higher levels of motion are based on laboratory and numerical modeling studies of site response [18].

Table A1-1-1 Site coefficient, *Fa*

Site class	Mapped Maximum Considered Earthquake Spectral Response Acceleration Parameter at Short Period				
	$S_s \leq 0.25$	$S_s = 0.5$	$S_s = 0.75$	$S_s = 1.0$	$S_s \geq 1.25$
A	0.8	0.8	0.8	0.8	0.8
B	1.0	1.0	1.0	1.0	1.0
C	1.2	1.2	1.1	1.0	1.0
D	1.6	1.4	1.2	1.1	1.0
E	2.5	1.7	1.2	0.9	0.9
F	--				

Table A1-1-2 Site coefficient, *Fv*

Site class	Mapped Maximum Considered Earthquake Spectral Response Acceleration Parameter at 1-s Period				
	$S_1 \leq 0.1$	$S_1 = 0.2$	$S_1 = 0.3$	$S_1 = 0.4$	$S_1 \geq 0.5$
A	0.8	0.8	0.8	0.8	0.8
B	1.0	1.0	1.0	1.0	1.0
C	1.7	1.6	1.5	1.4	1.3
D	2.4	2.0	1.8	1.6	1.5
E	3.5	3.2	2.8	2.4	2.4
F	--				

Table A1-1-3 Site classification

Site Class	$\overline{v}_s$	$\overline{N}$ or $\overline{N}_{ch}$	$\overline{s}_u$
A. Hard rock	>5,000 ft/s	NA	NA
B. Rock	2,500 to 5,000 ft/s	NA	NA
C. Very dense soil and soft rock	1,200 to 2,500 ft/s	>50	>2,000 psf
D. Stiff soil	600 to 1,200 ft/s	15 to 50	1,000 to 2,000 psf
E. Soft clay soil	<600 ft/s	<15	<1,000 psf
	Any profile with more than 10 ft of soil having the following characteristics: —Plasticity index $PI > 20$, —Moisture content $w \geq 40\%$, —Undrained shear strength $\overline{s}_u < 500$ psf		
F. Soils requiring site response analysis in accordance with Section 21.1	See Section 20.3.1		

For SI: 1 ft/s = 0.3048 m/s; 1 lb/ft^2 = 0.0479 kN/m^2.

A1.2 NBCC 2005

The Canadian Committee on Earthquake Engineering (CANCEE) advises on the seismic provisions of the National Building Code of Canada (NBCC) [106]. CANCEE essentially adopted the 1994 NEHRP provisions for establishing the free-field acceleration response spectrum and the NEHRP site classes. The short- and long-period amplification factors *Fa* and *Fv*, respectively, were adopted also with some minor modifications. The 2005 NBCC factors are listed in Tables 1-2-1 and 1-2-2. CANCEE adopted site class C in 1994 NEHRP as the reference site for amplification for the 2005 NBCC, instead of site class B as used in the 1994 NEHRP provisions. Therefore, for all intensities of earthquake shaking, the site factor for site C is 1.0.

Table A1-2-1 Site coefficient, *Fa*

Site class	Mapped Maximum Considered Earthquake Spectral Response Acceleration Parameter at Short Period				
	$S_s \leq 0.25$	$S_s = 0.5$	$S_s = 0.75$	$S_s = 1.0$	$S_s \geq 1.25$
A	0.7	0.8	0.8	0.8	0.8
B	0.8	0.8	0.9	1.0	1.0
C	1.0	1.0	1.0	1.0	1.0
D	1.3	1.2	1.1	1.1	1.0
E	2.1	1.4	1.1	0.9	0.9
F	--				

Table A1-2-2 Site coefficient, *Fv*

Site class	Mapped Maximum Considered Earthquake Spectral Response Acceleration Parameter at 1-s Period				
	$S_s \leq 0.25$	$S_s = 0.5$	$S_s = 0.75$	$S_s = 1.0$	$S_s \geq 1.25$
A	0.5	0.5	0.5	0.6	0.6
B	0.6	0.7	0.7	0.8	0.8
C	1.0	1.0	1.0	1.0	1.0
D	1.4	1.3	1.2	1.1	1.1
E	2.1	2.0	1.9	1.7	1.7
F	--				

A1.3 2005 Seismic Design Code for Buildings in Taiwan

Similar with those seismic codes introduced in section 1.1, site effects are also reflected by two site coefficients F_a and F_v, in 2005 Seismic Design Code for Buildings in Taiwan [107]. The F_a and F_v also, respectively, represent response spectral ratios for short period and long period (1s). But, the values for F_a and F_v shown in Tables 1-3-1 and 1-3-2 are different with those shown in section 1.1. And, the sites are divided into 3 classifications in terms of the V_{30}, as shown in Table 1-3-3.

Table A1-3-1 Site coefficient, *Fa*

Site class	Value of *Fa*				
	$S_s \le 0.5$	$S_s = 0.6$	$S_s = 0.7$	$S_s = 0.8$	$S_s \ge 0.9$
Hard site	1.0	1.0	1.0	1.0	1.0
Normal site	1.0	1.0	1.0	1.0	1.0
Soft site	1.2	1.2	1.1	1.0	1.0

Table A1-3-2 Site coefficient, *Fv*

Site class	Value of *Fv*				
	$S_1 \le 0.3$	$S_1 = 0.35$	$S_1 = 0.4$	$S_1 = 0.45$	$S_1 \ge 0.5$
Hard site	1.0	1.0	1.0	1.0	1.0
Normal site	1.5	1.4	1.3	1.2	1.1
Soft site	1.8	1.7	1.6	1.5	1.4

Table A1-3-3 Site classification

Site Class	V_{s30} (m/s)
S1 (Hard site)	$V_{s30} > 270$
S2 (Normal site)	$180 \le V_{s30} < 270$
S3 (Soft site)	$V_{s30} < 180$

A1.4 Eurocode 8 2004

Eurocode 8 [98] adopts only one soil factor S to reflect site effects. The values of the soil factor S for 5 site classes are listed in Table 1-4-1. The site classes are divided in terms of a representative average shear wave velocity, V_{30}, as shown in Table 1-4-2. The S represents amplification ratio of response spectrum, and S is considered to be constant and independent on the frequency. In Table 1, Type 1 and Type 2, respectively, represent high and moderate seismic regions and low seismicity regions. Thus, Eurocode 8 implicitly considers effect of soil nonlinearity on the site effects. It can be noted that, the values of S for Type 2 are larger than those for Type 1. The reason is because that, the soil damping is larger for high and moderate seismic regions.

Table A1-4-1 Soil factor S

Ground type	S (Type 1)	S (Type 2)
A	1.0	1.0
B	1.2	1.35
C	1.15	1.5
D	1.35	1.8
E	1.4	1.6

Table A1-4-2 Site classification

Site Class	Description of stratigraphic profile	V_{s30} (m/s)
A	Rock or other rock-like geological formation, including at most 5 m of weaker material at the surface.	$V_{s30} > 800$
B	Deposits of very dense sand, gravel, or very stiff clay, at least several tens of metres in thickness, characterized by a gradual increase of mechanical properties with depth.	$360 \le V_{s30} < 800$
C	Deep deposits of dense or medium-dense sand, gravel or stiff clay with thickness from several tens to nlany hundreds of meters.	$180 \le V_{s30} < 360$
D	Deposits of loose-to-medium cohesionless soil (with or without some soft cohesive layers), or of predonlinantly soft-to-firm cohesive soil.	$V_{s30} < 180$
E	A soil profile consisting of a surface alluviu111 layer with Vs values of type C or D and thickness varying between about 5 m and 20 m, underlain by stiffer material with Vs > 800 m/s.	

A1.5 Japanese seismic Code 2000

Japanese seismic Code reflects site effects by a amplification factor $G_s(T)$. The $G_s(T)$ represents amplification ratio of response spectrum on ground surface respect to the one on bedrock,

$$S_a(T) = G_s(T) S_0(T) \tag{A1-5-1}$$

where $S_a(T)$ is design acceleration response spectrum at ground surface, $S_0(T)$ is design response spectrum at engineering bedrock. And, the $G_s(T)$ is expressed as:

$$Gs = \begin{cases} Gs_2 \dfrac{T}{0.8T_2} & T \le 0.8T_2 \\ \dfrac{Gs_1 - Gs_2}{0.8(T_1 - T_2)} T + Gs_2 - 0.8\dfrac{Gs_1 - Gs_2}{0.8(T_1 - T_2)} T_2 & 0.8T_2 \le T \le 0.8T_1 \\ Gs_1 & 0.8T_1 \le T \le 1.2T_1 \\ \dfrac{Gs_1 - 1}{\dfrac{1}{1.2T_1} - 0.1}\dfrac{1}{T} + Gs_1 - 0.8\dfrac{Gs_1 - 1}{\dfrac{1}{1.2T_1} - 0.1} \times \dfrac{1}{1.2T_1} & 1.2T_1 \le T \end{cases} \tag{A1-5-2}$$

where T_1 is the fundamental period of the soil profile, T_2 is the second natural period of the soil profile, G_{s1} is amplification ratio respect to the fundamental period, and G_{s2} is amplification ratio respect to the second natural period.

The $G_s(T)$ is developed theoretically based on a simple soil model, a single-layer soil profile on bedrock. As shown in Fig.A1-5-1, the $G_s(T)$ is constructed to envelop the site transfer function of the simple soil model using four parameters, T_1, T_2, G_{s1} and G_{s2}. For the simple soil model these parameters can be obtained by following equations:

$$T_1 = \frac{4H}{V} \tag{A1-5-3}$$

$$T_2 = \frac{T_1}{3} \tag{A1-5-4}$$

$$Gs_1 = \frac{1}{1.57h + a} \tag{A1-5-5}$$

$$Gs_2 = \frac{1}{4.71h + a} \tag{A1-5-6}$$

where H is the soil thickness, V is the soil shear wave velocity, h is the soil damping ratio, and a is the impedance ratio of the soil layer with respect to the bedrock, which is defined as:

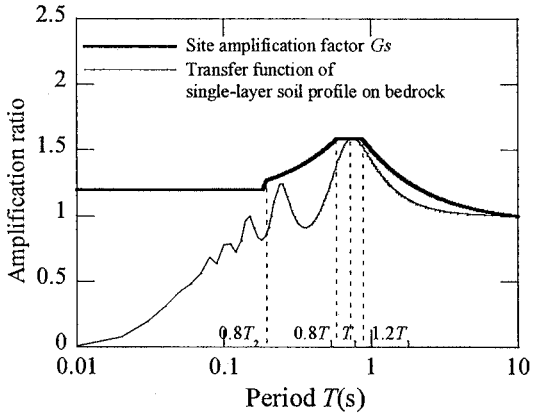

Fig. A1-5-1 Illustration of the concept to develop the equations for estimating site amplification factor, *Gs* in Japanese Seismic Code

$$a = \frac{\rho V}{\rho_B V_B} \tag{A1-5-7}$$

where V_B and ρ_B are the shear wave velocity and density of the bedrock, respectively.

For a multi-layer soil profile on bedrock, the multiple soil layers are replaced with an equivalent single layer by calculating the weighted averages of soil shear wave velocity and density as:

$$V = \frac{\sum_{m=1}^{N} V_m H_m}{\sum_{m=1}^{n} H_m} \tag{A1-5-8}$$

$$\rho = \frac{\sum_{m=1}^{N} \rho_m H_m}{\sum_{m=1}^{n} H_m} \tag{A1-5-9}$$

where m is soil layer number, each soil layer has finite thickness H_m, shear wave velocity V_m, and density ρ_m, and N is the number of soil layers. And, the damping ratio h is also calculated as the weighted average of all soil layers [22, 58] as follows:

$$h = \frac{\sum_{i=1}^{N} h_m E_m}{\sum_{i=1}^{m} E_m} \tag{A1-5-10}$$

where E_m is the energy stored in mth layer [58]. For linear analysis, the soil damping ratio of each layer, h_m, is constant, and is generally considered equal to 0.02. For nonlinear analysis, the damping ratio of each layer is dependent on the shaking level, and can be approximately estimated using the equivalent-linear method.

It is noted that, different with all seismic codes introduced above, the amplification factor $G_s(T)$ is a continuous function of period T. And the factor $G_s(T)$ is developed by taking account into the amplification properties for all periods instead of those for only one or two representative periods.

Soil nonlinear behavior

To consider the soil nonlinear behavior in estimating site effects, a simple response spectrum method developed by Kenji [67] is introduced into 2000 Japanese seismic code. The response spectrum method takes account of the soil nonlinear behavior utilizing the response spectrum defined on bedrock as input directly. The procedure including following steps to consider the soil nonlinear behavior. Firstly, using the bedrock response spectrum, maximum soil displacements at surface layer u_1, and on bedrock u_B, can be estimated by:

$$u_1 = (\frac{T_1}{2\pi})^2 A_s(T_1) \tag{A1-5-11}$$

$$u_B = (\frac{T_1}{2\pi})^2 A_b(T_1) \tag{A1-5-12}$$

where $A_s(T_1)$ and $A_b(T_1)$ are, respectively, Fourier spectrum amplitude at ground surface and bedrock, estimated by:

$$A_s(T_1) = \frac{1}{T_1} G_s(T_1, h, a) F_A(T_1) \tag{A1-5-13}$$

$$A_b(T_2) = \frac{1}{T_1} G_b(T_1, h, a) F_A(T_1) \tag{A1-5-14}$$

The $G_b(T_1, h, a)$ is amplification ratio of seismic motion on overlay bedrock respect to outcrop bedrock expressed as:

$$G_b(T_1, h, a) = \frac{1.57h}{1.57h + a} \tag{A1-5-15}$$

$F_s(T)$ is Fourier spectrum amplitude at outcrop bedrock, can be approximately related to undamped velocity response spectrum $S_V(T, h=0)$ by:

$$F_A(T) \approx S_V(T, h=0) \tag{A1-5-16}$$

The undamped velocity response spectrum can be in turn expressed in term of acceleration response spectrum as:

$$S_V(T, h=0) = (T/2\pi) S_A(T, h=0) \tag{A1-5-17}$$

Then, using the results of maximum soil displacements at surface layer, u_{s1}, and on bedrock, u_B, maximum soil displacement at any ith interface can be estimated by:

$$u_i = |u_{s1} - u_B| U_i \tag{A1-5-18}$$

where U_i is value of first mode shape at ith soil interface. U_i can be estimated using an eigenvalue analysis by discretizing the continuous soil profile into lumped-parameter multi-degree-of-freedom (MDOF) model, or using the simple Stodola method.

Then, based on the consideration of equivalent linear method, equivalent shear strain can be estimated by:

$$\gamma_i = 0.65(u_i - u_{i+1}) / H_i \tag{A1-5-19}$$

The soil nonlinear behaviors are characterized as shear modulus degradation and energy dissipation (damping) depending on the shear strains. Thus, during each interaction soil shear modular and damping should be update according to the estimated equivalent shear strain. It is noted that, the procedure is iterative; the calculation stops until the difference in the values of the fundamental period between two successive iterations is less than some specified value.

A1.6 MDOC 2012

In Mexico seismic code, site effects are reflected by a site amplification factor F_s and a nonlinear factor F_n^d . F_s represents amplification ratio of peak acceleration on ground surface respect to the one on bedrock, and factor F_n^d is used to account for the nonlinear soil behavior.

$$a_0 = F_n^d F_s a_g \tag{A1-6-1}$$

where a_0 is peak ground-surface acceleration, and a_g is peak rock acceleration.

F_s is a function of impedance ratio, p_s, and $T_s' = T_s\sqrt{F_d}$, where T_s is the fundamental period of soil profile, and F_d is a distance factor as $F_d = a_g / 500$. Values for F_s are listed in Table 1-6-1. And the nonlinear factor F_n^d is a function of level shaking F_d , impedance ratio p_s, and soil type, expressed as:

$$F_n^d = \begin{cases} 1-(1-\hat{F}_n^d)\dfrac{T_s}{1.5}, & T_s \le 1.5 \\ \hat{F}_n^d & T_s \ge 1.5 \end{cases} \tag{A1-6-2}$$

Values of the nonlinear factor $\hat{F}_n^d$ in Eq. (A1-6-2) for sands and clay are listed in Tables 1-6-2 and 1-6-3, respectively.

The values for these factors are based on site response analysis of a single-layer soil profile on bedrock, using the input power spectrum of the rock excitation and through application of the random vibration theory to predict peak responses.

Table A1-6-1 Values of the site amplification factor F_s.

p_s \ T_s'	0.00	0.05	0.10	0.20	0.50	1.00	2.00	3.00
1.000	1.00	1.00	1.00	1.00	1.00	1.00	1.00	1.00
0.625	1.00	1.08	1.23	1.12	1.00	1.00	1.00	1.00
0.250	1.00	1.18	1.18	1.98	1.40	1.12	1.00	1.00
0.125	1.00	1.20	2.64	2.01	1.69	13.2	1.00	1.00
0.000	1.00	1.22	4.51	3.17	2.38	1.75	1.19	1.00

Table A1-6-2 Values of the nonlinear factor $\hat{F}_n^d$ for sands and gravels.

p_s \ F_d	0.00	0.10	0.20	0.30	0.40	0.50	0.75	1.00
1.000	1.00	0.97	0.93	0.90	0.86	0.83	0.75	0.71
0.625	1.00	0.95	0.91	0.89	0.85	0.82	0.71	0.68
0.250	1.00	0.93	0.87	0.82	0.77	0.73	0.63	0.56
0.125	1.00	0.92	0.84	0.75	0.67	0.64	0.58	0.53
0.000	1.00	0.90	0.78	0.66	0.58	0.54	0.53	0.50

Table A1-6-3 Values of the nonlinear factor $\hat{F}_n^d$ for clays and cohesive soils.

p_s \ F_d	0.00	0.10	0.20	0.30	0.40	0.50	0.75	1.00
1.000	1.00	0.98	0.95	0.91	0.87	0.85	0.79	0.75
0.625	1.00	0.97	0.94	0.93	0.90	0.88	0.81	0.79
0.250	1.00	0.96	0.93	0.91	0.87	0.85	0.77	0.74
0.125	1.00	0.93	0.85	0.76	0.70	0.67	0.61	0.56
0.000	1.00	0.82	0.63	0.46	0.36	0.32	0.31	0.28

Appendix 2: Some theoretical methods for site effects

A2.1 Method by N.T.K. Lam *et al.*

N.T.K. Lam *et al.* developed a simple theoretical method to estimate site effects in construction of soil response spectra. The method considers the soil profile as a multi-storey moment-resisting frame (MRF) with rigid girders, and estimates site effects by vibrational analysis of the MRF model.

Specially, the procedure takes account of the site effects by following steps. Firstly, peak velocity on the soil surface (PGV) is estimated using the response spectral velocity of the bedrock motion at the natural period of the site, RSV (T_g) by

$$\mathrm{PGV} = \sqrt{(1.2\beta \mathrm{RSV}(T_g))^2 + (\mathrm{PRV})^2} \tag{A2-1-1}$$

where 1.2 is the adopted participation factor consistent with a parabolic displacement profile, and PRV is the peak velocity of the underlying bedrock. In situations where the value of T_g is close to the highest point on the rock spectrum, PRV can be approximated $\mathrm{RSV}(T_g)/2$. Eq. (A2-1-1) can therefore be simplified as follows:

$$\mathrm{PGV} = \sqrt{(1.2\beta \mathrm{RSV}(T_g))^2 + (\mathrm{RSV}(T_g)/2)^2} \tag{A2-1-2}$$

In contrast, if T_g is so remote from the highest point on the rock spectrum peak such that PRV is approximately equal to RSV (T_g), Eq. (A2-1-1) becomes:

$$\mathrm{PGV} = \sqrt{(1.2\beta \mathrm{RSV}(T_g))^2 + (\mathrm{RSV}(T_g))^2} \tag{A2-1-3}$$

Then using following equations, the maximum response spectral velocity $\mathrm{RSV_{max}}$ at T=T_g, in turn, the maximum response spectral displacement, $\mathrm{RSD_{max}}$ at T=T_g can be obtained.

$$\mathrm{RSV_{max}} = a\mathrm{PGV} \tag{A2-1-4}$$

$$\mathrm{RSD_{max}} = \mathrm{RSV_{max}}(T_g/2\pi) \tag{A2-1-5}$$

in which the coefficient a is the velocity amplification factor which relates the maximum velocity of the single degree-of-freedom (SDOF) system to the peak ground velocity.

In addition, based on the consideration of equivalent linear method, soil nonlinear behavior is also characterized by strain-dependent stiffness degradation and dissipation of hysteretic energy. The average shear strain in the soil (γ_{eq}) at maximum dynamic displacement is estimated in accordance with RSV (T_g) and soil depth (H)

$$\gamma_{eq} = 1.2\beta \mathrm{RSV}(T_g)(T_g/2\pi)/0.6H \tag{A2-1-6}$$

where β is the damping adjustment factor expressed as:

$$\beta = \sqrt{7/(\zeta + 2)} \tag{A2-1-7}$$

$$\beta = (5/\zeta)^{1/\eta} \tag{A2-1-8}$$

Eq. (A2-1-7) is used associate with Eqs. (A2-1-2), and (A2-1-7) is used associate with Eq. (A2-1-3).

The average shear strain determined by Eq. (A2-1-6) can be used to determine soil damping and stiffness degradation. The procedure is iteratively, the calculation stops until the difference in the values of the soil damping between two successive iterations is less than some specified value.

Moreover, the effect the shear wave velocity of the rock half-space on RSV_{max} is reflected by a reduction factor λ expressed as:

$$\lambda = 0.8 \qquad V_s < 1000 \text{ m/s} \tag{A2-1-9}$$

$$\lambda = 0.8 + 0.0001(V_s - 1000) \qquad 1000 \text{ m/s} < V_s < 3000 \text{m/s} \tag{A2-1-10}$$

$$\lambda = 1 \qquad V_s > 3000 \text{m/s} \tag{A2-1-11}$$

A2.2 Methods by Hing-Ho Tsang *et al.*

Hing-Ho Tsang *et al.* developed another simple method to estimate site effects [24]. The method reflects site effects using a single spectral ratio (SR) at site fundamental period, T_g, given by:

$$\mathrm{SR} = f(\alpha) \times \mathrm{PDR} \tag{A2-2-1}$$

$f(a)$ is a resonance factor expressed as:

$$f(\alpha) = \alpha^{-0.3} \leq 2.3 \tag{A2-2-2}$$

PDR represents ratio between the peak ground displacement on the surface of the soil sediment and that on the bedrock surface. Equation for PDR is derived according to multiple reflection of seismic waves based on a simple soil model, single-layer soil profile on bedrock; the equation is expressed as:

$$\mathrm{PDR} = \frac{2\alpha^{-1}}{1+\alpha^{-1}} \sqrt{\frac{\beta}{1-R^4\beta^4}} \tag{A2-2-3}$$

where, R is reflection coefficient, describes amplitude ratio of the upwardly propagating reflected wave and the downwardly propagating incident wave within the soil layer, expressed as:

$$R = \frac{1-\alpha^{-1}}{1+\alpha^{-1}} \tag{A2-2-4}$$

a is the impedance ratio of the soil layer with respect to the bedrock. β is half-period damping factor, and is introduced to represent the hysteretic damping (also known as anelastic attenuation) of seismic waves energy in the soil layer for every half-cycle of wave travel, which is defined as:

$$\beta = \exp(-\pi\varsigma) \tag{A2-2-5}$$

where ς is the soil damping ratio.

In addition, the soil nonlinear behavior is reflected by soil damming and period shifting. The soil damming is estimated according to bed-rock response spectrum, RSV_{T_g}, at the fundamental period,

$$\varsigma = 12.5 + 6.5\log(R_\gamma \lambda \psi) - 0.13\mathrm{PI} \tag{A2-2-6}$$

$$\psi = \frac{\mathrm{RSV}_{T_g}}{V_s} \tag{A2-2-7}$$

R_γ is the ratio of the effective shear strain to maximum shear strain, which has been found to vary between about 0.5 and 0.7 from empirical modelling (0.6 has been used in this study). The reduction factor λ, as developed in Reference [25], is needed to account for the bedrock rigidity effect

$$\lambda = \frac{\alpha^{-1}}{1+\alpha^{-1}}\sqrt{\frac{1-\beta^4}{1-R^4\beta^4}} \tag{A2-2-8}$$

Eq. (A2-2-6)) may be bounded by a 'practical' minimum damping ratio ς_{pi} and an upper bound damping ratio ς_{ub}:

$$\varsigma_{pi}(\%) = 2.5 + 0.03\mathrm{PI}(\%) \leq 6.8 \tag{A2-2-9}$$

$$\varsigma_{ub}(\%) = 17.5 - 0.07\mathrm{PI}(\%) \geq \varsigma_{pi} \tag{A2-2-10}$$

The period shifting due to the degrading of shear wave velocity is estimated by [25]:

$$\frac{T_g}{T_i} = 1 + R_\gamma \lambda \psi u \tag{A2-2-11}$$

u is defined as the 'Plasticity Factor' to allow for the effects of soil plasticity (u =1.6, 0.9, 0.4, 0.2 for PI=0, 15, 30, 50%)

Appendix 3: Input seismic motion at bedrock

This section describes the seismological model of Fourier spectral amplitude (FAS) of ground motion used in section 2.3. The FAS of acceleration at a rock site, $A(\omega)$, is described analytically as a function of the source, propagation path, and site characteristics (the site characteristics in this case represent the effect of the near-surface rock layers and not the effect of the overlying soil layers), expressed as:

$$A(\omega) = E(M_0, \omega)P(R, \omega)G(\omega) \tag{A3-1}$$

The Brune [108, 109] omega-squared model is the most common and simplest used source spectrum model. This source spectrum, $E(M_0, \omega)$, can be given by:

$$E(M_0, \omega) = CM_0S(\omega, \omega_c) \tag{A3-2}$$

The C is a constant expressed as:

$$C = \frac{R_{\theta\varphi}FV}{4\pi\rho\beta^3} \tag{A3-3}$$

where $R_{\theta\varphi}$ is the radiation pattern, usually averaged over a suitable range of azimuths and take-off angles (=0.71). V represents the partition of total shear-wave energy into horizontal components (= $1/\sqrt{2}$). F is the effect of the free surface (taken as 2 in almost all applications, which strictly speaking is only correct for SH waves), ρ and β are the density and shear-wave velocity in the vicinity of the source.

M_0 is the seismic moment, introduced into seismology in 1966 by K. AKI [110], it can be expressed in terms of moment magnitude M as:

$$M_0 = 10^{1.5M+10.7} \tag{A3-4}$$

$S(\omega, \omega_c)$ is the displacement source spectrum given by the equation

$$S(\omega, \omega_c) = \frac{\omega^2}{1+(\omega/\omega_c)} \tag{A3-5}$$

where ω_c is the corner frequency, it is affected by the seismic moment, M_0, and a parameter controlling the strength of the high-frequency radiation, stress drop $\Delta\sigma$,

$$f_c = 4.9 \bullet 10^6 \beta_0 (\Delta\sigma / M_0)^{1/3} \tag{A3-6}$$

The path effect $P(R,\omega)$ is given by the multiplication of the geometrical spreading and Q functions, expressed as:

$$P(R,\omega) = Z(R)\exp(-\omega R/2Q\beta) \tag{A3-7}$$

Geometrical spreading function $Z(R)$ is given by a piecewise continuous series of straight lines:

$$Z(R) = \begin{cases} \dfrac{R_0}{R} & R \le R_1 \\ Z(R_1)(\dfrac{R_1}{R})^{p_1} & \\ \cdots & \\ Z(R_n)(\dfrac{R_n}{R})^{p_n} & R_n \le R \end{cases} \tag{A3-8}$$

In this study, the three-segment geometrical spreading operator used in ATKINSON and BOORE's [111] predictions of ground motions in eastern North America is adopted.

And the Q functions is given by

$$Q = 680f^{0.38} \tag{A3-9}$$

The site effects are expressed by two parts, amplification ($A(\omega)$) and attenuation ($D(\omega)$) as follows:

$$G(\omega) = D(\omega)A(\omega) \tag{A3-10}$$

The amplification function, $A(\omega)$, accounts for the propagation of waves from the deeper crust, where the shear wave velocity of the rock is on the order of 3,500 m/ s, to the near surface, where the shear wave velocity of competent rock is generally 750 m/ s. Suggested values of $A(\omega)$ for generic rock sites in WNA can be found in Boore and Joyner [112]. These amplification values generally range between 1.0 and 4.0 over the frequency range of engineering interest.

The diminution function $D(\omega)$ is used to model the path-independent loss of energy, expressed as:

$$D(\omega) = \exp(-0.5k_0\omega) \tag{A3-11}$$

where k_0 is a diminution parameter, k_0 is adopted as 0.04 according to [112].

References

[1] Francisco J. Chfivez-Garcia, Pierre-Yves Bard. Site effects in Mexico City eight years after the September 1985 Michoacan earthquakes. Soil Dynamics and Earthquake Engineering, Vol.13, 229-247.
[2] Roger D. Burkhardt and Gary Glassmoyer. On the characteristics of local geology and their influence on ground motions generated by the Loma Prieta earthquake in the San Francisco bay region, California. Bulletin of the Seismological Society of America, Vol. 82, No. 2, 603-641, 1992.
[3] Roger D. Borcherdt. Empirical Evidence for Acceleration-Dependent Amplification Factors. Bulletin of the Seismological Society of America, Vol. 92, No. 2, 761–782, 2002.
[4] Masayuki D, Susumu, O, Kohji K and Kenichi K. Bedrock motions and site amplifications in Kobe city during the 1995 Hyogo-Ken earthquake, Journal of Structural and Construction Engineering AIJ, No.511, 77-84, 1998. (In Japanese)
[5] Hadi G, Gail M. A, Katsuichiro G. Implications of the 2011 M9.0 Tohoku Japan earthquake for the treatment of site effects in large earthquakes. Bull Earthquake Engineering, Vol. (11), 170-203, 2013.
[6] Xiaojun L, Zhenghua Z, Moh H, Ruizhi W, Haiyin Y, Dawei L, Yongnian Z, Jianwen C. Preliminary Analysis of Strong-Motion Recordings from the Magnitude 8.0 Wenchuan, China, Earthquake of 12 May 2008. Seismological Research Letters, Vol. 79, No.6, 844-854.
[7] Sumer C, Pallabee C. A study of response spectra for different geological conditions in Gujarat, India, Soil Dynamics and Earthquake Engineering, Vol. 31, 1551-1564, 2001.
[8] Mosato M and Masayuki N. Analysis on amplification characteristics of ground motions in Kobe city taking account of deep irregular underground structure – interpretation of heavily damaged belt zone during the 1995 Hyogo –ken Nanbu Earthquake, Journal of Structural and Construction Engineering AIJ, No.488, 39-48, 1996. (In Japanese)
[9] Anderson, J.G. *et al.* Strong ground motion from the Michoacán, Mexico, earthquake, Science, Vol, 233, 1043-1049, 1986.
[10] Esteva L. The Mexico earthquake of September 19, 1985- consequence, lesson, and impact on research and practice, Earthquake Spectra, Vol.4, 413-426, 1988.
[11] Uniform Building Code (UCB). Whittier (CA): International Conference of Building Official, 1997.
[12] International Building Code (IBC). Country Club Hill, Illinois, USA: International Code Council; 2003.
[13] International Building Code (IBC). Country Club Hill, Illinois, USA: International Code Council; 2012.
[14] International Building Code (IBC). Country Club Hill, Illinois, USA: International Code Council; 2015.
[15] ASCE/SEI 7-05, American Society of Civil Engineers. Minimum Design Loads for Buildings and other Structures; 2006.
[16] ASCE/SEI 7-10, American Society of Civil Engineers. Minimum Design Loads for Buildings and other Structures; 2010.
[17] Roger D. Borcherdt, M.EERI. Estimates of Site-Dependent Response Spectra for Design (Methodology and Justification). Earthquake spectra, Vol.10, No.4, 617-653, 1994.
[18] R. Dobry, R. D. Borcherdt, C. B. Crouse, I. M. Idriss, W. B. Joyner, G. R. Martin, M. S. Power, E. E. Rinne, and R. B. Seed. New Site Coefficients and Site Classification System Used in Recent Building Seismic Code Provisions. Earthquake Spectra, Vol. 16, No. 1, 41-67, 2000.
[19] Ministry of Land, Infrastructure and Transport (2000). Notification No.1457-2000, Technical Standard

for Structural Calculation of Response and Limit Strength of Buildings. (In Japanese)
[20] Mistumasa M, Izuru O, Masanori I, Masaomi T. Performance-Based Seismic Design Code for Buildings in Japan. Earthquake Engineering and Engineering Seismology, Vol. 4, No. 1, 15–25, 2003.
[21] Avilés J, Pérez-Rocha LE. Revisions to code provisions for site effects and soil-structure interaction in Mexico earthquake research and analysis, –New Frontiers in Seismology, Dr Sebastiano D'Amico (Ed.), 2012.
[22] Building Instruction Department, Housing administration, Ministry of Land, Infrastructure Transport and Tourism (2001). Examples and introduction of calculation method of response and limit strength. (In Japanese)
[23] Lam NTK, Wilson JL, Chandler AM. Seismic displacement response spectrum estimated from the analogy soil amplification model. Engineering Structures 2001, Vol. 23, No. 11, 1437–1452, 2001.
[24] Hing-Ho T, Adrian MC, Lam NTK. Estimating non-linear site response by single period approximation. Earthquake engineering and structural dynamics, Vol. 35, 1053–1076, 2006.
[25] Hing-Ho T, Adrian MC, Lam NTK. Simple models for estimating period-shift and damping in soil. Earthquake engineering and structural dynamics, Vol. 35, 1925–1947, 2006.
[26] Tsang HH, Wilson JL, Lam NTK, Su RKL. A design spectrum model for flexible soil sites in regions of low-to-moderate seismicity. Soil Dynamics and Earthquake Engineering, Vol. 92 36–45, 2017.
[27] Yasuhiro H, Takeshi M, Sadatomo O, Masataka Y. Study on ground amplification ratio in the calculation method of response and limit strength. Journal of Structural and Construction Engineering AIJ, Vol. 567, 41–46, 2003. (In Japanese)
[28] Kehji K. Practical evaluation for soil response and pile stress in a liquefiable site using response spectrum method. J Technol Des AIJ, Vol. 19, 47–52, 2004. (In Japanese)
[29] Wakako I, Yasuhiro H, Hiroshi A, Shoichi N, Masanori IIBA. A study on method to evaluate seismic amplification ratios of surface strata. J Technol Des AIJ, Vol. 16,107–112, 2010. (In Japanese)
[30] Zhao JX, Zhang J, Irikura K. Side-effect of using response spectral amplification ratios for soil sites—variability and earthquake-magnitude and source-distance dependent amplification ratios for soil sites. Soil Dynamics and Earthquake Engineering Vol.29, 1262–73, 2009.
[31] Zhao JX, Zhang J. Side-effect of using response spectral amplification ratios for soft soil sites—Earthquake source-type dependent amplification ratios. Soil Dynamics and Earthquake Engineering, Vol.30, 258–269, 2010.
[32] Dobry, R., 1991, Soil properties and earthquake response, Proceeding of X European Conference of Soil Mechanics and Foundation Engineering, IV, 1171-1187, Florence, Italy, May 26-30.
[33] Rosenblueth E, Arciniega A. Response spectral ratios. Earthquake Engineering and Structural Dynamics, Vol.21, 483–492, 1992.
[34] Joyner, W.B., Fumal, T. E., and Glassmoyer, G., 1994, Empirical spectral response ratios for strong motion data from the 1989 Loma Perieta, California, earthquake, Proceedings of the 1992 NCEER/SEAOC/BSSC Workshop on Site Response During Earthquakes and Seismic Code Provisions, G.R. Martin, ed., University of Southern California, Los Angeles, November 18-20, 1992, National center for Earthquake Engineering Research Special Publication NCEER-94-SP01, Buffalo, NY.
[35] Strong-motion Seismograph Networks (K-NET, KIK-net), http://www.kyoshin.bosai.go.jp/kyoshin/; [accessed 16.04.13].
[36] Boore, D. M. Stochastic simulation of high-frequency ground motions based on seismological models of the radiated spectra, Bulletin of the Seismological Society of America, Vol .73, 1865–1894, 1983.
[37] Boore, D. M., and W. B. Joyner. A note on the use of random vibration theory to predict peak amplitudes

of transient signals, Bulletin of the Seismological Society of America, Vol .74, No. 5, 2035–2039, 1984.
[38] Liu, L., and S. Pezeshk. An improvement on the estimation of pseudo response spectral velocity using RVT method, Bulletin of the Seismological Society of America, Vol. 89, No. 5, 1384–1389, 1999.
[39] Boore, D. M., and E. M. Thompson. Empirical improvements for estimating earthquake response spectra with random-vibration theory, Bulletin of the Seismological Society of America, Vol .102, No. 2, 761–772, 2012.
[40] Boore, D. M., and E. M. Thompson. Revisions to some parameters used in stochastic-method simulations of ground motion, Bulletin of the Seismological Society of America, Vol .105, No. 2A, 1029–1041, 2015.
[41] Cartwright, D E. and M. S. Longuet-Hlggms. The statistmal distribution of the maxima of a random function, Proc. Roy Soc. London, Ser A237, 212-223, 1956.
[42] Davenport, A G. Note on the distribution of the largest value of a random function with application to gust loading, Proc Institution of Cwil Engineers, Vol .28, 187-196,1964.
[43] Vanmarcke, E. H. On the distribution of the first-passage time for normal stationary random processes, Journal of Applied Mechanics, Vol .42, No. 1, 215–220, 1975.
[44] Boore, D. M. Simulation of ground motion using the stochastic method, Pure Appl. Geophys. Vol .160, 635–676, 2003.
[45] Rathje, E. M., and M. C. Ozbey. Site-specific validation of random vibration theory-based seismic site response analysis, Journal of geotechnical and geoenvironmental engineering, Vol .132, No. 7, 911–922, 2006.
[47] Dieter D. Pfaffinger. M. Calculation of power spectra from response spectra. Journal of Engineering Mechanics. Vol .109, No 1, 357-372, 1983.
[48] Eduardo Reinoso, Mario Ordaz, Francisco J. Sanchez-Sesma. A note on the fast computation of response spectra estimates, Earthquake engineering and structural dynamics, Vol. 19, 971-976, 1990.
[49] H. Afra, A. Pecker. Calculation of free field response spectrum of a non-homogeneous soil deposit from bed rock response spectrum, Soil Dynamics and Earthquake Engineering, Vol. 22, No.2, 157-165, 2002.
[50] Vanmarcke, E. H. On the distribution of the first-passage time for normal stationary random processes, Journal of Applied Mechanics, Vol.42, no. 1, 215–220, 1975.
[51] Rosenblueth E. and J.I. Bustamante: Distribution of Structural Response to Earthquakes, Journal of the Engineering Mechanics Division, ASCE, EM3, 75-106, 1962.
[52] Kottke, A. R., and E. M. Rathje. Comparison of time series and random-vibration theory site-response methods, Bull, Bulletin of the Seismological Society of America, Vol. 103, No. 3, 2111–2127, 2013.
[53] X. Wang and E. M. Rathje. Influence of Peak Factors on Site Amplification from Random Vibration Theory Based Site-Response Analysis, Bulletin of the Seismological Society of America, Vol.106, No. 4, 1–14, 2016.
[54] Yousuke I, Kenji M. Study on the rationalization of foundation input motion in Japan's performance-based building code. Journal of Structural and Construction Engineering AIJ, Vol. 616, 57–65, 2007. (In Japanese)
[55] Thomson WT. Transmission of elastic waves through a stratified solid medium. J Appl Physics, Vol. 21, 89–93, 1950.
[56] Haskell NA. The dispersion of surface waves on multilayered media. Bulletin of the Seismological Society of America, Vol. 43, 17–34, 1953.
[57] Idriss IM, Sun JI. SHAKE91: a computer program for conducting equivalent linear seismic response analyses of horizontally layered soil deposits. User's Guide, University of California, Davis, 1992.
[58] Jose MR, Robert VW, Ricardo D. Modal analysis for structures with foundation interaction, J Struct Div

Vol.99, No.3, 399–416, 1973.
[59] Building Instruction Department, housing administration, Ministry of Land, Infrastructure Transport and Tourism. Structure-related technical standard commentary book of the building (2007). (In Japanese)
[60] J. X. Zhao, Estimating modal parameters for a simple soft-soil site having a linear distribution of shear wave velocity with depth, Earthquake engineering and structural dynamics, Vol. 25, 163-178, 1996.
[61] Sarma SK. Analytical solution to the seismic response of visco-elastiv soil layers. Geotechnique Vol.44, 265–275, 1994.
[62] Vijayendra KV, Sitaram N, Prasad SK. An Alternative Method to Estimate Fundamental Period of Layered Soil Deposit. Indian Geotechnical Journal Vol.45, 192–99, 2015.
[63] JARA. Specifications for highway bridges. Japan Road Association, 2012. (In Japanese)
[64] Yuki S, Seiji T, Kazuyoshi K, Toshimi K. Simplified method to evaluate ground surface amplification assuming the input motions on the engineering bedrock in the revised enforcement order of the building standard law. Journal of Structural and Construction Engineering AIJ, Vol. 565, 73–78, 2003. (In Japanese)
[65] Madera GA. Fundamental period and amplification of peak acceleration in layered systems. Research Report R 70-37, June. Cambridge, MA: MIT Press; 1970.
[66] Hadjian AH. Fundamental period and mode shape of layered soil profiles. Soil Dynamics and Earthquake Engineering, Vol. 22, No.9-12, 885–891, 2002.
[67] Kenji M, Kohji K, Masanori I. Response spectrum method for evaluating nonlinear amplification of surface strata. Journal of Structural and Construction Engineering AIJ, Vol. 539, 57–62, 2001. (In Japanese)
[68] Francesca Dezia, Sandro Carbonarib, Graziano Leonic. Static equivalent method for the kinematic interaction analysis of single piles. Soil Dynamics and Earthquake Engineering, Vol. 30, 679–690, 2010.
[69] Sheikh, M. Neaz., Tsang, H., Yaghmaei-Sabegh, S. and Anbazhagan, P. Evaluation of damping modification factors for seismic response spectra. In S. Anderson (Eds.), Australian Earthquake Engineering Society Conference 1-13, 2013.
[70] George D. Hatzigeorgiou. Damping modification factors for SDOF systems subjected to near-fault, far-fault and artificial earthquakes. Earthquake engineering and structural dynamics, Vol. 39, 1239–1258, 2010.
[71] Lin YY, Chang KC. Effects of site classes on damping reduction factors. Journal of Structural Engineering, Vol.130, No.11, 1667–1675, 2004.
[72] Lin YY, Chang KC. Study on damping reduction factor for buildings under earthquake ground motions. Journal of Structural Engineering, Vol.129, No.2, 206–214, 2003.
[73] Anmin Hao, DeyuanZhou, YamingLi, HuiZhang. Effects of moment magnitude, site conditions and closest distance on damping modification factors. Soil Dynamics and Earthquake Engineering, Vol. 31, 1232-1247, 2011.
[74] Hardin BO, Drnevich VP. Shear modulus and damping in soils: measurement and parameter effects. Journal of Soil Mechanics and Foundations (ASCE), Vol. 98, No.SM6, 603–624, 1972.
[75] J. X. ZHAO. Modal analysis of soft-soil sites including radiation damping, Earthquake engineering and structural dynamics, Vol. 26, No. 26, 93-113, 1997.
[76] Dobry R, Oweis I, Urzua A. Simplified procedures for estimating the fundamental period of a soil profile. Bulletin of the Seismological Society of America ,Vol. 66,1293–1321, 1976.
[77] Shibata, A. Dynamic Analysis of Earthquake Resistant Structures, Tohoku University, Sendaishi, Miyagi, Japan, 2010.
[78] Asteris, P.G., Repapis, C., Cavaleri, L., Sarhosis, V. and Athanasopoulou, A. On the fundamental period of infilled RC frame buildings, Structural Engineering and Mechanics, Vol. 54, No. 6, 1175-1200, 2015.

[79] Young, K. and Adeli, H., Fundamental period of irregular moment-resisting steel frame structures, The structural design of tall and special buildings, Vol.23, No.15, 1141-1157, 2014.
[80] Asteris, P.G., Repapis, C.C., Tsaris, A.K., Di Trapani, F. and Cavaleri, L. Parameters affecting the fundamental period of infilled RC frame structures, Earthquakes and Structures, Vol.9, No.5, 999-1028, 2015.
[81] Asteris, P.G., Repapis, C.C., Repapi, E.V. and Cavaleri, L. Fundamental period of infilled reinforced concrete frame structures, Structure and Infrastructure Engineering, Vol.13, No.7, 929-941, 2016.
[82] Asteris, P.G., Tsaris, A.K., Cavaleri, L., Repapis, C.C., Papalou, A., Di Trapani, F. and Karypidis, D.F., Prediction of the fundamental period of infilled RC frame structures using artificial neural networks, Computational Intelligence and Neuroscience, Vol. 2016, 2016.
[83] Asteris, P.G., Repapis, C.C., Foskolos, F., Fotos, A. and Tsaris, A.K., Fundamental period of infilled RC frame structures with vertical irregularity, Structural Engineering and Mechanics, Vol.61, No.5, 663-674, 2017.
[84] Kose, M.M., Parameters affecting the fundamental period of RC buildings with infill walls, Engineering Structures, Vol.31, No.1, 93-102, 2009.
[85] Shafei, A. and Alirezaei, M. Evaluation of the fundamental period of vibration of irregular steel structures, International Journal of Engineering Sciences & Research Technology, Vol.3, No.4, 6083-6090, 2014.
[86] Hatzigeorgiou, G.D. and Kanapitsas, G. Evaluation of fundamental period of low-rise and mid-rise reinforced concrete buildings, Earthquake engineering and structural dynamics, Vol. 42, No.11, 1599-1616, 2013.
[87] Kwon, O.S. and Kim, E.S. Evaluation of building period formulas for seismic design, Earthquake engineering and structural dynamics, Vol. 39, No.14, 1569-1583, 2010.
[88] Crowley, H. and Pinho, R. Period-height relationship for existing European reinforced concrete buildings, Journal of Earthquake Engineering, Vol.8, 93-119, 2004.
[89] Balkaya, C. and Kalkan, E. Estimation of fundamental periods of shear-wall dominant building structures, Earthquake engineering and structural dynamics, Vol.32, No.7, 985-998, 2003.
[90] Goel, R.K. and Chopra, A.K. Period formulas for moment-resisting frame buildings, Journal of Structural Engineering, Vol.123, No.11, 1454-1461, 1997.
[91] Goel, R.K. and Chopra, A.K. Period formulas for concrete shear wall buildings, Journal of Structural Engineering, Vol.124, No.4, 426-433, 1998.
[92] Hsiao, J.K. Computation of fundamental periods for moment frames using a hand-calculated approach, Electronic Journal of Structural Engineering, Vol.9, 16-28, 2009.
[93] Yao Zuoqiu. Two new and simple approximate formulas on natural frequencies. Journal of South China University of Technology, Vol. 16, No.1, 28-33, 1988. (In Chinese)
[94] GUO Zhi-yong, LU Hong-yu, LI Jian-an, AN Xiao-ning. A simple formula for finding basic frequency. Journal of xi' an mining institute, Vol. 19, No.4, 368-370, 1999. (In Chinese)
[95] GUO Zhi-yong. A simple formula for finding n-order natural frequency. Journal of xi' an university of science and technology, Vol. 23, No.3, 354-356, 2003. (In Chinese)
[96] CHEN Kuifu ZHANG Senwen. Algorithm to estimate the minimum natural frequency of multi-degree freedom vibration system. Journal of Mechanical Strength, Vol. 25, No.2, 141-143, 2003. (In Chinese)
[97] LENG Bing-lin YAN Xiang-cheng LIN Ke-xin. Analysis on natural frequency calculation formula of vibration system. Shanxi architecture, Vol. 39, No.21, 20-22, 2013. (In Chinese)
[98] European Committee for Standardization CEN (2004), Eurocode 8: design of structures for earthquake resistance—part 1: general rules, seismic actions and rules for buildings, European Standard EN 1998-1:2004.

[99] Tatsuya AZUHATA, et al. Study on dynamic soil-building structure interaction based on strong motion observation. National Institute for Land and Infrastructure Management No.866, 2015. (In Japanese)
[100] ARIMOTO Shinichi, et al. Considerations on diagnosis and repair of earthquake-resistant structures. ~Case in Wakayama Pref.~. Summaries of Technical Papers of Annual Meeting AIJ, 229-230, 2004. (In Japanese)
[101] INOUE, Yoshio, et al. Study on Seismic Input to Apartment House of HUDC (part-3 Application to 5 storied houses). Summaries of Technical Papers of Annual Meeting AIJ, 131-132, 1985. (In Japanese)
[102] MANABU KAWASHIMA, et al. Pseudo-Damage Detection in a Five-Story Structure Based on Shaking Test. Reports of Technical Research and Development Center of SUMITOMO MITSUI CONSTRUCTION CO.,LTD., No.8, 101-108. (In Japanese)
[103] Midori Koiwai, Taiju Hamasaki, Nagayuki Yoshida. A Study on Structural Vibration Property by Optimization Method-Structural Identification from Microtremor-. Bulletin of Research Center for Computing and Multimedia Studies, Hosei University, No.27, 61-67, 2013. (In Japanese)
[104] MIZUHATA Koji et al. Observed Earthquake Record of a Middle Height Building with # Shaped Large Frame Halfway up Mt. Rokko. Summaries of Technical Papers of Annual Meeting AIJ, 553-556, 1988. (In Japanese)
[105] Crouse CB, McGuire JW. Site response studies for purpose of revising NEHRP seismic provisions. Earthquake Spectra, Vol. 12, No.3, 407– 439, 1996.
[106] W.D. Liam Finn and Adrian Wightman. Ground motion amplification factors for the proposed 2005 edition of the National Building Code of Canada. Can. J. Civ. Eng. 30: 272–278, 2003.
[107] 2005 Seismic Design Code for Buildings in Taiwan, National Center for Research on Earthquake Engineering.
[108] Brune, J. N. Tectonic stress and the spectra of seismic shear waves from earthquakes, J. Geophys Res 75, 4997-5009, 1970.
[109] Brune, J. N. (1971). Correction, J Geophys. Res 76, 5002.
[110] AKI, K. Generation and Propagation of G Waves from the Niigata Earthquake of June 16, 1964. Part 2. Estimation of Earthquake Moment, Released Energy, and Stress-strain Drop from the G-Wave Spectrum, Bull. Earthq. Res. Inst. 44, 73–88, 1966.
[111] ATKINSON, G. M. and BOORE, D. M., Ground Motion Relations for Eastern North America, Bulletin of the Seismological Society of America, Vol. 85, 17–30, 1995.
[112] BOORE, D. M. and JOYNER, W. B., Site amplifications for Generic Rock Sites, Bulletin of the Seismological Society of America, Vol. 87, 327–341, 1997.

List of Publications

Journal papers

[1] Haizhong Zhang, Takasuke Saito, Yan-Gang Zhao. Simple calculation method of seismic motion amplification ratio corresponding to fundamental period. *Journal of Structural and Construction Engineering AIJ* 2017; **82** (734): 597-604. (In Japanese)
[2] Haizhong Zhang, Takasuke Saito, Yan-Gang Zhao. Calculation method of seismic motion amplification ratio corresponding to fundamental period of layered soil profiles. *Journal of Structural Engineering* 2017; **63B**: 343-349. (In Japanese)
[3]Yan-Gang Zhao, Haizhong Zhang, Takasuke Saito. A simple approach for the fundamental period of MDOF structures. *Earthquakes and structures* 2017; **13** (3): 231-239. (Corresponding author)
[4] Haizhong Zhang, Yan-Gang Zhao. A simple procedure for estimating the first resonance peak in layered soil profiles. *Journal of Earthquake and Tsunami.* (Accepted)
[5] Haizhong Zhang, Yan-Gang Zhao. A simple approach for analysis of first vibration mode of layered soil profiles *Journal of Earthquake and Tsunami.* (Under review)

International Conference :

[6]Haizhong Zhang, Yan-gang Zhao. An Empirical Power Spectrum on Engineering Bedrock corresponding to Standard Response Spectrum, *International Symposium on Reliability Engineering and Risk Management 2014*, pp. 161-164, Taipei, Taiwan.
[7]Haizhong Zhang, Yan-gang Zhao. A Response Spectrum Method for Surface Strata Site-Amplification, *International Symposium on Reliability Engineering and Risk Management 2015*, pp. 305-314, Taipei, Taiwan.
[8]Haizhong Zhang, Takasuke Saito, Yan-gang Zhao. Response Spectrum Method for Surface Strata Site Amplification.*16th World Conference on Earthquake 2017*, Paper No.1430, Santiago, Chile.
[9] Haizhong Zhang, Fangwen Ge, Yan-gang Zhao. Comparison of response spectral ratio and Fourier spectral ratio based on statistical analysis of ground-motion records. *International Symposium on Life-cycle Engineering and Sustainability of Infrastructure 2017*, Taipei, Taiwan.

Domestic Conference:

[10] Haizhong Zhang, Takasuke Saito, Yan-gang Zhao. Prediction of Site Amplification for the Calculation of Acceleration Response Spectrum on Ground Surface, *Summaries of Technical Papers of Annual Meeting, AIJ 2013*, pp.1525-1526, Hokkaido.
[11] Haizhong Zhang, Takasuke Saito, Yan-gang Zhao. Prediction of Site Amplification for Response Spectrum. *Summaries of Technical Papers of Annual Meeting, AIJ 2014*, pp.379-380, Kinki.
[12] Deyin Jin, Haizhong Zhang, Takasuke Saito, Yan-gang Zhao. A Study on Ground Amplification Ratios in the Calculation Method of Response Limit Strength (Part 1), *Summaries of Technical Papers of Annual*

Meeting, AIJ 2015,pp.83-84, Kanto.
[13] Haizhong Zhang, Takasuke Saito, Yan-gang Zhao. A Study on Ground Amplification Ratios in the Calculation Method of Response Limit Strength (Part 2). *Summaries of Technical Papers of Annual Meeting, AIJ 2015*,pp.85-86, Kanto.
[14] Haizhong Zhang, Takasuke Saito, Yan-gang Zhao. Simplified procedure for estimating amplification ratio corresponding to the fundamental period of layered soil profile, *Summaries of Technical Papers of Annual Meeting, AIJ*, 2016, pp1037-1038, Kyushu.
[15] Haizhong Zhang, Takasuke Saito, Yan-gang Zhao. A simple approach for analysis of fundamental mode shape of layered soil profiles, *Summaries of Technical Papers of Annual Meeting, AIJ*, 2017, pp363-364, Chugoku.
[16] Yan-gang Zhao, Haizhong Zhang, Takasuke Saito. A simple approach for fundamental period of MDOF structures, *Summaries of Technical Papers of Annual Meeting, AIJ*, 2017, pp1037-1038, Chugoku.
[17] Fangwen Ge, Haizhong Zhang, Takasuke Saito, Yan-gang Zhao. Relationship between response spectral ratio and Fourier spectral ratio based on statistics, *Summaries of Technical Papers of Annual Meeting, AIJ*, 2017,pp.83-84, Chugoku.